COMPLEX MODAL ANALYSIS OF ROTATING MACHINERY

A dissertation submitted to the

Division of Research and Advanced Studies
of the University of Cincinnati

in partial fulfillment of the
requirements for the degree of

DOCTORATE OF PHILOSOPHY (Ph.D.)

In the Department of Mechanical, Industrial, and Nuclear Engineering
of the College of Engineering

1999

by

Charles L. Kessler

B.S., Wright State University, 1986
M.S., University of Dayton, 1991

Committee Co-Chairs:	Dr. Jay Kim
	Dr. David Thompson
Committee Members:	Dr. Randy Allemang
	Dr. David Brown
	Dr. Bob Rost

ABSTRACT: COMPLEX MODAL ANALYSIS OF ROTATING MACHINERY

Rotor dynamics is a subset of vibration analysis that deals with the dynamic characteristics of spinning machines. The problem is characterized by generally nonsymmetric system matrices whose elements depend upon the rotor speed.

An approach to complex analysis of rotating systems is described which results in improved physical understanding of solutions to the eigenvalue problem and stresses commonality with conventional modal analysis. In the approach, a natural mode of the rotor is represented as the sum of two sub-modes which are rotating to the forward (i.e., with rotor rotation) and backward (i.e., against rotor rotation) directions. This definition of the natural mode allows complex analysis of free and forced vibration of anisotropic systems, which had not been reported previously. The complex mode representation enables clear definition of the forward mode and the backward mode, and more importantly enables one to complete the complex rotor analysis procedure.

Concepts are illustrated with a general rigid rotor model and a reduced form which is a two degree of freedom anisotropic model including gyroscopic effects. In order to verify the approach, a pendulum-mounted multi-axis force sensor was used as an impact device to excite the spinning rotor. This enabled measurement of the normal impact as well as the tangential force component induced by friction. Complex modal analysis was then applied to clearly distinguish forward and backward modes and separate them in the frequency domain.

ACKNOWLEDGMENTS:

Reflecting upon the effort summarized in this document it is clear that it is the result of contributions from many people. My professors, dissertation committee, coworkers, and family members all supported me during this endeavor and earned my sincere gratitude.

Most responsible for the direction of the research conducted during this dissertation was Dr. Jay Kim. As my advisor his professionalism, dedication, and patience were often tested. He was willing to accept this dissertation topic, outside of his normal area of expertise, and provide me continuous support. I will always be grateful for his efforts.

My co-advisor, Dr. Dave Thompson, was also very helpful in the early stages of the dissertation when its direction was unclear. Discussions on magnetic bearings between a controls person, a vibration person, and an aspiring Ph.D. candidate may have seemed fruitless at the time but proved extremely beneficial. The support and inputs from the remaining committee members are also gratefully acknowledged.

While this effort could not have been completed without the encouragement and support of Dr. Kim, the attempt could not have been made without support from the Power Division of the Propulsion Directorate of the Air Force Research Laboratory. Their willingness to allow me to invest the time and resources necessary to complete this effort is acknowledged. Special thanks must be expressed to Dr. Buryl McFadden for his unwillingness to allow me to decline this opportunity. My immediate supervisor, Mr. Phil Colegrove, is also acknowledged for leaving me alone when I told him that I would

be successful if he would just leave me alone. My coworkers who shouldered the work I would have done are also very much appreciated.

Thanks are also due to those family members and coworkers who stopped inquiring as to my progress after about the two year point of the dissertation phase; I hereby formally apologize for my replies. The tolerance of my wife in allowing me to pursue this goal was very much appreciated. Finally, I thank my kids for their consistent optimism as to how good life will be after Dad gets his Ph.D.; in a few years they may have some appreciation for the meaning of the letters.

Sincerely,

Chuck Kessler

TABLE OF CONTENTS:

LIST OF TABLES AND FIGURES:

NOMENCLATURE:

$Y, Z =$ non-rotating Cartesian coordinate system

$y(t), z(t)$ = real position of geometric center of rotor station in Y and Z coordinates

$f_Y(t), f_Z(t)$ = real excitation in Y and Z coordinates

Y_k, Z_k = coefficients of complex Fourier series of $y(t)$ and $z(t)$

F_{Yk}, F_{Zk} = coefficients of complex Fourier series of $f_Y(t)$ and $f_Z(t)$

$p(t)$ = complex response

$g(t)$ = complex excitation

P_f, P_b = coefficients of complex Fourier series of $p(t)$

G_f, G_b = coefficients of complex Fourier series of $g(t)$

$[T]$ = transformation matrix

s = complex frequency

$\omega =$ frequency

ω_k = FFT spectral line or frequency bin

λ_i = eigenvalue

r_i, l_i = right, left modal vector

R_i, L_i = right, left eigenvector

Ω = rotor speed

$\alpha =$ dimensionless rotary inertia ratio: $I_{polar} / I_{transverse}$

$\Omega_p =$ dimensionless rotor speed parameter

Δ = dimensionless anisotropy parameter

C_{ij} = viscous damping coefficient relating force at i to velocity at j

K_{ij} = stiffness coefficient relating force at i to displacement at j

$e =$ base of the natural logarithms, mass eccentricity (context-dependent)

$[X]^+ =$ pseudoinverse of matrix [X]

$j = \sqrt{-1}$

$\bar{x}$ = complex conjugate of x

CHAPTER 1: INTRODUCTION

1.1 Chapter Abstract

This chapter explains the motivation to pursue the complex modal analysis approach for analysis and testing of rotor systems as well as the overall objectives of the work. A survey of relevant literature is included, as is a brief preview of the contents of remaining chapters.

1.2 Motivations of the Work

Most of the important concepts or topics in rotor dynamics are related to classical vibration theory. For example, natural frequencies, natural modes, and critical speeds are all found in rotor dynamics as well as in vibration analysis. The major distinction between rotor dynamics and classical vibration is the effect of rotation, which induces many unique features such as whirling, forward and backward modes, gyroscopic terms, non-symmetric equation of motion, and others. The rotation effect also makes formulation and solution of the system equation, as well as interpretation of the solution, much more difficult to understand. This difficulty may be understood as "interference between rotation and harmonic motion", which needs further explanation as follows.

In vibration analysis, rotating motion is used to describe harmonic motion using the Euler identity. For example, when the expression $f(t) = F_0 e^{j\omega t}$ is used to define a force varying harmonically in time, it implies that one is interested in only the real or imaginary part of the complex variable; for graphical convenience this concept is represented in the phasor diagram. In rotor systems two more rotating quantities must be considered as well: spinning and whirling (i.e., motion of an axial rotor station in the plane perpendicular to the spin axis) of the rotor. This "interference" creates difficulties

in describing motions, formulating equations, and generally understanding, interpreting and visualizing the responses. This is mainly because while rotor spin and whirl are actually physical "rotation", harmonic motion as described by the complex exponential in vibration analysis is not; all of these variables are used in rotor dynamics with the same mathematical form.

In the complex rotor analysis method advocated in this work the harmonically vibrating variable is expressed by a complex variable which is in turn composed of two complex exponentials which rotate in opposite directions. This allows all of the variables that appear in rotor analysis to represent quantities that actually rotate in a two dimensional plane. Therefore, this simplifies all analysis procedures in rotor dynamics: formulation, solution, and interpretation of the equation of motion. It also eliminates possibilities of confusion or mis-interpretations. Among all the advantages, this is considered the biggest.

It is noted here that the term "complex mode" in classical vibration typically refers to a mode for which the modal vector cannot be normalized such that its elements are all purely real, as results from a system with non-proportional damping. As used here "complex modal analysis" refers to the application of modal analysis principles to systems whose inputs and outputs are described by complex variables. This approach has been shown to have significant advantages in the study of rotor systems but the theory has not been well received. It is believed that this has been caused by complexities of the theory itself, very complicated notations adopted by the people who pioneered it (i.e., Chong-Won Lee and his collaborators[8-16]) and most importantly by lack of a definition of one fundamental concept: the complex natural mode. Despite its many advantages

these factors have contributed to prevent the method from being used more widely, as one can see from the fact that virtually all papers adopting this method have been published by Lee and his students.

This discussion identifies the motivations of this work, and therefore the contributions gained from it, as follows:

- Develop an easy-to-use and easy-to-understand analysis procedure for free and forced vibration problems in rotor dynamics.
- Develop a firm definition of complex natural modes.
- Develop concrete understanding of the rotor responses, especially in complex notation.
- Develop an experimental frequency response function estimation and modal identification procedure using the complex analysis concept.

1.3 Literature Survey and Background

Modal analysis concepts have not been applied to rotor systems as extensively as they have to other structural dynamic systems. Rotor systems force the reconsideration of some of the basic assumptions applied in modal analysis of other structures. In particular, rotor systems do not in general obey Maxwell's reciprocity theorem; system matrices are nonsymmetric. System matrices also depend upon rotor speed due to the presence of gyroscopic effects which lead to skew-symmetry in the damping matrix; this is a linear function of rotor speed. Also, support characteristics are nonsymmetric for commonly-used bearing types and they vary widely with rotor speed.

Nordmann[1] examined modal analysis of rotor systems at fixed rotational speed considering their unique features which lead to a non-self-adjoint eigenvalue problem. He proposed that a natural mode be described by the free response of the point in the plane. To enable this, two complex conjugate eigensolutions (i.e., the combination of an eigenvalue and an eigenvector) were summed to result in a physically meaningful motion which could be plotted as a planar curve at each rotor station.

Ehrich[2] showed that when natural solutions are presented as Nordmann proposed, some modes are corotating (i.e., in the same direction as shaft rotation) and some are counter-rotating. He also represented the equations of motion for a single disk system in complex form, and assumed the solution form:

$$\bar{\gamma} = \bar{\gamma}_0 e^{j\omega t} \tag{1.1}$$

which he termed a "rotational natural mode". He showed that the eigenvalue with a positive frequency denoted a corotating mode and the eigenvalue with a negative frequency denoted a counter-rotating mode. The system that he used for this example was an isotropic single disk system, though he did not make this clarification.

Muszynska[3] proposed testing to identify forward and backward modes separately by applying perturbation forces which rotate with and against the rotor spin direction. The design of the excitation device is a disk attached to the outer race of a rolling element bearing the inner race of which is fixed to the rotor. On the disk is an arrangement of springs; moving the end of one spring circumferentially places a unidirectional force on the rotor. The disk is attached to a variable speed motor through a soft belt so that the speed and direction of disk rotation is varied independent of the rotor speed. Forward and backward rotating excitations are thus applied independently.

Bently, et. al. [4-6] have recently discussed advantages of applying forward/backward concepts to rotating machinery diagnostics. In particular, rotor motion is measured in orthogonal directions at the stations of interest. These real signals are Fourier transformed and added according to the definition of the complex position variable:

$$p(t) = y(t) + jz(t) \tag{1.2}$$

where rotor rotation is from Y toward Z. Fourier coefficients corresponding to positive exponents in the complex series are forward (i.e., they represent rotation from Y toward Z) and those corresponding to negative exponents are backward. The magnitude of the forward response component is plotted on the positive frequency domain and the magnitude of the backward component is plotted on the negative frequency domain. Their term for this presentation is the "full spectrum plot". A recent article[7] explains basic observations such as the response of the isotropic rotor to mass imbalance excitation should be purely forward, as indicated by a line on the positive frequency side at synchronous frequency. The work has not considered excitation sources in general and has not investigated relationships between excitation and responses or the modal contributions to these relationships.

Lee, et. al. [8-16] developed complex modal analysis theory and showed it to offer significant advantages in the study of rotor systems. The main advantage is the ability to incorporate directionality. In particular, it separates the contributions of forward and backward modes into different frequency response functions; he termed these directional frequency response functions (dFRFs) for this reason.

Separation of the forward and backward modes is significant for several reasons. The frequency difference between pairs of modes is often small; modal parameters of the two physically different modes can be difficult to estimate due to overlapping of the closely spaced modes. Also, the rotor system responds very differently to forward and backward excitations; this fact is not clear from looking at the conventional FRFs.

Lee algebraically derived the dFRF matrix by transforming the frequency response matrix of the system formulated with a real variable description. Complex free vibration analysis, which results in the complex natural modes of the system, was done only for the case of isotropic rotors. Forced vibration analysis was based upon work by Nordmann[1] and Lancaster[17] which deals with modal superposition of non-self-adjoint systems.

Lee[13-16] further developed the theory and extended it to complex modal testing and recommended several excitation approaches. Two of these forms are not different than conventional experimental modal analysis in which a force is applied in a certain line of action and responses are measured along this or other lines of action; the dFRFs are then algebraically calculated from these measurements. "Unidirectional" excitation involves exciting the rotor station in a single linear direction at a time and monitoring orthogonal translations; "bidirectional" stationary excitation is similar with independent linear excitations applied in two directions simutaneously. Neither of these are different than conventional modal analysis; one is single-input multi-output and the other is multi-input multi-output. The third approach Lee has defined is called "bidirectional rotating" excitation and involves synchronizing orthogonal exciters so that a broad-spectrum force is generated which rotates in a particular direction; this is done by requiring the Z-

direction force to lead the Y-direction force by 90°. This requires very precise synchronization of excitations in order to generate forces of the form mechanically generated on a frequency-by-frequency basis by Muszynska. Each of these approaches can be implemented in a magnetically-levitated rotor by injecting an excitation current into the magnetic bearing stator but application to other systems is limited.

In addition to the speed-dependent and non-self-adjoint nature of rotor systems, there are several practical issues which make modal testing of spinning rotors difficult. Solving these practical issues was not the objective of this work; experimental verification of the complex modal analysis concepts developed herein avoided these issues as much as possible and was a relatively small portion of the effort.

Non-contact response sensors are required to directly measure rotor motion. Two common choices are eddy-curent proximity sensors ("Bently" probes) and laser sensors[18]. When shaft position is measured by the probe, the signal includes not only the motion of the shaft but also surface imperfections of the rotor, typically called mechanical runout. Probe performance is also affected by local variations in the electrical characteristics of the rotor target material, called electrical runout. Rogers and Ewins[19] discussed many of the practical difficulties associated with testing spinning rotor systems.

An additional consideration is that whenever the rotor is spinning, it is subject to excitation by mass imbalance, machine processes, and possibly rolling element bearing surface imperfections, all of which are likely uncharacterized. The measured response to perturbation includes this baseline response as well as the desired response to the

perturbation. Signal processing techniques to improve FRF estimates in the presence of these synchronous excitations have been extensively studied[20-22].

Exciting the rotor is also more difficult due to the fact that it is spinning. One approach[19] is to mount a stinger to the outer race of a rolling element bearing and use a controlled electrodynamic exciter. This requires adding a bearing to the rotor which may not be possible in the field and which may alter its dynamic characteristics. Impacting the spinning rotor through a stationary flap with a small coefficient of friction has also been used[20] successfully.

Much of the work in rotor dynamics in recent years has related to magnetic levitation systems. In this case, the bearing stator provides a convenient non-contact excitation mechanism[10,16]. An electrical perturbation applied to the stator coil generates a force perturbation on the rotor. A non-contact electromagnetic exciter applicable to laboratory rotors has been developed[18] which has an integral piezoelectric force transducer; this allows applied force to be measured directly as opposed to estimating it based upon measured current and the assumed invariant transfer function between force and stator current. These approaches eliminate the unknown tangential excitation due to friction but are of limited use in field testing.

The fairly recent introduction of the triaxial force transducer enables, at least in theory, direct measurement of not only the primary impact excitation but also the tangential component induced by friction. No references were located which discussed measuring the tangential component of excitation during impact testing of a spinning rotor.

Concepts developed to support complex modal analysis led to the development of a practical complex testing theory which can be applied to rotors installed in the field. The triaxial force transducer, which is a ring configuration, was fitted with an impact cap and used as a triaxial impact hammer. Two axes of the sensor were used to measure the primary force applied to the rotor as well as the tangential component due to friction. A pendulum was used to control the impact orientation.

1.4 Scope of the Work

This document is organized into chapters which form a logical progression through the complex modal analysis approach. An overview of the chapter contents follows.

In Chapter 2 some fundamental concepts of rotor dynamics are discussed in order to prepare the reader for future chapters. The most basic rotor system possible, named the Jeffcott rotor after its original developer, is used to discuss rotor whirl, natural frequencies and modes, mass imbalance response, and critical speeds. The anisotropic variant of the model is used to introduce the fact that anisotropic rotors are capable of a mass imbalance response which is backward (i.e., counter to the direction of rotor spin). A commonly-used plot which shows typical variation of natural frequencies with rotor speed as well as intersections with lines of asynchronous excitation frequency which indicate critical speeds, known as the RPM spectral map or Campbell diagram, is introduced. Also, typical analyses in modern rotor dynamics are briefly discussed.

In Chapter 3 the method for complex free vibration analysis of the general anisotropic rotor is established. The purpose of the chapter is to establish the most

fundamental concepts of complex rotor analysis. Natural modes (i.e., frequencies, mode shapes and directions) of general anisotropic rotors are concretely established. At first, describing planar motions with a complex variable is explained as a basic concept. The complex matrix equation of motion is derived by applying a transformation matrix to the real equation of motion. The most important achievements of the work, the definition of the complex natural mode and the solution method to obtain it, are presented. Interpretations of the physical significance of the complex description of these modes is explained. This allows definition of the directivity of modes and establishes the concept of forward modes and backward modes, which has been used for a long time by many researchers without clear definition.

In Chapter 4 the complex method is extended to the forced vibration problem. Forced vibration analysis is conducted based on the mode superposition method, using the complex natural modes which were defined in Chapter 3. Input-output relations are considered in terms of frequency response functions (FRFs) for the general anisotropic rotor in complex notation. Because of the directivity of natural modes built into the complex description, the FRFs are identified with directivity relations which makes them "directional FRFs" (dFRFs). Directional FRFs are newly defined in this work as the relation between forward and backward excitations and forces. The modal contributions to these relations are explained.

In Chapter 5 experimental identification of complex natural modes of rotors is established. Again, definitions of the complex modes and dFRFs made in Chapters 3 and 4 are effectively used. Methods to excite the system, measure the responses and extract the modes are explained and developed. The procedure is implemented in a test rig. The

importance of experimental verification of the theory is recognized but this was not the main objective of this work. Therefore, the experimental set-up is a simple impact test using a multi-axis impact hammer.

Throughout this work, the rigid rotor is used as the model to develop the theory and related concepts. The rigid rotor is chosen for two main reasons:

- The analytic solution is available in closed form.
- It is the simplest rotor model which includes the gyroscopic effect, which is considered one of the unique characteristics of general rotors (as compared to the classic Jeffcott rotor).

Equations of motion of the 4 degree of freedom (DOF) rigid body rotor are derived in Appendix A. When the rotor has symmetric geometry it is recognized that the antisymmetric motion ("pitch" type motion) of the rotor represents 2 DOF gyroscopic rotor motion, and is the simplest analytical case of such motion.

Chapter 6 provides a summary and conclusions drawn from this work. Main achievements are briefly summarized and necessary future works based on the foundation laid by this work are identified. They are:

- Extension of the theory to the analysis of asymmetric rotors (i.e., those which are not axisymmetric).
- Application of the theory to practical rotor systems for analysis, particularly on-line monitoring and control problems.
- Extension of the work to include more realistic bearing models, such as hydraulic bearings, rolling element bearings riding on squeeze film dampers and actively

controlled magnetic bearings. The last type is discussed as a useful non-contact excitation mechanism.

- Refining experimental and on-line monitoring techniques in hardware, software and algorithims related to signal processing.
- Application of the complex analysis approach to continuous systems, particularly applying forward and backward descriptions to rotating shell vibration.

CHAPTER 2: OVERVIEW OF FUNDAMENTAL CONCEPTS OF ROTOR DYNAMICS

2.1 Chapter Abstract

A brief overview of the study of rotor dynamics is presented in this chapter. Classic simple models are introduced and used to explain fundamental concepts. The need for directivity in rotor analysis is illustrated by examining the mass imbalance response of the anisotropic Jeffcott rotor; this illustration motivates the work presented in Chapter 3. Current industrial practices in this area are very briefly summarized.

2.2 The Rotor as a Vibrating System

A rotor system can be considered a vibrating system in the classical sense. It is represented by a system of equations which relates excitations and responses, where responses of interest are motions of the geometric center of the shaft. Excitations can be due to rotating mass imbalance, aerodynamic or hydrodynamic loading due to process flows, gravity, or many other sources. The homogeneous solution determines the system's natural frequencies and mode shapes. A resonance condition exists when the frequency of excitation due to any source coincides with a natural frequency.

The rotating system has several unique features compared to other vibrating systems due to its rotation. Mass imbalance provides excitation which is present whenever the rotor spins; for this reason mass imbalance is sometimes considered an integral part of the analysis as opposed to an excitation term. The tendency of a rotor disk's angular momentum, or the momentum of the rotor itself, to couple with rotations about the bearing axis is called the "gyroscopic effect" and causes natural frequencies to vary with rotor speed.

In the following sections, the so-called Jeffcott rotor model, the simplest rotor system, is used to explain some basic concepts and terminologies of rotor dynamics which will be used in this work.

2.3 Jeffcott Rotor on Isotropic Supports

Some of the basic features of rotor dynamic analysis can be presented with the Jeffcott rotor[2,8,23-25] model which dates to 1919 and was the first to explain why a rotor experiences large lateral vibration at a certain speed and why the rotor could safely operate above this speed. It consists of a single disk rotor, the disk of which has a mass imbalance and is attached to a massless elastic shaft at mid-span. Supports are ideally rigid with frictionless bearings. The two degrees of freedom are translations in the plane of the disk. The geometry is illustrated in Figure 2.1:

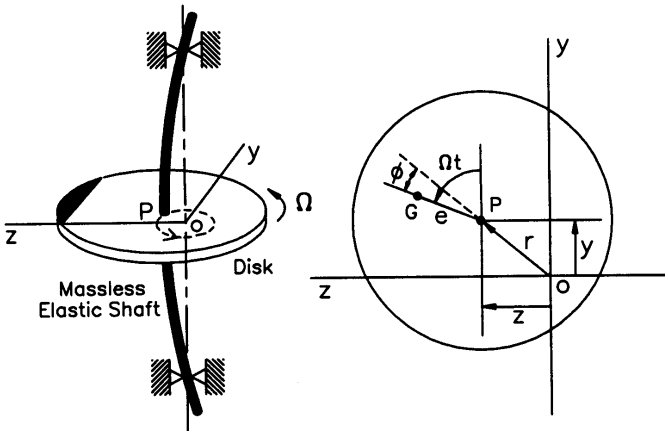

Figure 2.1: Jeffcott Rotor Geometry[8]

Variables in the figure are defined as follows:

Y, Z = stationary coordinate axes
P = geometric center of disk
G = center of gravity of disk
O = intersection point of bearing axis with disk
Ω = rotational speed of shaft (assumed constant)
$y(t), z(t)$ = position of geometric center of disk
ϕ = angle by which disk displacement lags imbalance force

For constant Ω, the position of point P is governed by:

$$m\ddot{y}(t) + c\dot{y}(t) + ky(t) = me\Omega^2 \cos\Omega t \tag{2.1a}$$

$$m\ddot{z}(t) + c\dot{z}(t) + kz(t) = me\Omega^2 \sin\Omega t \tag{2.1b}$$

where the disk mass is m, the shaft stiffness in the Y and Z coordinate directions is k, and viscous damping (provided by the ambient environment) is represented by c.

Equations (2.1) can be represented by one equation using the complex variable $r(t)$ [1,2,8,23-25]:

$$r(t) = y(t) + jz(t) \tag{2.2}$$

This allows Equations (2.1) to be combined to result in:

$$m\ddot{r}(t) + c\dot{r}(t) + kr(t) = me\Omega^2 e^{j\Omega t} \tag{2.3}$$

where the forcing function is the centrifugal force generated by the eccentric disk rotating about the shaft elastic axis. This form results from applying Euler's identity to the Y and Z force components.

The context in which this equation is presented in the texts is important: it is a convenient way to algebraically combine the two equations. Functions $y(t)$ and $z(t)$ are of interest and they can be retrieved as the real or imaginary parts of the complex whirl radius, respectively. The algebraic equality of the two forms is easily shown. Conceptually, this forms the basis for the use of complex variables for the rotor dynamics applications.

The solution of the homogeneous version of Equation (2.3) can be obtained by assuming $r(t) = P_0 e^{\lambda t}$, which results in the two eigenvalues of the system:

$$\lambda_{1,2} = \left(-\zeta \pm j\sqrt{1-\zeta^2}\right)\omega_n \tag{2.4}$$

where:

$$\omega_n = \sqrt{\frac{k}{m}}; \zeta = \frac{c}{2\sqrt{mk}} \tag{2.5}$$

The eigenvalue with a positive (negative) imaginary part represents forward (backward) rotation of the shaft. The signs of the eigenvalues can be related to so-called forward and backward modes; however, related discussions are delayed to later chapters. In fact, forward or backward modes, even though used very often in rotor dynamics, have not been a clearly defined concept. In Chapter 3, the definition of the rotor's forward and backward modes is established by considering a gyroscopic rotor on anisotropic supports.

A rotor speed such that $\Omega = \omega_n$ results in resonance and is called a mass imbalance critical speed, or synchronous critical speed. The Jeffcott rotor is isotropic meaning that the rotor and the stator, i.e. the support system, are both axisymmetric and key issues to be related later in this work are not apparent in the deceptively simple solution.

The response of the Jeffcott rotor to mass imbalance parallels response characteristics of non-rotating systems. Response of the Jeffcott rotor system of Equation (2.3) is:

$$r(t) = \left(\frac{me\Omega^2}{k - m\Omega^2 + cj\Omega}\right)e^{j\Omega t} \tag{2.6}$$

At low speeds the system response is dominated by stiffness and the rotation of the heavy spot of the disk tends to pull the geometric center of the shaft radially outward; the rotor

whirls in a circular pattern nearly in phase with the disk's heavy spot. At high frequencies (well above the natural frequency) the response is dominated by the disk's inertia and the response is such that the rotor whirls around its center of gravity. At the natural frequency, the response magnitude is determined by the level of viscous damping and a 90° phase lag exists between the vectors orienting the disk heavy spot and response. For the isotropic system, each of these responses is circular as indicated by the dotted trace in the left portion of Figure 2.1.

2.4 Jeffcott Rotor on Anisotropic Supports

If supports are anisotropic ($k_Y \neq k_Z$) in the Jeffcott rotor of Figure 2.1 the undamped equations of motion can be written in real form as:

$$m\ddot{y}(t) + k_Y y(t) = me\Omega^2 \cos\Omega t \tag{2.7a}$$

$$m\ddot{z}(t) + k_Z z(t) = me\Omega^2 \sin\Omega t \tag{2.7b}$$

or in the complex form as:

$$m\ddot{r}(t) + kr(t) + \Delta k\bar{r}(t) = me\Omega^2 e^{j\Omega t} \tag{2.8}$$

where:

$$k = \frac{k_Y + k_Z}{2}; \Delta k = \frac{k_Y - k_Z}{2} > 0 \tag{2.9}$$

and the overbar denotes the complex conjugate. Two eigenvalues can be obtained from the homogeneous form of the real Equations (2.7) as:

$$\lambda_{1,2} = \pm j\omega_{nY} \tag{2.10a}$$

$$\lambda_{3,4} = \pm j\omega_{nZ} \tag{2.10b}$$

where:

$$\omega_{nY} = +\sqrt{\frac{k_Y}{m}}; \omega_{nZ} = +\sqrt{\frac{k_Z}{m}} \tag{2.11}$$

However, information in the form of Equation (2.11) is very insufficient due to the following reasons:

- As will become evident in later chapters, the motion corresponding to a single natural frequency does not occur. The natural motion, i.e. mode, always occurs as a combination of sub-modes associated with positive and negative natural frequencies of the same magnitude.
- In conventional vibration analysis, natural modes are obtained by substituting the natural frequencies back to the equation of motion; in the above case, substituting Equations (2.10a) and (2.10b) into homogeneous forms of Equations (2.7a) and (2.7b). However, full information on natural modes of rotors is not obtained by doing so. Therefore, directivity must be incorporated into the natural mode description as will be shown in Chapter 3 in order to describe the full characteristics of natural modes.

The need for directivity in defining natural modes becomes evident if one assumes the standard harmonic solution form $r(t) = P_0 e^{\lambda t}$ and substitutes into the complex equation of motion in Equation (2.8). One immediately finds that the complex exponential on the left does not divide out to give an eigenvalue problem in λ. As the physical implication, which will be explained more in detail later, natural modes have to be of the form:

$$r = R_1 e^{\lambda t} + R_2 e^{\bar{\lambda} t} \tag{2.12}$$

The steady state mass imbalance response can be obtained from Equation (2.8) using the method of undetermined coefficients and assuming the response is elliptical as described by the form:

$$r(t) = P_f e^{j\Omega t} + P_b e^{-j\Omega t} \tag{2.13}$$

Substituting *r(t)* from Equation (2.13) and its complex conjugate into Equation (2.8) results in:

$$\begin{aligned} m\left[-\Omega^2\left(P_f e^{j\Omega t} + P_b e^{-j\Omega t}\right)\right] + k\left(P_f e^{j\Omega t} + P_b e^{-j\Omega t}\right) + \\ \Delta k\left(\overline{P}_f e^{-j\Omega t} + \overline{P}_b e^{j\Omega t}\right) = me\Omega^2 e^{j\Omega t} + 0e^{-j\Omega t} \end{aligned} \tag{2.14}$$

From which two equations are extracted which correspond to the positive and negative exponentials:

$$\left(k - m\Omega^2\right)P_f + \Delta k\overline{P}_b = me\Omega^2 \tag{2.15}$$

and

$$\left(k - m\Omega^2\right)P_b + \Delta k\overline{P}_f = 0 \tag{2.16}$$

The complex conjugate of Equation (2.16) can be combined with Equation (2.15):

$$\begin{bmatrix} k - m\Omega^2 & \Delta k \\ \Delta k & k - m\Omega^2 \end{bmatrix}\begin{Bmatrix} P_f \\ \overline{P}_b \end{Bmatrix} = \begin{Bmatrix} me\Omega^2 \\ 0 \end{Bmatrix} \tag{2.17}$$

or,

$$\begin{Bmatrix} P_f \\ \overline{P}_b \end{Bmatrix} = \begin{bmatrix} k - m\Omega^2 & \Delta k \\ \Delta k & k - m\Omega^2 \end{bmatrix}^{-1}\begin{Bmatrix} me\Omega^2 \\ 0 \end{Bmatrix} \tag{2.18}$$

The magnitude of the forward and backward rotating components for this simple case are:

$$\left|\frac{P_f}{e}\right| = \frac{\left(\omega_{nY}^2 + \omega_{nZ}^2 - 2\Omega^2\right)\Omega^2}{2\left(\omega_{nY}^2 - \Omega^2\right)\left(\omega_{nZ}^2 - \Omega^2\right)} \tag{2.19}$$

and

$$\left|\frac{P_b}{e}\right| = \frac{\left(\omega_{nY}^2 - \omega_{nZ}^2\right)\Omega^2}{2\left(\omega_{nY}^2 - \Omega^2\right)\left(\omega_{nZ}^2 - \Omega^2\right)} \tag{2.20}$$

In this way, forward and backward rotating components of the response can be calculated for each Ω. Figure 2.2 shows the ratio of forward and backward response strengths as a function of rotor speed for a typical system with a disk mass of unity and $K_Z=0.25K_Y$. Obviously, the magnitude of the response of the undamped system is unbounded at speeds corresponding frequencies ω_{nZ} and ω_{nY}. It is also known that equal response strengths for each component would make the whirl orbit a straight line at those speeds. This is expected since the mass imbalance force is composed of simultaneous excitations in the Y and Z directions; at $\Omega=\omega_{nZ}$ the Z response dominates so that motion is linear in the Z direction (i.e, unbounded Z response and finite Y response) and at $\Omega=\omega_{nY}$ the Y response dominates so that motion is linear in the Y direction. In general, the ratio becomes non-zero and non-unity which makes the whirl orbit an elliptical shape. It is also interesting that the orbit becomes purely circular, in the backward direction, at one speed between ω_{nY} and ω_{nZ}. If $\omega_{nY}=\omega_{nZ}$ (i.e., the system becomes isotropic) it is easily seen that the backward response in Equation (2.20) disappears; therefore, the motion is always in the forward direction along a circular orbit.

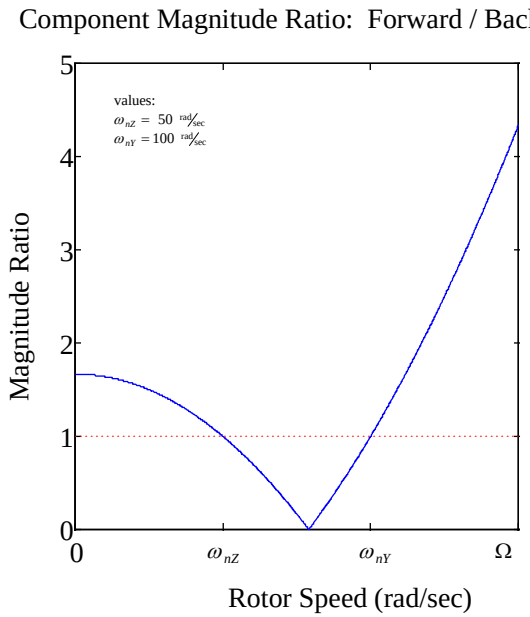

Figure 2.2: Anisotropic Flexible Rotor Mass Imbalance Response

At frequencies below ω_{nZ} the response is forward elliptical as indicated by the magnitude ratio exceeding unity. At natural frequencies ω_{nZ} and ω_{nY} the response collapses to a line (i.e., equal magnitudes) as expected from the uncoupled real solution. Between ω_{nZ} and ω_{nY} the response is backward elliptical and it becomes backward circular at the point where the curve touches the abscissa indicating zero forward component magnitude. Above ω_{nY}, the response becomes forward elliptical and approaches forward circular in the limit as speed increases.

Dynamically, the Jeffcott rotor and its anisotropic variant are not different than a bar subjected to rotating excitation. In particular, they do not demonstrate the effect of gyroscopic coupling since the model does not possess rotational degrees of freedom in any direction except the rotor spin direction. Gyroscopic coupling leads to skew-symmetric terms in the damping matrix which vary linearly with rotor speed. This tends to separate zero-speed repeated natural frequencies as speed increases. Therefore, one can consider that the gyroscopic effect is what truly separates rotors from other vibrating

systems. Figure 2.3 illustrates variation of the eigenvalues with rotor speed for a typical rigid rotor on soft supports. Motion of the rigid rotor is described by four second order degrees of freedom, so that the homogeneous solution of the governing equations has eight eigenvalues. Two of the natural modes are described by the rotor bouncing on the springs; these are repeated due to symmetry. The other two modes are described by a pitching motion; this rotation about axes perpendicular to the spin axis couples with the rotor angular momentum to cause variation of the natural frequencies with rotor speed. When the problem is modeled using real variables the eigenvalues occur in complex conjugate pairs as shown in the figure.

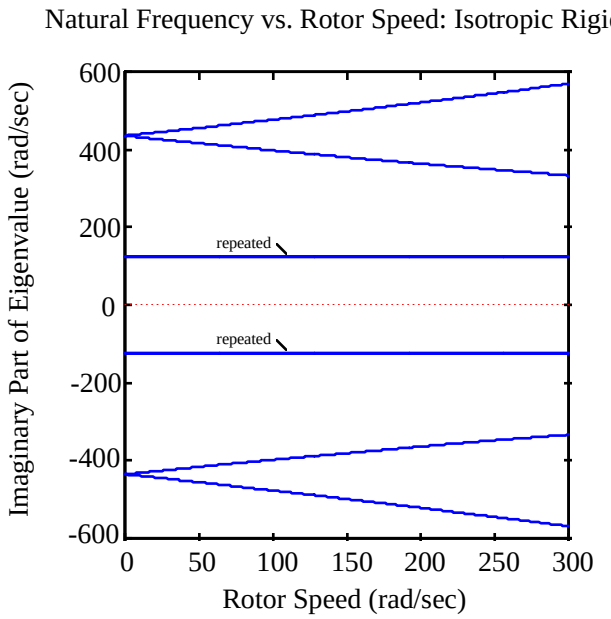

Figure 2.3: Typical Variation of Natural Frequency with Rotor Speed

2.5 Synchronous and Asynchronous Critical Speeds

A synchronous critical speed of the rotor is when the system natural frequency matches with the rotor's spinning velocity. The large response of the rotor excited by

mass imbalance can be considered to be the forward synchronous response. The rotor may operate at a speed much higher than the critical speed as long as it is not operated in the vicinity of the critical speeds. Obviously, operation of the rotor at any of the natural frequencies of the forward modes, which will be solidly defined in Chapter 3, must be avoided. For this reason, natural frequencies of the rotor as well as the directivity of the modes associated with these frequencies, must be found accurately; the latter has not been well defined so far.

Sometimes, excitations other than synchronous mass imbalance are of interest. Asynchronous excitations are characterized by the form:

$$\omega = n\Omega \tag{2.21}$$

and may arise due to ball bearing surface imperfections, gravity, or others. For example, n in Equation (2.21) becomes the number of balls in case of a ball bearing which has a defective retainer, *2* in case of the gravity loading, and approximately *0.49* in the case of oil whip. The concepts of critical speed, speed-dependent natural frequencies, and asynchronous excitation are combined in a plot commonly referred to as the Campbell diagram or the "RPM spectral map". The abscissa is rotor speed and the ordinate is frequency; natural frequencies are plotted as a function of rotor speed. Lines of various slopes are also plotted which represent various values of the parameter n of Equation (2.21). Figure 2.4 shows an example of such a graph for the pitch modes of the anisotropic rigid rotor, where Ω_p represents rotor speed:

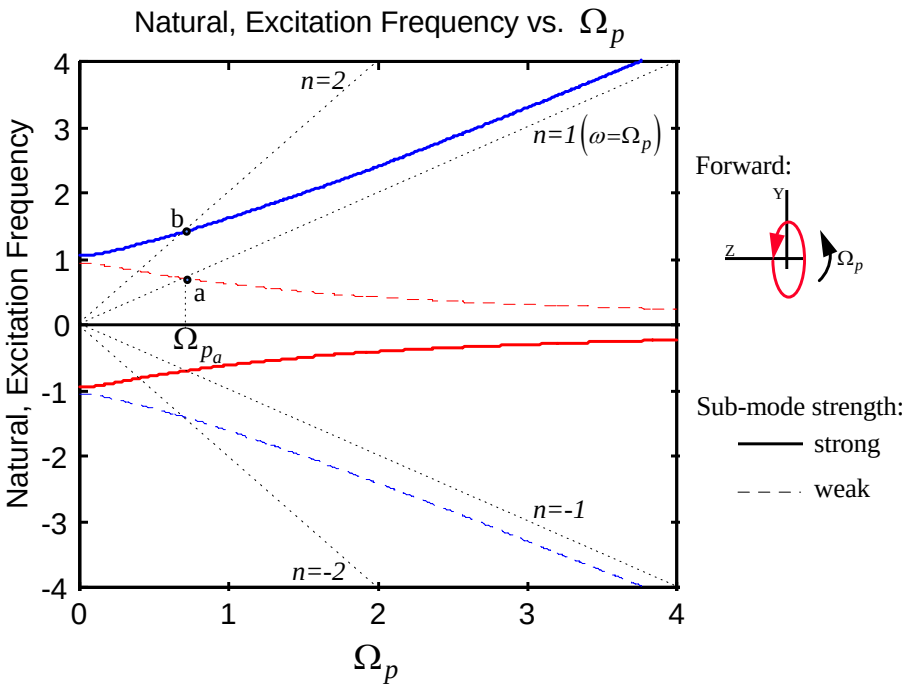

Figure 2.4: Modified Campbell Diagram

Notice that Figure 2.4 is not the common Campbell diagram which includes no directivity concept. Intersections of the *n*=1 line with natural frequency curves indicate mass imbalance critical speeds. The diagram shown in Figure 2.4 is modified to include the directivity of the modes and the strength of the sub-modes, which will be explained in detail in Chapter 3. In the figure, frequencies of weak sub-modes are plotted in a dashed line. In this way, possible false conclusions are eliminated. For example, a designer may try to avoid a false critical speed such as the intersection of the synchronous ($\omega = \Omega_p$) speed and the natural frequency of a backward sub-mode, indicated as Ω_{pa} in the figure, the response of which is much weaker than a forward sub-mode.

2.6 Typical Issues in Modern Rotor Dynamics

In current industry practice rotors are modeled using finite element analysis. Each bearing support is described by eight coefficients which may be a function of rotor speed:

$$\begin{Bmatrix} f_Y(t) \\ f_Z(t) \end{Bmatrix}_{bearing} = -\begin{bmatrix} K_{YY}(\Omega) & K_{YZ}(\Omega) \\ K_{ZY}(\Omega) & K_{ZZ}(\Omega) \end{bmatrix} \begin{Bmatrix} y(t) \\ z(t) \end{Bmatrix} - \begin{bmatrix} C_{YY}(\Omega) & C_{YZ}(\Omega) \\ C_{ZY}(\Omega) & C_{ZZ}(\Omega) \end{bmatrix} \begin{Bmatrix} \dot{y}(t) \\ \dot{z}(t) \end{Bmatrix} \tag{2.22}$$

Support systems which are not well-described by these coefficients, such as magnetic bearings, are approximated. Magnetic support characteristics are frequency-dependent as opposed to rotor speed dependent; rotor dynamic codes do not currently support their analysis. "Effective" stiffness and damping characteristics are estimated during the controls analysis and provided as input to the rotor analysis.

Rotor stability is of fundamental concern. Hydrodynamic (i.e., journal) bearings are characterized by cross-coupled stiffness terms which can either add to or subtract from the damping provided by external sources. Also, magnetic bearing systems can provide phase lead in their force over rotor position transfer function (corresponding to positive damping which acts to remove energy from the vibrating system) only over a finite frequency range; above this range they become an excitation source or a source of effectively negative damping.

Typical analysis also includes generation of the RPM spectral map (Campbell diagram) to determine the critical speeds for expected forcing functions. Mode shapes (which are also speed-dependent in general) are examined to assure that bearings are not located at nodal points which would prevent their damping properties from being realized.

Since the rotor system can be represented in state space similarly to any other vibrating system, the forced response can be simulated easily with software tools such as MATLAB®[1]. The distinction is that system parameters depend upon the rotor speed, therefore not only forced responses but also the natural frequencies and modes have to be calculated at each rotational speed of the rotor, perhaps repeating the calculation while incrementing the speed of the rotor. Lee proposed a method to use the Lambda Matrix method which allows solution of the eigenvalue problem and forced response solution in a manner analogous to other classical vibration problems[8]. The method is indeed ingenuous, however at the cost of mathematical complications. With the advent of powerful and inexpensive modern computers direct analysis at each frequency, even at hundreds of frequencies, seems to no longer be a major issue.

The objective of machinery diagnostics is to infer the condition of installed machinery by passive observation of whirl orbits over time. Rotors of interest are often applied in processes which run continuously and down time for testing and inspection is simply not available. Whirl orbits, obtained from orthogonally mounted proximity sensors at key rotor stations, and the frequency content of these signals provide operating information from which some limited information on bearing condition or the presence of rotor damage (e.g., cracks induced by material fatigue) can be detected. The difficulty with using such observations is that excitations are uncharacterized, variable, and from many sources.

This chapter has provided a brief overview of some fundamental concepts in rotor dynamics in order to give the reader a necessary foundation for later chapters.

[1] MATLAB is a registered trademark of The MathWorks, Inc.

CHAPTER 3: COMPLEX FREE VIBRATION OF GENERAL ROTOR SYSTEMS

3.1 Chapter Abstract

The objective of this chapter is to present the complex analysis method for the free vibration of general anisotropic rotors. The approach developed in this work represents the natural mode of the rotor as the sum of two sub-modes, one that rotates in the forward direction and the other in the backward direction. It is shown that the complex mode has to be described as such to satisfy the complex equation of motion of general rotor systems. Physical interpretation of results from the analysis of a model of the anti-symmetric motion of the rigid rotor shows that the complex mode contains modal directivity information as well as the conventional modal information. Proposed representation of the complex mode enables one to make clear definition of the forward mode and the backward mode, and more importantly enables one to complete the complex rotor analysis procedure.

3.2 Introduction

Dimentberg[25], Childs[23], Vance[24], Lee[8], and others have applied an assumed response form for the mass imbalance response of single disk rotors which includes independent forward and backward response components. Especially, Lee, et. al.,[9-16] pioneered the complex analysis method for general rotor dynamics taking advantage of the fact that a complex description conveys both magnitude and directionality, and demonstrated advantages of the method over real analysis. However, the complex natural mode has not been defined or understood enough to be applied to general anisotropic rotor systems. In this work, a new concept of the "complex natural mode" is introduced.

The new concept is that a natural mode of the rotor is considered to be composed of the sum of a forward rotating sub-mode and a backward rotating sub-mode. While the complex analysis method has many significant advantages, it has not been widely used by researchers in the rotor dynamics community, which may have been caused by the lack of solid definition and understanding of the complex natural mode.

The definition of the complex natural mode and corresponding analysis technique proposed in this work allow conventional modal analysis procedures to be applied to rotor systems with one additional, important advantage: modal directivity information. The definition allows forced vibration analysis of rotors, and also experimental modal analysis, to be done based on the complex description and complex modes in a manner completely analogous to conventional real modal analysis.

3.3 Complex Description of Planar Motions

A vector moving in a plane can be represented by a single complex variable as shown in Figure 3.1, with real and imaginary parts representing vector components in two orthogonal directions. The position of point *P* along an arbitrary path in the *YZ* plane at time *t* is identified by the complex variable *p(t)*:

$$p(t) = y(t) + jz(t) \tag{3.1}$$

where, $j = \sqrt{-1}$.

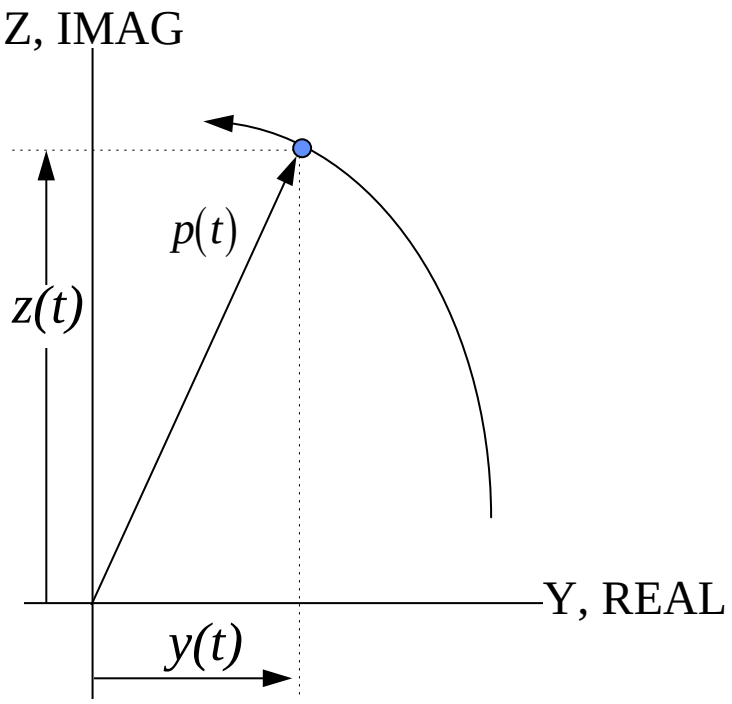

Figure 3.3: Planar Motion of Point P

The transformation between the real and complex representations is:

$$\begin{Bmatrix} y(t) \\ z(t) \end{Bmatrix} = \frac{1}{2}\begin{bmatrix} 1 & 1 \\ -j & j \end{bmatrix}\begin{Bmatrix} p(t) \\ \overline{p}(t) \end{Bmatrix} \tag{3.2}$$

Expanding *y(t)* and *z(t)* by their complex Fourier series results in:

$$\begin{aligned} p(t) = y(t) + jz(t) &= \sum_{k=0}^{\infty}\left\{\left(Y_k e^{j\omega_k t} + \overline{Y}_k e^{-j\omega_k t}\right) + j\left(Z_k e^{j\omega_k t} + \overline{Z}_k e^{-j\omega_k t}\right)\right\} \\ &= \sum_{k=0}^{\infty}\left\{\left(Y_k + jZ_k\right)e^{j\omega_k t} + \left(\overline{Y}_k + j\overline{Z}_k\right)e^{-j\omega_k t}\right\} \\ &= \sum_{k=0}^{\infty}\left\{P_{f_k} e^{+j\omega_k t} + P_{b_k} e^{-j\omega_k t}\right\} \end{aligned} \tag{3.3}$$

Equation (3.3) indicates that each harmonic component representing arbitrary plane motion can be considered to be composed of two independent components: one rotating forward and one rotating backward. Two important observations are emphasized here:

- With the complex description, now $e^{j\omega t}$ is not just a complex variable but is a vector which is actually rotating in the physical two dimensional space. A linear harmonic motion in non-rotating vibration analysis is a special case whose forward and backward rotating components have the same amplitudes, i.e. $|P_{fk}| = |P_{bk}|; k = 0,1,2,\ldots,\infty$.
- A real variable such as *y(t)*, which defines linear motion along the *Y* axis in Figure 3.1, can be considered a special case in which components are such that $Y_k = \overline{Y}_k, Z_k = \overline{Z}_k = 0; k = 0,1,2,\ldots,\infty$.

The above thought that led to Equation (3.3) suggests that the complex description of natural modes of rotors, obviously being planar motions, must also be composed of two sub-modes: one rotating forward and one rotating backward.

3.4 Complex Formulation of the Problem

Dynamics of the general rotor system can be represented by the standard equations for vibrating lumped-mass systems:

$$[M]\{\ddot{x}\} + [C]\{\dot{x}\} + [K]\{x\} = \{f\} \tag{3.4}$$

where the vector of displacements $\{x\} = \begin{Bmatrix}\{y\}\\ \{z\}\end{Bmatrix}$ and the excitation is $\{f\} = \begin{Bmatrix}\{f_Y\}\\ \{f_Z\}\end{Bmatrix}$. The length of $\{y\}$ and $\{z\}$ vectors is *n*; they define motion in a plane orthogonal to the bearing axis at each of *n* rotor stations. Coefficient matrices are speed-dependent and in general nonsymmetric due to bearing properties and the gyroscopic effect.

The relationship between real and complex descriptions of shaft position as

discussed previously can be generalized and considered a transformation defined by the matrix [*T*]:

$$[T] = \frac{1}{2}\begin{bmatrix} I(n) & I(n) \\ -jI(n) & jI(n) \end{bmatrix} \tag{3.5}$$

and $$\begin{Bmatrix} \{y\} \\ \{z\} \end{Bmatrix} = [T]\begin{Bmatrix} \{p\} \\ \{\bar{p}\} \end{Bmatrix} \tag{3.6}$$

where *I(n)* denotes an *n* x *n* identity matrix. Complex governing equations result from substituting Equation (3.6) into Equation (3.4) and premultiplying by $[T]^{-1}$:

$$[T]^{-1}[M][T]\begin{Bmatrix} \{\ddot{p}\} \\ \{\ddot{\bar{p}}\} \end{Bmatrix} + [T]^{-1}[C][T]\begin{Bmatrix} \{\dot{p}\} \\ \{\dot{\bar{p}}\} \end{Bmatrix} + [T]^{-1}[K][T]\begin{Bmatrix} \{p\} \\ \{\bar{p}\} \end{Bmatrix} = \begin{Bmatrix} \{g\} \\ \{\bar{g}\} \end{Bmatrix} \tag{3.7}$$

where the complex excitation vector is:

$$\begin{Bmatrix} \{g\} \\ \{\bar{g}\} \end{Bmatrix} = [T]^{-1}\begin{Bmatrix} \{f_Y\} \\ \{f_Y\} \end{Bmatrix} \tag{3.8}$$

or, $$\begin{Bmatrix} \{g\} \\ \{\bar{g}\} \end{Bmatrix} = \begin{Bmatrix} \{f_Y\} + j\{f_Z\} \\ \{f_Y\} - j\{f_Z\} \end{Bmatrix} \tag{3.9}$$

It is this transformation of the vector of excitations from the real form to the complex form that motivates premultiplication by $[T]^{-1}$; the purpose is not to decouple the governing equations as is often done using the orthogonality properties of modal vectors.

Representing Equation (3.7) as:

$$\left[M_c\right]\begin{Bmatrix}\ddot{p}\\ \ddot{\bar{p}}\end{Bmatrix}+\left[C_c\right]\begin{Bmatrix}\dot{p}\\ \dot{\bar{p}}\end{Bmatrix}+\left[K_c\right]\begin{Bmatrix}p\\ \bar{p}\end{Bmatrix}=\begin{Bmatrix}g\\ \bar{g}\end{Bmatrix} \tag{3.10}$$

uses the subscript *c* to emphasize that this formulation is based upon complex variables.

3.5 Free Vibration Analysis in Complex Description

For homogeneous problems the excitation vector is zero:

$$\begin{Bmatrix}\{g\}\\ \{\bar{g}\}\end{Bmatrix}=\begin{Bmatrix}\{0\}\\ \{0\}\end{Bmatrix} \tag{3.11}$$

The natural mode is assumed to be of the form in Equation (3.12), where the real part of the complex frequency *s* is zero since system damping is not considered in this discussion:

$$p(t)=P_f e^{st}+P_b e^{\bar{s}t}=P_f e^{j\omega t}+P_b e^{-j\omega t} \tag{3.12}$$

This is a very important definition. It makes complex natural mode analysis of the anisotropic rotor possible, thus enabling complete complex analysis of the general rotor system. Indeed, a function of the form shown in Equation (3.12) is the only form that can satisfy the homogeneous complex equation of motion of anisotropic rotors. Notice that Equation (3.12) implies that each natural mode is composed of two sub-modes: one rotating in the positive (forward) direction and the other in the negative (backward) direction.

Substituting Equation (3.12) into Equation (3.10) and grouping e^{st} terms and $e^{\bar{s}t}$ terms results in:

$$[M_c]\begin{Bmatrix} s^2 P_f e^{st} + \bar{s}^2 P_b e^{\bar{s}t} \\ \bar{s}^2 \bar{P}_f e^{\bar{s}t} + s^2 \bar{P}_b e^{st} \end{Bmatrix} + [C_c]\begin{Bmatrix} sP_f e^{st} + \bar{s} P_b e^{\bar{s}t} \\ \bar{s}\bar{P}_f e^{\bar{s}t} + s\bar{P}_b e^{st} \end{Bmatrix} + [K_c]\begin{Bmatrix} P_f e^{st} + P_b e^{\bar{s}t} \\ \bar{P}_f e^{\bar{s}t} + \bar{P}_b e^{st} \end{Bmatrix} = \begin{Bmatrix} \{0\} \\ \{0\} \end{Bmatrix} \tag{3.13}$$

This equation should be closely examined; it is satisfied only if coefficients of e^{st} terms and $e^{\bar{s}t}$ terms are independently zero. Thus, two equations result from Equation (3.13):

$$\left[s^2[M_c] + s[C_c] + [K_c]\right]\begin{Bmatrix} P_f \\ \bar{P}_b \end{Bmatrix} = \begin{Bmatrix} 0 \\ 0 \end{Bmatrix} \tag{3.14}$$

and

$$\left[\bar{s}^2[M_c] + \bar{s}[C_c] + [K_c]\right]\begin{Bmatrix} \bar{P}_f \\ P_b \end{Bmatrix} = \begin{Bmatrix} 0 \\ 0 \end{Bmatrix} \tag{3.15}$$

These equations are not complex conjugates since coefficient matrices are complex. However, it can be shown that they carry the same information, therefore only one of them must be solved.

EXAMPLE: 2 Degree of Freedom Anisotropic Rotor

As an example, consider the undamped gyroscopic motion of a simple anisotropic rotor as derived in Appendix A:

$$\begin{Bmatrix} \ddot{y} \\ \ddot{z} \end{Bmatrix} + \begin{bmatrix} 0 & \Omega_p \\ -\Omega_p & 0 \end{bmatrix}\begin{Bmatrix} \dot{y} \\ \dot{z} \end{Bmatrix} + \begin{bmatrix} 1+\Delta & 0 \\ 0 & 1-\Delta \end{bmatrix}\begin{Bmatrix} y \\ z \end{Bmatrix} = \begin{Bmatrix} 0 \\ 0 \end{Bmatrix} \tag{3.16}$$

where Ω_p is nondimensional rotor speed including the ratio of polar to transverse rotary inertia and Δ is nondimensional anisotropy. It should be noted that a general damping matrix (i.e., the matrix which multiplies the vector of derivatives) can be decomposed into symmetric and skew-symmetric parts. The skew-symmetric matrix does not affect

system stability (i.e., the real parts of the eigenvalues). The symmetric part of the matrix is assumed to be null, leading to purely imaginary eigenvalues as indicated in Equation (3.12).

Equation (3.16) is the simplest rotor equation that includes the gyroscopic effect. The equation represents the anti-symmetric motion of the geometrically symmetric rigid body rotor shown in Figure 3.2. Notice that the coordinate system is a body-fixed non-rotating system which translates with the rotor. The motion is commonly referred to as "pitch".

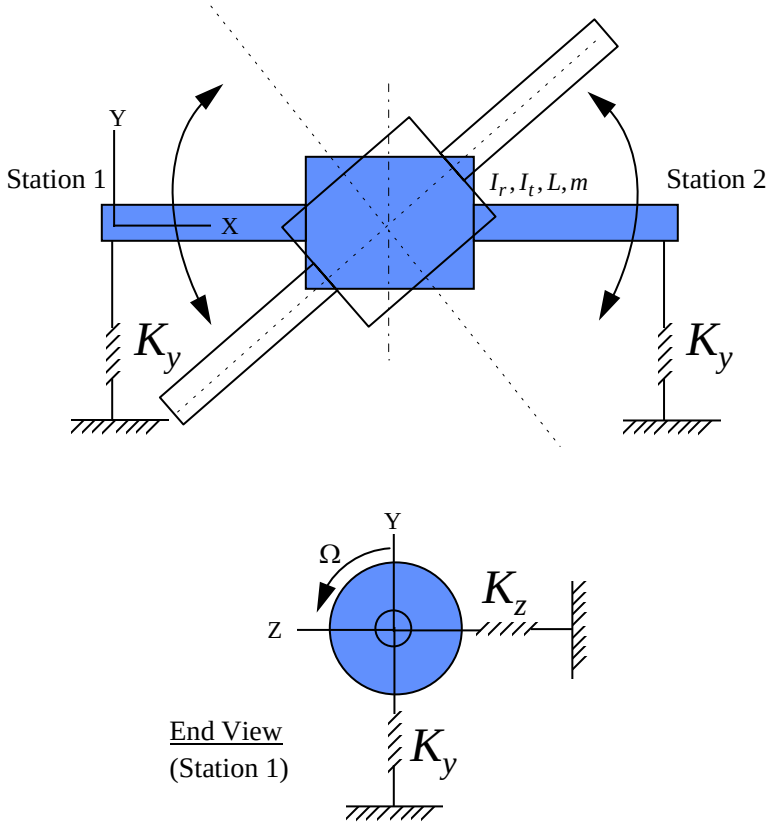

Figure 3.2: Anti-Symmetric Motion of Symmetric Rigid Rotor

The complex version of Equation (3.16) is obtained with the transformation matrix [*T*]:

$$[T]^{-1}[T]\begin{Bmatrix}\ddot{p}\\ \ddot{\bar{p}}\end{Bmatrix}+[T]^{-1}\begin{bmatrix}0 & \Omega_p\\ -\Omega_p & 0\end{bmatrix}[T]\begin{Bmatrix}\dot{p}\\ \dot{\bar{p}}\end{Bmatrix}+[T]^{-1}\begin{bmatrix}1+\Delta & 0\\ 0 & 1-\Delta\end{bmatrix}[T]\begin{Bmatrix}p\\ \bar{p}\end{Bmatrix}=\begin{Bmatrix}0\\ 0\end{Bmatrix} \tag{3.17}$$

It becomes:

$$\begin{Bmatrix}\ddot{p}\\ \ddot{\bar{p}}\end{Bmatrix}+\begin{bmatrix}-j\Omega_p & 0\\ 0 & j\Omega_p\end{bmatrix}\begin{Bmatrix}\dot{p}\\ \dot{\bar{p}}\end{Bmatrix}+\begin{bmatrix}1 & \Delta\\ \Delta & 1\end{bmatrix}\begin{Bmatrix}p\\ \bar{p}\end{Bmatrix}=\begin{Bmatrix}0\\ 0\end{Bmatrix} \tag{3.18}$$

As discussed, the assumed solution form is:

$$p(t)=P_f e^{j\omega t}+P_b e^{-j\omega t} \tag{3.19}$$

Substituting Equation (3.19) into Equation (3.18) results in:

$$\begin{bmatrix}-\omega^2+\omega\Omega_p+1 & \Delta\\ \Delta & -\omega^2-\omega\Omega_p+1\end{bmatrix}\begin{Bmatrix}P_f\\ \bar{P}_b\end{Bmatrix}e^{j\omega t}+\begin{bmatrix}-\omega^2+\omega\Omega_p+1 & \Delta\\ \Delta & -\omega^2-\omega\Omega_p+1\end{bmatrix}\begin{Bmatrix}\bar{P}_f\\ P_b\end{Bmatrix}e^{-j\omega t}=0 \tag{3.20}$$

As one can see, two equations are obtained:

$$\begin{bmatrix}-\omega^2+\omega\Omega_p+1 & \Delta\\ \Delta & -\omega^2-\omega\Omega_p+1\end{bmatrix}\begin{Bmatrix}P_f\\ \bar{P}_b\end{Bmatrix}=\begin{Bmatrix}0\\ 0\end{Bmatrix} \tag{3.21}$$

and

$$\begin{bmatrix}-\omega^2+\omega\Omega_p+1 & \Delta\\ \Delta & -\omega^2-\omega\Omega_p+1\end{bmatrix}\begin{Bmatrix}\bar{P}_f\\ P_b\end{Bmatrix}=\begin{Bmatrix}0\\ 0\end{Bmatrix} \tag{3.22}$$

Because the system is undamped in this case, the coefficient matrix becomes real and the two equations become essentially the same.

The characteristic equation of Equation (3.21) is:

$$\left(1-\omega^2\right)^2-\omega^2\Omega_p^2-\Delta^2=0 \tag{3.23}$$

or:

$$\omega^4-\left(2+\Omega_p^2\right)\omega^2+1-\Delta^2=0 \tag{3.24}$$

The four roots are obtained as natural frequencies:

$$\omega_{1,2,3,4}=\pm\sqrt{\frac{2+\Omega_p^2}{2}\pm\sqrt{\left(\frac{2+\Omega_p^2}{2}\right)^2-1+\Delta^2}} \tag{3.25}$$

From Equation (3.21), natural modes corresponding to the characteristic values are:

$$\begin{Bmatrix}P_f\\P_b\end{Bmatrix}_i=\begin{Bmatrix}P_f\\\overline{P}_b\end{Bmatrix}_i=\begin{Bmatrix}-\dfrac{\Delta}{-\omega_i^2+\omega_i\Omega_p+1}\\1\end{Bmatrix} \tag{3.26}$$

where the modal vectors are real.

Isotropic Case

First consider the isotropic (Δ=0) case. From Equation (3.21):

$$\begin{bmatrix}-\omega^2+\omega\Omega_p+1 & 0\\0 & -\omega^2-\omega\Omega_p+1\end{bmatrix}\begin{Bmatrix}P_f\\\overline{P}_b\end{Bmatrix}=\begin{Bmatrix}0\\0\end{Bmatrix} \tag{3.27}$$

The characteristic equation is:

$$\left(-\omega^2-\omega\Omega_p+1\right)\left(-\omega^2+\omega\Omega_p+1\right)=0 \tag{3.28}$$

From which four characteristic values are found as natural frequencies:

$$\omega_{1,2} = -\frac{\Omega_p}{2} \pm \sqrt{\left(\frac{\Omega_p}{2}\right)^2 + 1} \tag{3.29}$$

and

$$\omega_{3,4} = \frac{\Omega_p}{2} \pm \sqrt{\left(\frac{\Omega_p}{2}\right)^2 + 1} \tag{3.30}$$

Natural modes can be obtained by evaluating Equation (3.27) at these frequencies.

For $\omega_{1,2}$:

$$\begin{matrix} \left(-\omega_i^2 + \omega_i \Omega_p + 1 \neq 0\right) P_f + 0\overline{P}_b = 0 \\ 0P_f + \left(-\omega_i^2 - \omega_i \Omega_p + 1 = 0\right)\overline{P}_b = 0 \end{matrix} ; i = 1,2 \tag{3.31}$$

so that the modal vector is of the form:

$$\begin{Bmatrix} P_f \\ \overline{P}_b \end{Bmatrix}_{1,2} = \begin{Bmatrix} P_f \\ P_b \end{Bmatrix}_{1,2} = \begin{Bmatrix} 0 \\ 1 \end{Bmatrix} \tag{3.32}$$

and the corresponding homogeneous solutions from Equation (3.19) are:

$$\begin{matrix} p_1(t) = 1e^{-j\omega_1 t} \ ; \ \omega_1 > 0 \\ p_2(t) = 1e^{-j\omega_2 t} \ ; \ \omega_2 < 0 \end{matrix} \tag{3.33}$$

Natural modes corresponding to $\omega_{3,4}$ are found from:

$$0P_f + \left(-\omega_i^2 - \omega_i \Omega_p + 1 \neq 0\right)\overline{P}_b = 0 \ ; \ \mathrm{i} = 3,4 \tag{3.34}$$

and are of the form:

$$\left\{\begin{matrix} P_f \\ \overline{P}_b \end{matrix}\right\}_{3,4} = \left\{\begin{matrix} P_f \\ P_b \end{matrix}\right\}_{3,4} = \left\{\begin{matrix} 1 \\ 0 \end{matrix}\right\} \tag{3.35}$$

Corresponding homogeneous solutions are:

$$\begin{aligned} p_3(t) &= 1e^{j\omega_3 t} \;;\; \omega_3 > 0 \;;\; |\omega_3| = |\omega_2| \\ p_4(t) &= 1e^{j\omega_4 t} \;;\; \omega_4 < 0 \;;\; |\omega_4| = |\omega_1| \end{aligned} \tag{3.36}$$

Physically, solutions $p_1(t)$and $p_4(t)$ represent a mode which is characterized by backward conical whirl as shown in Figure 3.3:

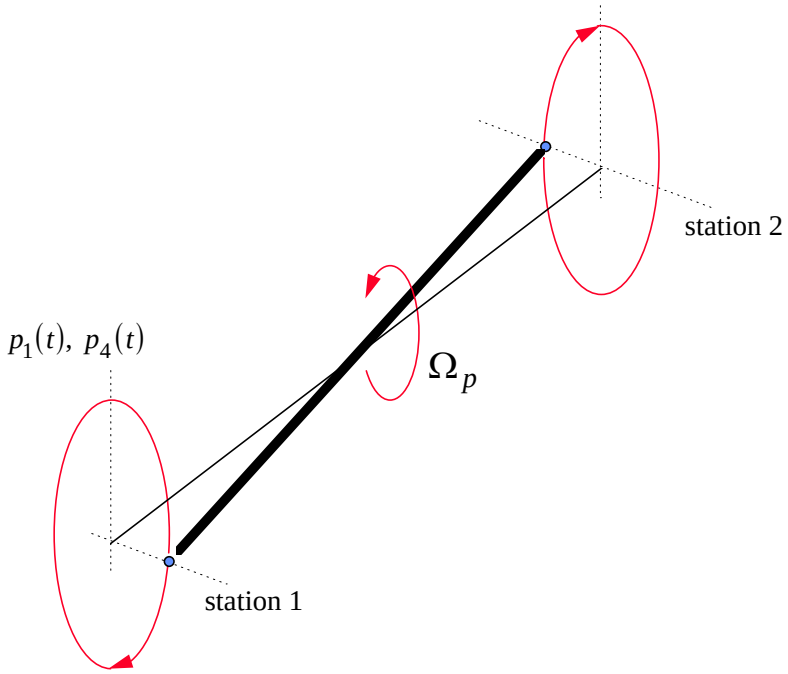

Figure 3.3: Backward Conical Whirl Mode

Solutions $p_2(t)$ and $p_3(t)$ represent a mode characterized by forward conical whirl as shown in Figure 3.4.

Natural frequencies $\omega_{1,2,3,4}$ in Equations (3.29) and (3.30) are plotted as functions

of the nondimensional rotor speed in Figure 3.5. If one considers the sign of natural frequencies together with the implied direction of the natural modes as defined in Equation (3.19), one can visualize the actual rotating shape of the mode as depicted in the

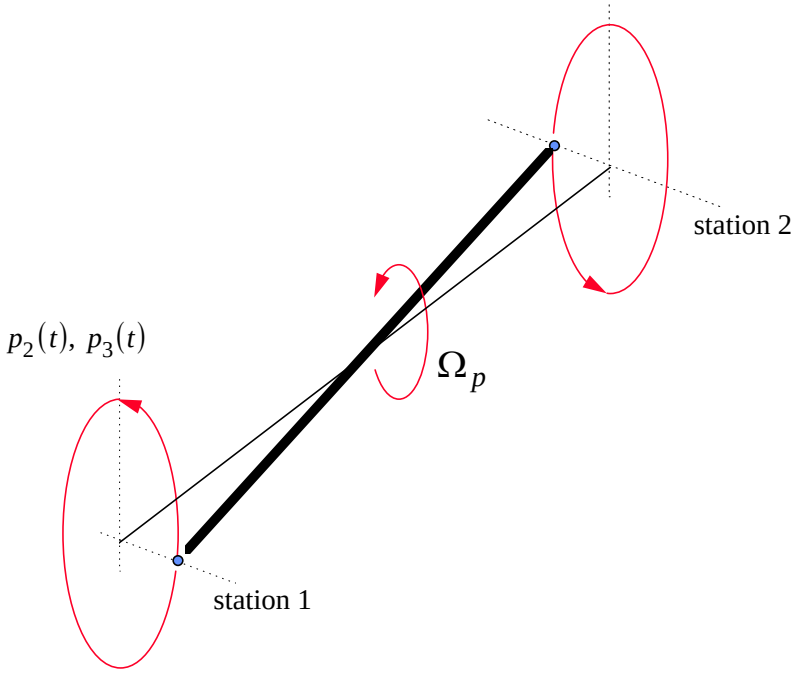

Figure 3.4: Forward Conical Whirl Mode

figure, where the direction of the mode is shown as viewed from station 1.

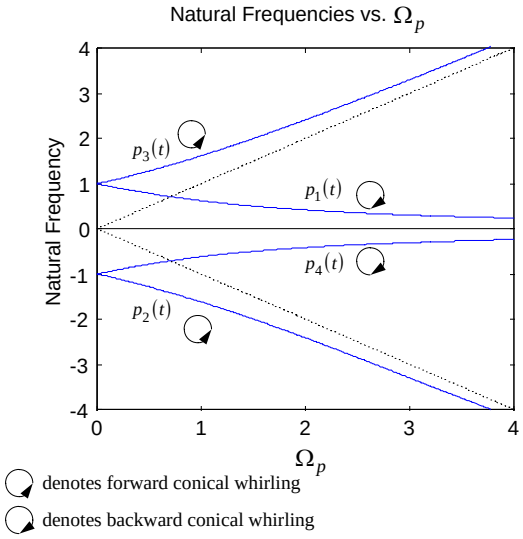

Figure 3.5: Homogeneous Solutions vs. Nondimensional Rotor Speed (Δ=0)

From the figure, one realizes that $p_2(t)$ and $p_3(t)$ represent the same mode, as do $p_1(t)$ and $p_4(t)$. Therefore, there are only two unique natural modes of the isotropic rotor.

Allowing the algebraic sign of the frequency to denote direction (i.e., letting $+\omega$ represent the forward mode and $-\omega$ the backward mode), the natural modes are represented by two curves as shown in Figure 3.6. Presenting the solutions in this way exploits the ability of the complex representation to indicate direction as well as frequency.

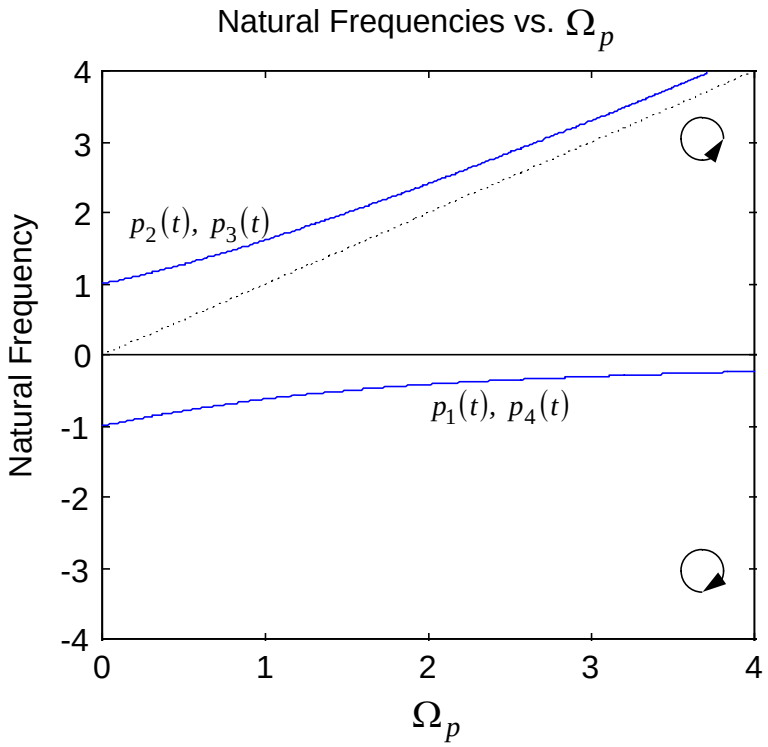

Figure 3.6: Two Natural Modes of Isotropic Rotor (Δ=0)

From Figure 3.6 it is clear that there are two independent modes, one forward and one backward.

Rotating mass imbalance is an excitation source which is purely in the forward

direction. A critical speed is generally defined to be a rotating speed at which the magnitude of the response to mass imbalance is a local maximum. It is known[8] that there will be no synchronous (1-x excitation) critical speed associated with the pitch (conical) mode for values of the inertia ratio $\alpha \geq 1$, where $\alpha = I_{\text{polar}} / I_{\text{transverse}}$. The normalization used in the model includes this ratio in the nondimensional rotor speed, so that lines in the Campbell diagram of Figure 3.7 are based upon both rotor speed and inertia ratio. The synchronous $\alpha=1$ line is shown as a reference. As the rotor geometry approaches a thin disk $\alpha \to 2$, and as the rotor becomes a long narrow stick $\alpha \to 0$. The effect of these geometric changes is a rotation of this reference line as Figure 3.7 shows:

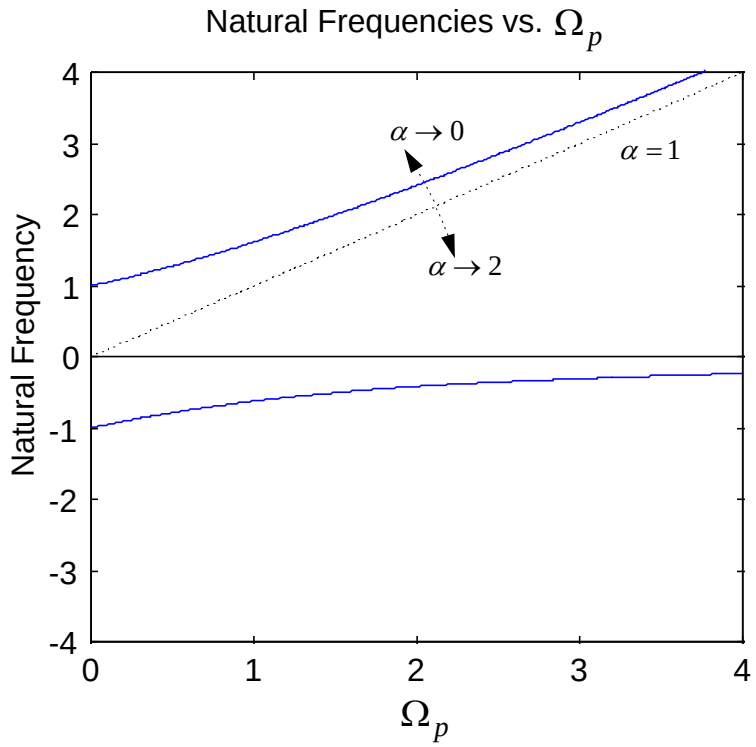

Figure 3.7: Nondimensional Campbell Diagram of the Isotropic Rotor (Δ=0)

The value $\alpha=1$ is a geometric threshold above which a synchronous critical speed of the

conical mode will not be observed.

For the $\alpha=1$ rotor, an intersection of twice-synchronous (2-x) excitation with the curve on the positive frequency side (i.e., the curve defining the forward mode natural frequency) indicates a forward mode critical speed, as may exist due to gravity excitation of an orthotropic rotor[23] or other 2-x supersynchronous excitation.

Figure 3.7 can be generalized to consider asynchronous (i.e., an arbitrary real multiple of rotor speed) excitation. The parameter determining whether a critical speed of the conical mode will be observed for an excitation of the form:

$$g(t) = G_f e^{jn\Omega t} \tag{3.37}$$

is the product $n\alpha$, where n can have positive or negative values. Figure 3.8 illustrates the concept for three positive values of this product, which indicate forward mode critical speeds. Corresponding lines could be drawn on the negative frequency side to indicate backward mode critical speeds.

Anisotropic Case

Now consider the anisotropic case ($\Delta \neq 0$). There are four natural frequencies defined by Equation (3.25):

$$\omega_1 = \sqrt{\frac{2+\Omega_p^2}{2} + \sqrt{\left(\frac{2+\Omega_p^2}{2}\right)^2 - 1 + \Delta^2}} = -\omega_2 \tag{3.38}$$

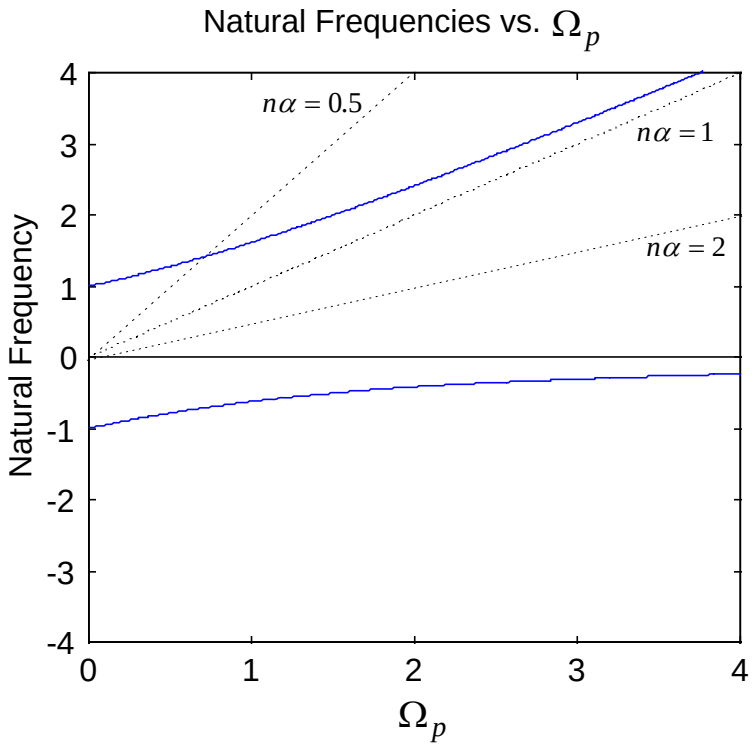

Figure 3.8: Nondimensional Campbell Diagram of the Isotropic Rotor (Δ=0)

and

$$\omega_3 = \sqrt{\frac{2+\Omega_p^2}{2} - \sqrt{\left(\frac{2+\Omega_p^2}{2}\right)^2 - 1 + \Delta^2}} = -\omega_4 \tag{3.39}$$

The natural mode is found for each characteristic value from Equation (3.21):

$$\begin{Bmatrix} P_f \\ P_b \end{Bmatrix}_i = \begin{Bmatrix} 1 \\ \dfrac{\Delta}{\omega_i^2 + \omega_i \Omega_p - 1} \end{Bmatrix} \tag{3.40}$$

Consider the case $\Delta=0.1$, $\Omega_p=0.9$ as a numerical example. The natural frequencies are:

$$\begin{aligned} \omega_1 &= 1.5482 = -\omega_2 \\ \omega_3 &= 0.6427 = -\omega_4 \end{aligned} \tag{3.41}$$

Natural modes for $\omega_{1,2}$ are:

$$\begin{Bmatrix} P_f \\ P_b \end{Bmatrix}_1 = \begin{Bmatrix} 1 \\ 0.0354 \end{Bmatrix} \Rightarrow p_1(t) = 1e^{1.5482\,jt} + 0.0354e^{-1.5482\,jt} \tag{3.42}$$

and

$$\begin{Bmatrix} P_f \\ P_b \end{Bmatrix}_2 = \begin{Bmatrix} 0.0354 \\ 1 \end{Bmatrix} \Rightarrow p_2(t) = 0.0354e^{-1.5482\,jt} + 1e^{1.5482\,jt} \tag{3.43}$$

so that $p_1(t)$ and $p_2(t)$ represent the same mode which is characterized by a forward elliptical whirl orbit. Natural modes for $\omega_{3,4}$ are:

$$\begin{Bmatrix} P_f \\ P_b \end{Bmatrix}_3 = \begin{Bmatrix} -0.0858 \\ 1 \end{Bmatrix} \Rightarrow p_3(t) = -0.0858e^{0.6427\,jt} + 1e^{-0.6427\,jt} \tag{3.44}$$

$$\begin{Bmatrix} P_f \\ P_b \end{Bmatrix}_4 = \begin{Bmatrix} 1 \\ -0.0858 \end{Bmatrix} \Rightarrow p_4(t) = 1e^{-0.6427\,jt} - 0.0858e^{0.6427\,jt} \tag{3.45}$$

Solutions $p_3(t)$ and $p_4(t)$ represent the same mode which is characterized by a backward elliptical whirl orbit.

One pair of natural frequencies which have the same magnitude but opposite signs are necessary to completely define one natural mode as seen in the expressions in Equation sets (3.42),(3.43) and (3.44),(3.45). Notice that the strengths of the two opposite rotating components are markedly different.

Figure 3.9 shows the natural frequencies as functions of the nondimensional rotor speed:

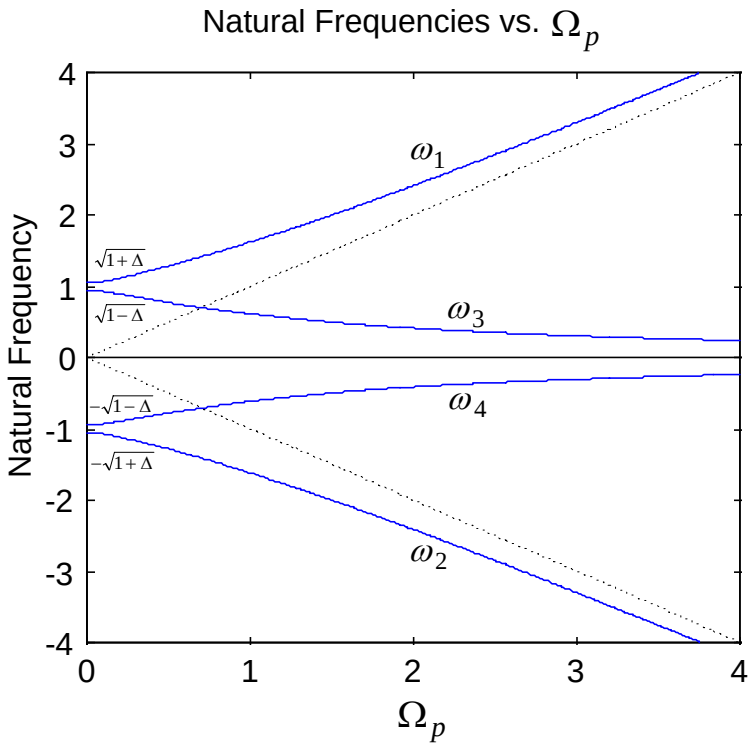

Figure 3.9: Nondimensional Campbell Diagram ($\Delta \neq 0$)

Figure 3.9 does not accurately depict the physical situation and may lead to confusion; in particular, the fact that the sub-modes are of very different strengths is not shown. Figure 3.10 includes this information (it is assumed that $\alpha=1$). The intersection shown as Point **a** in Figure 3.10 illustrates that a 1-x critical speed exists for the anisotropic rotor; however, this intersection is with the weak sub-mode component of the backward mode. At the frequency Ω_{pa} the response of the system to mass imbalance excitation will take the form of the modal vector. I.e.,

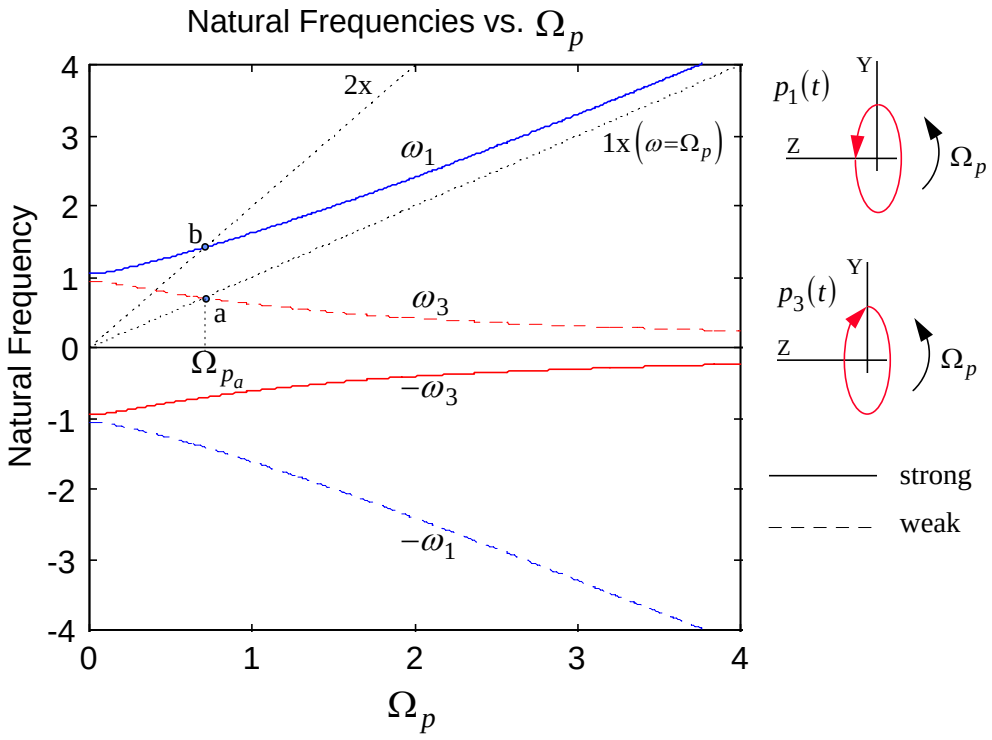

Figure 3.10: Homogeneous Physical Solutions vs. Nondimensional Rotor Speed (Δ≠0)

$$p_3(t) = \beta\left(\varepsilon_3 e^{j|\omega_3|t} + 1e^{-j|\omega_3|t}\right) \tag{3.46}$$

where $$\varepsilon_3 = \frac{\Delta}{\omega_3^2 + \omega_3\Omega_p - 1} << 1 \tag{3.47}$$

and in an actual system the the scale factor β is determined by the level of excitation and damping. Since the synchronous frequency line intersects the weak sub-mode curve, the critical speed response is not expected to be as large as the forward critical speed case.

Point **b** represents an intersection between the strong sub-mode component of the forward mode and the 2-x line. If a significant 2-x excitation were present a relatively

severe critical response would be expected at this point.

3.6 Results / Conclusions

Basic theory for free vibration analysis of general anisotropic rotor systems by the complex description has been presented. Interpretation of the complex representation of planar motion, formulation of the equation of motion, solution of the free vibration equation, natural frequencies and complex natural modes were explained. Most importantly, it was proposed that complex natural modes should be expressed using two sub-components: a forward rotating component and a backward rotating component. It was shown that assuming such a form is the only way to satisfy the complex free vibration equation. The resulting complex mode description carries not only the frequency and amplitude information but also the direction of the motion.

One benefit of the concept of complex modes is the clear definition of forward and backward modes made possible by the physical interpretation of the homogeneous solution, the complex modal vector and natural frequency. Using an anisotropic rotor system as an example, it was shown that the forward (backward) mode can be defined as the mode whose forward (backward) sub-mode is stronger than its backward (forward) sub-mode. Physically the forward (backward) mode represents an elliptic whirl motion rotating forward (backward).

The definition of complex modes and the complex formulation method proposed in this work enable all existing techniques and procedures in classical modal analysis theory to be utilized for rotor analysis. For example, experimental analysis for mode identification and forced vibration analysis by the modal superposition theory can be

implemented in the complex description for general rotor systems exactly the same way as it has been done in the real analysis of non-rotating structures.

CHAPTER 4: COMPLEX ANALYSIS OF ROTOR FORCED VIBRATION

4.1 Chapter Abstract

An approach to complex modal analysis of rotating systems is described which results in improved physical understanding of eigensolutions and stresses commonality with conventional modal analysis. In the approach, a natural mode of the rotor is represented as the sum of two sub-modes which are rotating to the forward and backward directions. This definition of the natural mode leads to some interesting insights into the procedure of the complex analysis of free and forced vibration problems of rotating systems, and interesting results. It is shown that the proposed method is the generalized version of classical modal analysis. For clarity, concepts are illustrated with simulated results of a general rigid rotor and a two degree of freedom anisotropic rotor model with gyroscopic effects.

4.2 Introduction

The purpose of this chapter is to present a complex modal analysis method for general rotor systems, where “complex” refers to a complex variable representation of system excitation and response. Complex modal analysis is a very powerful tool to aid in understanding the dynamic behavior of rotor systems because it implicitly incorporates rotation and directionality.

Ehrich[2] and Lee[8] have discussed the representation of general elliptical motion by complex variables representing forward and backward rotating components. Laws [7] has recently discussed applying this interpretation in the diagnostics of rotating machinery.

Lee, et. al., [9-16] have developed, verified, and applied complex modal analysis and testing theories, the derivation of which is based upon a transformation of the real frequency response matrix. The transformed matrix thus relates complex signals.

This work complements that of Lee, et. al., by presenting a complex modal analysis approach based upon relations between the rotating components of complex excitation and response signals as opposed to the complex signals themselves. The development follows a classical vibration approach and stresses physical interpretations.

4.3 Complex Description of Natural Modes of Rotating Systems

As shown in Chapter 3, a two-dimensional vector can be represented by a single complex variable as shown in Figure 4.1, where real and imaginary parts represent vector components in two orthogonal directions.

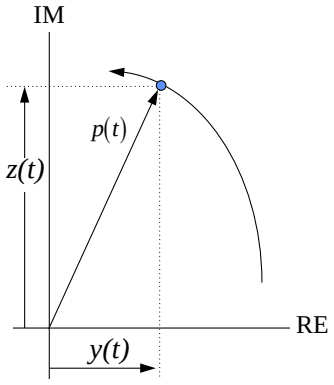

Figure 4.4: Planar Motion of Point P

The position of the point *P* along an arbitrary path in the *YZ* plane at any time *t* is identified by the complex variable *p(t)*:

$$p(t) = y(t) + jz(t) \tag{4.1}$$

The transformation between the real and complex representations is:

$$\begin{Bmatrix} y(t) \\ z(t) \end{Bmatrix} = \frac{1}{2}\begin{bmatrix} 1 & 1 \\ -j & j \end{bmatrix}\begin{Bmatrix} p(t) \\ \overline{p}(t) \end{Bmatrix} \tag{4.2}$$

where $\overline{p}(t)$ is the complex conjugate of *p(t)*. Expanding *y(t)* and *z(t)* by their complex Fourier series results in:

$$\begin{aligned} p(t) &= y(t) + jz(t) \\ &= \sum_{k=0}^{\infty}\left\{\left(Y_k e^{j\omega_k t} + \overline{Y}_k e^{-j\omega_k t}\right) + j\left(Z_k e^{j\omega_k t} + \overline{Z}_k e^{-j\omega_k t}\right)\right\} \\ &= \sum_{k=0}^{\infty}\left\{\left(Y_k + jZ_k\right)e^{j\omega_k t} + \left(\overline{Y}_k + j\overline{Z}_k\right)e^{-j\omega_k t}\right\} \\ &= \sum_{k=0}^{\infty}\left\{P_{f_k} e^{+j\omega_k t} + P_{b_k} e^{-j\omega_k t}\right\} \end{aligned} \tag{4.3}$$

Equation (4.3) indicates that each harmonic component representing any arbitrary planar motion can be considered to be composed of one forward rotating component and one backward rotating component. Two important observations that evoked the main ideas in this chapter are emphasized here:

- With the complex description, now $e^{j\omega t}$ is not just a complex variable but is a vector which is actually rotating in the physical two dimensional space. A linear harmonic motion in non-rotating vibration analysis is a special case whose forward and backward rotating components have the same amplitudes.
- The form in Equation (4.3) suggests that natural modes of rotors also may be described as a combination of two sub-modes; one rotating forward and the other rotating backward.

4.4 Formulation of Eigenvalue Problem

The equation of motion of a linear rotor system of *n*-stations is represented by:

$$[M]\begin{Bmatrix}\{\ddot{y}\}\\{\ddot{z}\}\end{Bmatrix}+[C]\begin{Bmatrix}\{\dot{y}\}\\{\dot{z}\}\end{Bmatrix}+[K]\begin{Bmatrix}\{y\}\\{z\}\end{Bmatrix}=\begin{Bmatrix}\{f_Y\}\\{f_Z\}\end{Bmatrix} \tag{4.4}$$

where *{{y},{z}}* is a *2n* by *1* vector representing the planar motion of the center of the shaft at *n* stations. Coefficient matrices depend on the rotating speed.

The relationship between the real and complex displacement variables in Equation (4.2) can be generalized by the following transformation:

$$\begin{Bmatrix}\{y\}\\{z\}\end{Bmatrix}=[T]\begin{Bmatrix}\{p\}\\{\overline{p}\}\end{Bmatrix} \tag{4.5}$$

where,

$$[T]=\frac{1}{2}\begin{bmatrix} I(n) & I(n)\\ -jI(n) & jI(n)\end{bmatrix} \tag{4.6}$$

and *I(n)* denotes the identity matrix of size *n*. The complex formulation of the governing equations results from substituting Equation (4.5) into Equation (4.4) and pre-multiplying by $[T]^{-1}$:

$$[T]^{-1}[M][T]\begin{Bmatrix}\{\ddot{p}\}\\{\ddot{\overline{p}}\}\end{Bmatrix}+[T]^{-1}[C][T]\begin{Bmatrix}\{\dot{p}\}\\{\dot{\overline{p}}\}\end{Bmatrix}+[T]^{-1}[K][T]\begin{Bmatrix}\{p\}\\{\overline{p}\}\end{Bmatrix}=\begin{Bmatrix}\{g\}\\{\overline{g}\}\end{Bmatrix} \tag{4.7}$$

Premultiplication by $[T]^{-1}$ transforms the real representation of the excitation vector to the complex representation. For free vibration analysis, the complex force vector $\{\{g\},\{\overline{g}\}\}$ of Equation (4.7) is zero. Equation (4.7) is shortened:

$$[M_c]\begin{Bmatrix}\{\ddot{p}\}\\{\ddot{\overline{p}}\}\end{Bmatrix}+[C_c]\begin{Bmatrix}\{\dot{p}\}\\{\dot{\overline{p}}\}\end{Bmatrix}+[K_c]\begin{Bmatrix}\{p\}\\{\overline{p}\}\end{Bmatrix}=\begin{Bmatrix}\{0\}\\{0\}\end{Bmatrix} \tag{4.8}$$

where the subscript *c* in the transformed matrices M_c, C_c, and K_c of Equation (4.8) emphasizes that the matrices are complex. From previous discussion it is very natural to

assume the natural mode for the undamped system (i.e., neglecting the symmetric portion of the matrix *C* of Equation (4.4)) is of the form:

$$p(t) = P_f e^{j\omega t} + P_b e^{-j\omega t} \tag{4.9}$$

or, with $s = j\omega$:

$$p(t) = P_f e^{st} + P_b e^{\bar{s}t} \tag{4.10}$$

where *p(t)*, P_f, and P_b are each vectors of length *n*. Substitution results in:

$$[M_c]\begin{Bmatrix} s^2 P_f e^{st} + \bar{s}^2 P_b e^{\bar{s}t} \\ \bar{s}^2 \overline{P}_f e^{\bar{s}t} + s^2 \overline{P}_b e^{st} \end{Bmatrix} + [C_c]\begin{Bmatrix} sP_f e^{st} + \bar{s} P_b e^{\bar{s}t} \\ \bar{s}\overline{P}_f e^{\bar{s}t} + s\overline{P}_b e^{st} \end{Bmatrix} + [K_c]\begin{Bmatrix} P_f e^{st} + P_b e^{\bar{s}t} \\ \overline{P}_f e^{\bar{s}t} + \overline{P}_b e^{st} \end{Bmatrix} = \begin{Bmatrix} \{0\} \\ \{0\} \end{Bmatrix} \tag{4.11}$$

Equation (4.11) is satisfied if and only if e^{st} terms and $e^{\bar{s}t}$ terms become zero respectively, which results in two characteristic equations:

$$\left[s^2[M_c] + s[C_c] + [K_c]\right]\begin{Bmatrix} P_f \\ \overline{P}_b \end{Bmatrix} = \begin{Bmatrix} 0 \\ 0 \end{Bmatrix} \tag{4.12}$$

and

$$\left[\bar{s}^2[M_c] + \bar{s}[C_c] + [K_c]\right]\begin{Bmatrix} \overline{P}_f \\ P_b \end{Bmatrix} = \begin{Bmatrix} 0 \\ 0 \end{Bmatrix} \tag{4.13}$$

Natural mode solutions obtained from the two equations represent the same physical information. Notice that Equations (4.12) and (4.13) are not conjugate forms of each other.

One can formulate the problem as a generalized eigenvalue problem in state space:

$$\begin{bmatrix} [0] & [M_c] \\ [M_c] & [C_c] \end{bmatrix}\begin{Bmatrix} \begin{Bmatrix} \{\ddot{p}\} \\ \{\dddot{p}\} \end{Bmatrix} \\ \begin{Bmatrix} \{\dot{p}\} \\ \{\ddot{p}\} \end{Bmatrix} \end{Bmatrix} = \begin{bmatrix} [M_c] & [0] \\ [0] & -[K_c] \end{bmatrix}\begin{Bmatrix} \begin{Bmatrix} \{\dot{p}\} \\ \{\ddot{p}\} \end{Bmatrix} \\ \begin{Bmatrix} \{p\} \\ \{\overline{p}\} \end{Bmatrix} \end{Bmatrix} + \begin{Bmatrix} \begin{Bmatrix} \{0\} \\ \{0\} \end{Bmatrix} \\ \begin{Bmatrix} \{0\} \\ \{0\} \end{Bmatrix} \end{Bmatrix} \tag{4.14}$$

Substitution and retaining the problem in *s* results in:

$$\left[s\begin{bmatrix} [0] & [M_c] \\ [M_c] & C_c \end{bmatrix} - \begin{bmatrix} [M_c] & [0] \\ [0] & -[K_c] \end{bmatrix} \right] \begin{Bmatrix} s\begin{Bmatrix} P_f \\ \overline{P}_b \end{Bmatrix} \\ \begin{Bmatrix} P_f \\ \overline{P}_b \end{Bmatrix} \end{Bmatrix} = \{0\} \tag{4.15}$$

which is recognized as the generalized eigenvalue problem of the form:

$$[s[A] - [B]]\{X\} = \{0\} \tag{4.16}$$

The lower half of the eigenvector contains the modal vector which together with the eigenvalue λ_i, i.e. that value of *s* resulting in a zero determinate of $[s[A] - [B]]$, describes the natural modes.

4.5 Interpretation of Eigensolutions by Example

Consider a rigid rotor on soft flexible supports. Motion is completely described by translations at each of two stations. Governing equations, geometric definitions, and specific parameters are given in Appendix A.

Eigensolutions of the rigid rotor are described by the eigenvalue λ_i and the corresponding modal vector of the form*:*

$$\begin{Bmatrix} P_{f1} \\ P_{f2} \\ \overline{P}_{b1} \\ \overline{P}_{b2} \end{Bmatrix}_i \tag{4.17}$$

where element P_{f1} is the relative amplitude and phase of the forward rotating sub-mode at station 1, P_{f2} is the amplitude and phase of the forward rotating sub-mode at station 2, $\overline{P}_{b1}$ is the complex conjugate of the amplitude and phase of the backward rotating sub-mode at station 1, and $\overline{P}_{b2}$ is the complex conjugate of the amplitude and phase of the

backward rotating sub-mode at station 2. Here, the forward (backward) direction is defined as the same (opposite) direction as the rotor spin.

Eigensolutions of the isotropic rigid rotor are:

	Backward Bounce	Forward Bounce	Backward Pitch	Forward Pitch
λ (rad/sec)	-.47+123.2j	-.47+123.2j	-5.7+416.8j	-6.2+456.9j
P_{f1}	0	1	0	1
P_{f2}	0	1	0	-1
$\overline{P}_{b1}$	1	0	1	0
$\overline{P}_{b2}$	1	0	-1	0

Table 4.1: Isotropic Rigid Rotor Eigensolutions

The modes in Table 4.1 are illustrated in Figure 4.2:

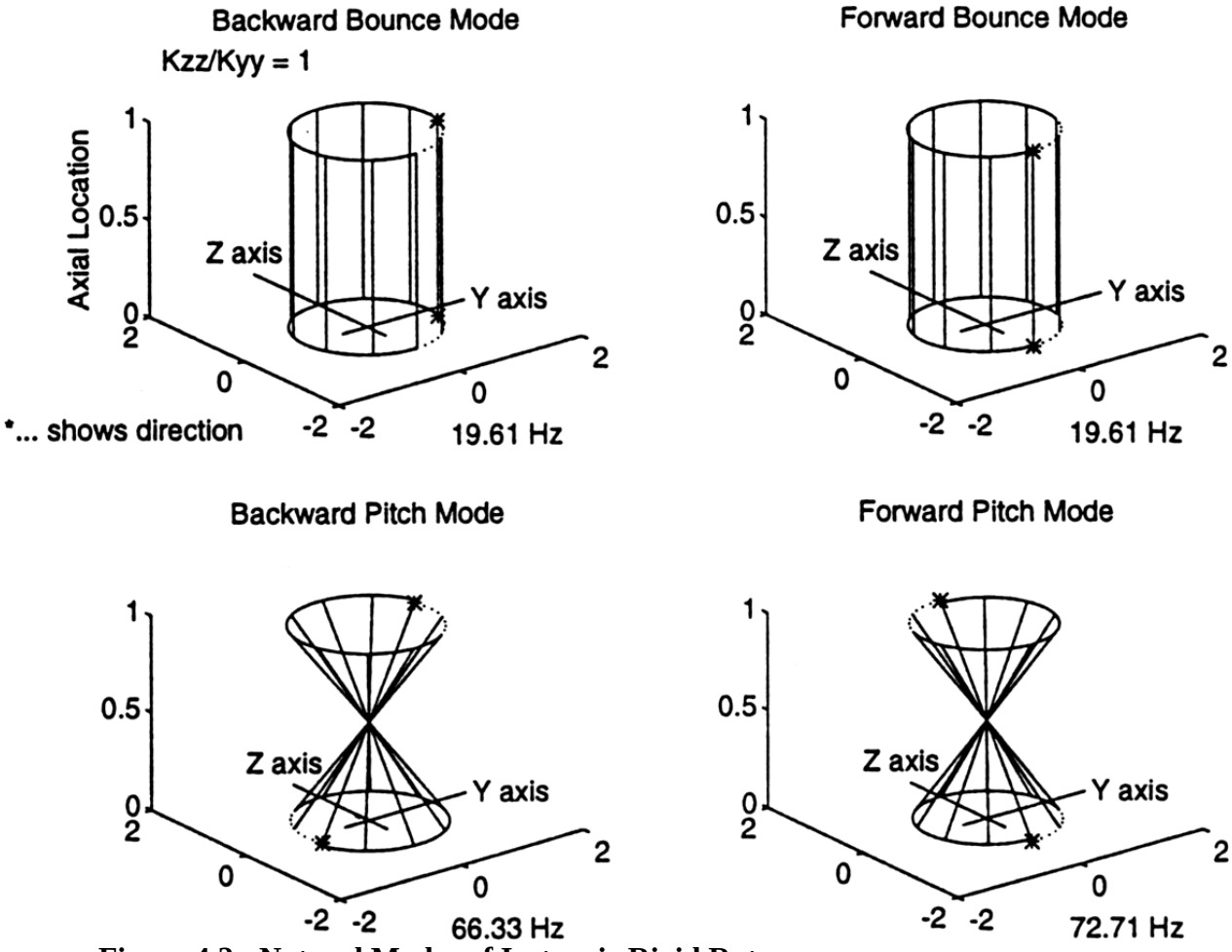

Figure 4.2: Natural Modes of Isotropic Rigid Rotor

When supports are anisotropic ($K_{YYi} \neq K_{ZZi}; i = 1,2$), the eigensolutions become:

	Backward Bounce	Forward Bounce	Backward Pitch	Forward Pitch
λ (rad/sec)	-.47+116.9j	-.47+123.2j	-5.7+402.7j	-6.2+448.6j
P_{f1}	1	1	-.27+.0033j	1
P_{f2}	1	1	.27-.0033j	- 1
$\overline{P}_{b1}$	-1	1	1	.25-.003j
$\overline{P}_{b2}$	-1	1	-1	-.25+.003j

Table 4.2: Anisotropic Rigid Rotor Eigensolutions

It is considered necessary to define *forward modes* and *backward modes* as defined herein. The forward mode is defined as the mode whose forward direction sub-mode has larger amplitude than the backward direction sub-mode. The backward mode is defined accordingly. The mode shapes in Table 4.2 are illustrated in Figure 4.3:

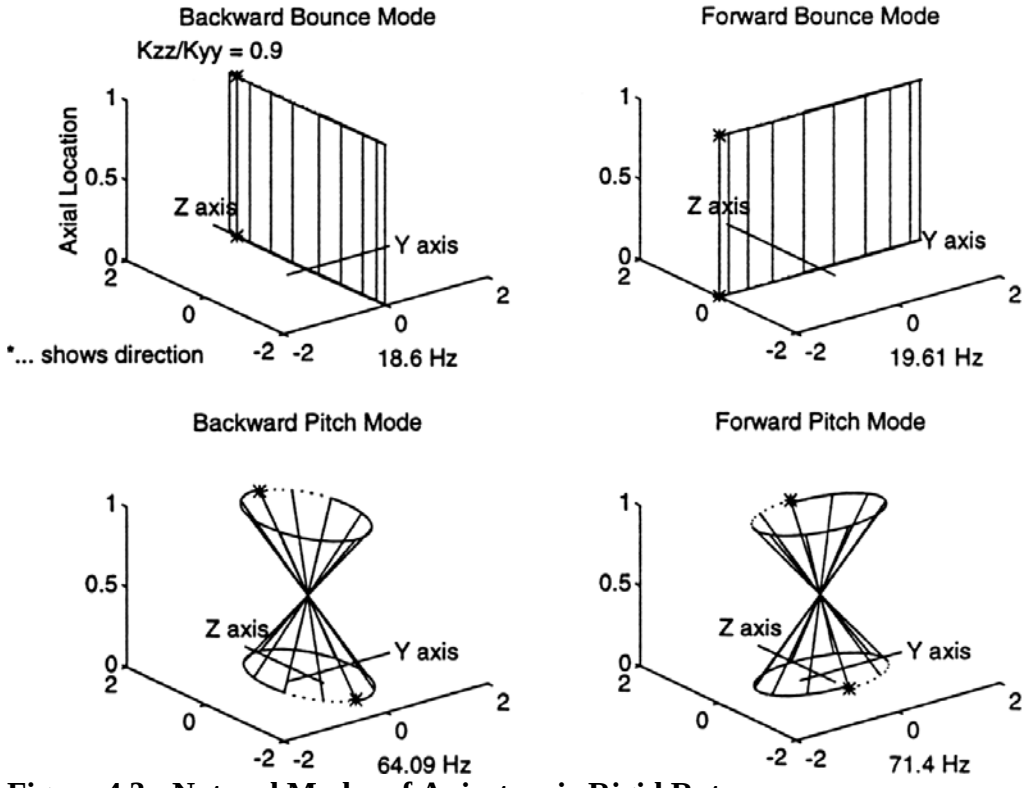

Figure 4.3: Natural Modes of Anisotropic Rigid Rotor

In this case, the natural solution for the bounce modes is motion along a line. The real

description would result in uncoupled *Y*-direction and *Z*-direction modes. The same physical solution is found with complex analysis.

Geometric simplifications as described in Appendix A for the symmetric rotor pitch mode result in the reduced set of equations:

$$\begin{Bmatrix} \ddot{p} \\ \ddot{\bar{p}} \end{Bmatrix} + \begin{bmatrix} -j\Omega_p & 0 \\ 0 & j\Omega_p \end{bmatrix} \begin{Bmatrix} \dot{p} \\ \dot{\bar{p}} \end{Bmatrix} + \begin{bmatrix} 1 & \Delta \\ \Delta & 1 \end{bmatrix} \begin{Bmatrix} p \\ \bar{p} \end{Bmatrix} = \begin{Bmatrix} 0 \\ 0 \end{Bmatrix} \tag{4.18}$$

Natural frequencies and modes are obtained by assuming that:

$$p(t) = P_f e^{st} + P_b e^{\bar{s}t} \tag{4.19}$$

Figure 4.4 illustrates the form of the modal vector as a function of the anisotropic parameter Δ for the value of $\Omega_p = 0.1$. Shown are the ratio $\left| \bar{P}_b / P_f \right|$ for the forward mode and $\left| P_f / \bar{P}_b \right|$ for the backward mode:

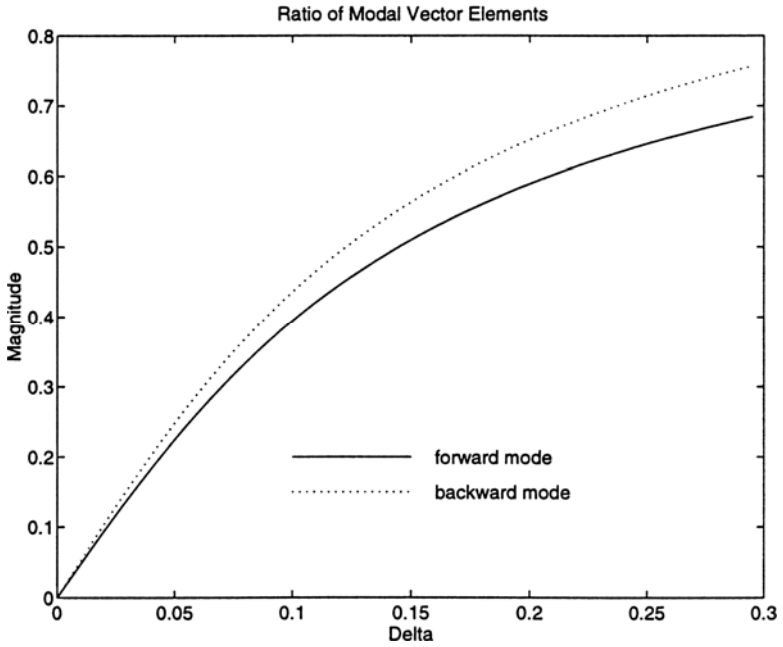

Figure 4.4: Mode Shapes of Symmetric Rigid Rotor Pitch Modes as Function of Δ

The figure indicates that as the system becomes isotropic the forward mode becomes purely forward (no backward sub-mode component) and the backward mode purely backward. Since all four eigenvalues will be obtained in real analysis without the concept of the sub-modes and their strengths, this will be viewed as the number of natural frequencies of a system with infinitesimal anisotropy which is twice as many as those of its isotropic version. This situation was discussed as a paradox by Lee[11].

4.6 Discussion

Physical interpretation of eigensolutions follows from the assumed solution form. Elements of the modal vector indicate the relative magnitude of forward and backward rotating components of the natural response at each station. Directivity of the mode is immediately apparent from noting which terms of the modal vector are of dominant magnitude. For the isotropic system one of these terms becomes zero. Not considering rotational degrees of freedom, the *n*-station rotor has *2n* modes whether the system is isotropic or anisotropic.

The rigid rotor has two stations so it has two sets of modes. Bounce modes are lower in frequency and characterized by motion in which the rotor revolves around the bearing axis with stations 1 and 2 in phase. Pitch modes, which separate in frequency with shaft speed due to gyroscopic coupling, are characterized by similar motion with stations 1 and 2 out of phase.

4.7 dFRFs Obtained by Forced Response Analysis Using Mode Superposition Method

Limiting discussion to harmonic excitations, the complex excitation *g(t)* acting on the *n*-station rotor is represented as:

$$\begin{aligned} g(t) &= f_Y(t) + jf_Z(t) \\ &= \left(F_Y e^{j\omega t} + \overline{F}_Y e^{-j\omega t}\right) + j\left(F_Z e^{j\omega t} + \overline{F}_Z e^{-j\omega t}\right) \\ &= G_f e^{j\omega t} + G_b e^{-j\omega t} \end{aligned} \tag{4.20}$$

where $g(t)$, G_f, and G_b are each vectors of length n. The response will be:

$$p(t) = P_f e^{j\omega t} + P_b e^{-j\omega t} \tag{4.21}$$

Substituting Equations (4.20) and (4.21) into Equation (4.8) leads to:

$$\left[-\omega^2[M_c] + j\omega[C_c] + [K_c]\right]\begin{Bmatrix} P_f \\ \overline{P}_b \end{Bmatrix} = [B(\omega)]\begin{Bmatrix} P_f \\ \overline{P}_b \end{Bmatrix} = \begin{Bmatrix} G_f \\ \overline{G}_b \end{Bmatrix} \tag{4.22}$$

or,

$$\begin{Bmatrix} P_f \\ \overline{P}_b \end{Bmatrix} = [B(\omega)]^{-1}\begin{Bmatrix} G_f \\ \overline{G}_b \end{Bmatrix} = [H(\omega)]\begin{Bmatrix} G_f \\ \overline{G}_b \end{Bmatrix} = \begin{bmatrix} H_{gp}(\omega) & H_{\hat{g}p}(\omega) \\ H_{g\hat{p}}(\omega) & H_{\hat{g}\hat{p}}(\omega) \end{bmatrix}\begin{Bmatrix} G_f \\ \overline{G}_b \end{Bmatrix} \tag{4.23}$$

The matrix *H* is called the directional frequency response matrix (dFRM) and its elements, *n*x*n* partitions in general which relate the forward and backward rotating components of excitation and response, are the dFRFs. Functions H_{gp} and $H_{\hat{g}\hat{p}}$ are called "normal" dFRFs because they relate excitations and responses in the same direction; $H_{\hat{g}p}$ and $H_{g\hat{p}}$ relate excitations and responses which are in opposite directions and are called "reverse" dFRFs.

Equation (4.22) cannot be decoupled into modal equations directly because orthogonality among natural modes does not exist since the system matrix is not symmetric. However, the modal superposition method, completely analogous to that for

non-self-adjoint real systems, can be conducted if the state space form of Equation (4.22) is used:

$$s\begin{bmatrix} [0] & [M_c] \\ [M_c] & [C_c] \end{bmatrix}\begin{Bmatrix} s\begin{Bmatrix} P_f \\ \overline{P}_b \end{Bmatrix} \\ \begin{Bmatrix} P_f \\ \overline{P}_b \end{Bmatrix} \end{Bmatrix} = \begin{bmatrix} [M_c] & [0] \\ [0] & -[K_c] \end{bmatrix}\begin{Bmatrix} s\begin{Bmatrix} P_f \\ \overline{P}_b \end{Bmatrix} \\ \begin{Bmatrix} P_f \\ \overline{P}_b \end{Bmatrix} \end{Bmatrix} + \begin{Bmatrix} \begin{Bmatrix} 0 \\ 0 \end{Bmatrix} \\ \begin{Bmatrix} G_f \\ \overline{G}_b \end{Bmatrix} \end{Bmatrix} \tag{4.24}$$

or,

$$[s[A]-[B]]\begin{Bmatrix} s\begin{Bmatrix} P_f \\ \overline{P}_b \end{Bmatrix} \\ \begin{Bmatrix} P_f \\ \overline{P}_b \end{Bmatrix} \end{Bmatrix} = \begin{Bmatrix} \{0\} \\ \begin{Bmatrix} G_f \\ \overline{G}_b \end{Bmatrix} \end{Bmatrix} \tag{4.25}$$

The forced response is:

$$\begin{Bmatrix} s\begin{Bmatrix} P_f \\ \overline{P}_b \end{Bmatrix} \\ \begin{Bmatrix} P_f \\ \overline{P}_b \end{Bmatrix} \end{Bmatrix} = [s[A]-[B]]^{-1}\begin{Bmatrix} \{0\} \\ \begin{Bmatrix} G_f \\ \overline{G}_b \end{Bmatrix} \end{Bmatrix} \tag{4.26}$$

System dynamics are contained in the inverted matrix which can be expanded[17] in terms of the appropriately-scaled right and left eigenvectors of Equation (4.16):

$$\begin{aligned} [s[A]-[B]]^{-1} &= \sum_{i=1}^{4n} \frac{R_i L_i^T}{s-\lambda_i} = \sum_{i=1}^{4n} \frac{\begin{Bmatrix} \lambda_i r_i \\ r_i \end{Bmatrix}\begin{Bmatrix} \lambda_i l_i \\ l_i \end{Bmatrix}^T}{s-\lambda_i} \\ &= \sum_{i=1}^{4n} \frac{\begin{bmatrix} \lambda_i^2 r_i l_i^T & \lambda_i r_i l_i^T \\ \lambda_i r_i l_i^T & r_i l_i^T \end{bmatrix}}{s-\lambda_i} \end{aligned} \tag{4.27}$$

where right and left eigenvectors associated with eigenvalue λ_i are:

$$R_i = \begin{Bmatrix} \lambda_i r_i \\ r_i \end{Bmatrix} \text{ and } L_i = \begin{Bmatrix} \lambda_i l_i \\ l_i \end{Bmatrix} \tag{4.28}$$

and right and left modal vectors are of the form:

$$\{r\}_i = \begin{Bmatrix} P_f \\ \overline{P}_b \end{Bmatrix}_i \text{ and } \{l\}_i = \begin{Bmatrix} L_f \\ \overline{L}_b \end{Bmatrix}_i \tag{4.29}$$

Provided $s \neq \lambda_i$, the harmonic response is:

$$\begin{Bmatrix} s\begin{Bmatrix} P_f \\ \overline{P}_b \end{Bmatrix} \\ \begin{Bmatrix} P_f \\ \overline{P}_b \end{Bmatrix} \end{Bmatrix} = \begin{bmatrix} \sum_{i=1}^{4n} \frac{\begin{bmatrix} \lambda_i^2 r_i l_i^T & \lambda_i r_i l_i^T \\ \lambda_i r_i l_i^T & r_i l_i^T \end{bmatrix}}{s-\lambda_i} \end{bmatrix} \begin{Bmatrix} \{0\} \\ \begin{Bmatrix} G_f \\ \overline{G}_b \end{Bmatrix} \end{Bmatrix} \tag{4.30}$$

or,

$$\begin{aligned} \begin{Bmatrix} s\begin{Bmatrix} P_f \\ \overline{P}_b \end{Bmatrix} \\ \begin{Bmatrix} P_f \\ \overline{P}_b \end{Bmatrix} \end{Bmatrix} &= \begin{Bmatrix} \begin{bmatrix} \sum_{i=1}^{4n} \frac{\lambda_i^2 r_i l_i^T}{s-\lambda_i} \end{bmatrix} \{0\} + \begin{bmatrix} \sum_{i=1}^{4n} \frac{\lambda_i r_i l_i^T}{s-\lambda_i} \end{bmatrix} \begin{Bmatrix} G_f \\ \overline{G}_b \end{Bmatrix} \\ \begin{bmatrix} \sum_{i=1}^{4n} \frac{\lambda_i r_i l_i^T}{s-\lambda_i} \end{bmatrix} \{0\} + \begin{bmatrix} \sum_{i=1}^{4n} \frac{r_i l_i^T}{s-\lambda_i} \end{bmatrix} \begin{Bmatrix} G_f \\ \overline{G}_b \end{Bmatrix} \end{Bmatrix} \\ &= \begin{Bmatrix} \begin{bmatrix} \sum_{i=1}^{4n} \frac{\lambda_i r_i l_i^T}{s-\lambda_i} \end{bmatrix} \begin{Bmatrix} G_f \\ \overline{G}_b \end{Bmatrix} \\ \begin{bmatrix} \sum_{i=1}^{4n} \frac{r_i l_i^T}{s-\lambda_i} \end{bmatrix} \begin{Bmatrix} G_f \\ \overline{G}_b \end{Bmatrix} \end{Bmatrix} \end{aligned} \tag{4.31}$$

The position response is described by:

$$\begin{Bmatrix} P_f(\omega) \\ \overline{P}_b(\omega) \end{Bmatrix} = \begin{bmatrix} \sum_{i=1}^{4n} \frac{r_i l_i^T}{j\omega - \lambda_i} \end{bmatrix} \begin{Bmatrix} G_f(\omega) \\ \overline{G}_b(\omega) \end{Bmatrix} \tag{4.32}$$

Recalling the definition of the dFRM:

$$\begin{Bmatrix} P_f(\omega) \\ \overline{P}_b(\omega) \end{Bmatrix} = \begin{bmatrix} H_{gp}(\omega) & H_{\hat{g}p}(\omega) \\ H_{g\hat{p}}(\omega) & H_{\hat{g}\hat{p}}(\omega) \end{bmatrix} \begin{Bmatrix} G_f(\omega) \\ \overline{G}_b(\omega) \end{Bmatrix} \tag{4.33}$$

it is shown that there are 4*n* contributions to each dFRF over the two-sided frequency range; 2*n* natural modes exist. Associated with each mode are two eigensolutions which contribute to the dFRF and which are redundant descriptions of the same physical mode.

Normal dFRF H_{gp} relates the forward response to the forward excitation and $H_{\hat{g}\hat{p}}$

relates the backward response to the backward excitation. Normal dFRFs relating excitation and response at station 1 for the isotropic rigid rotor considered previously and described in Appendix A are shown in Figure 4.5:

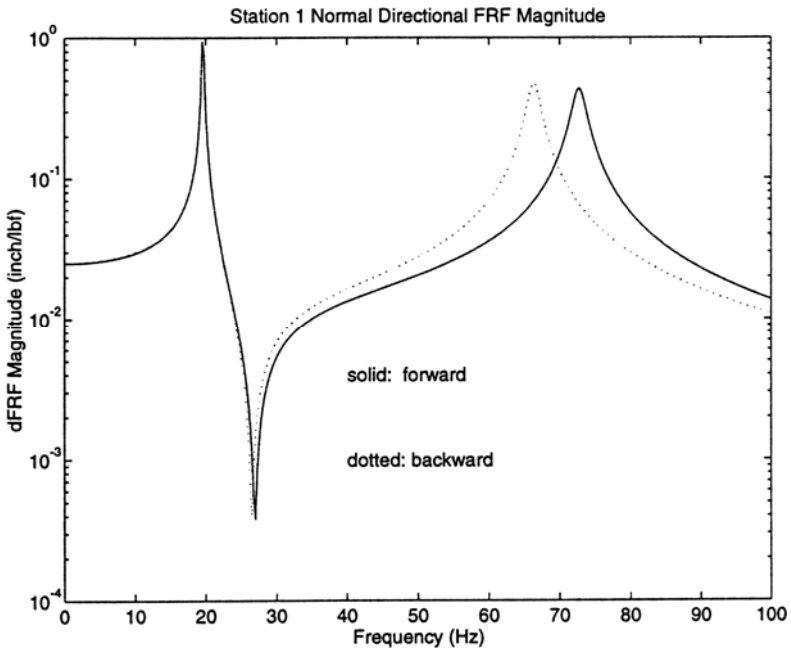

Figure 4.5: Magnitude of Normal dFRFs of Isotropic Rigid Rotor at Station 1

Since the rotor is isotropic the reverse dFRFs are zero[8] ($H_{\hat{g}ipj} = H_{gi\hat{p}j} \equiv 0; i, j = 1,2$). See reference [8] for the rigorous definition of an isotropic system.

The forward pitch mode, which increases in frequency by gyroscopic stiffening, appears only in H_{g1p1}; the backward pitch mode does not contribute to this dFRF. The backward pitch mode, the frequency of which is decreased by the gyroscopic effect, appears only in $H_{\hat{g}1\hat{p}1}$; the forward pitch mode does not contribute to this dFRF. Forward and backward bounce modes exist at the same frequency near 20 Hz and contribute to their respective dFRFs.

For comparison, the driving point *Y*-direction FRF at station 1 (H_{Y1Y1}) as obtained from real analysis is shown in Figure 4.6. The forward and backward modes all contribute to the FRF and are not distinguished from each other.

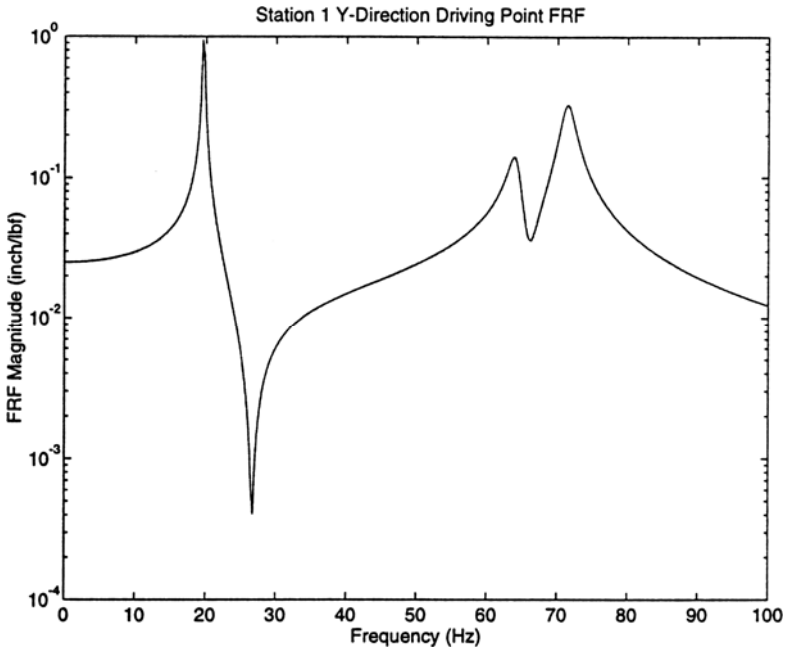

Figure 4.6: Magnitude of Y-Direction Driving Point Real FRF of Isotropic Rigid Rotor at Station 1

Now consider the case when the support system is anisotropic as described in Appendix A. Reverse dFRFs are nonzero, and elements of residue matrices corresponding to forward (backward) modes are nonzero so that they contribute to $H_{\hat{g}1\hat{p}1}$ (H_{g1p1}) and appear as local maxima in Figure 4.7.

The magnitude of the reverse dFRFs is shown in Figure 4.8. The reverse dFRFs are not identical; in this example they have the same magnitude but opposite phase. Only magnitude plots have been included here since they sufficiently illustrate the important concepts.

The magnitude of the forward and backward normal dFRFs and the forward and backward reverse dFRFs are all equal at the bounce mode frequencies, although Figures 4.7 and 4.8 do not reflect this due to innacuracy at the peaks of the curves (which follows

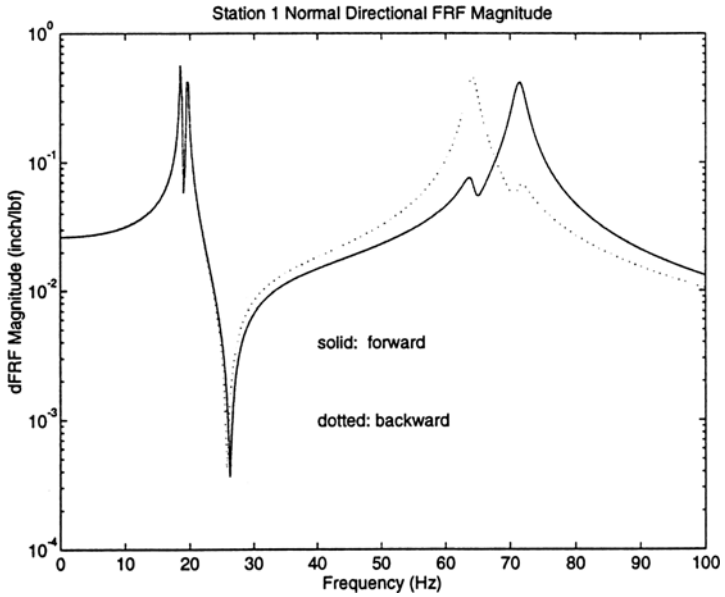

Figure 4.7: Magnitude of Normal dFRFs of Anisotropic Rigid Rotor at Station 1

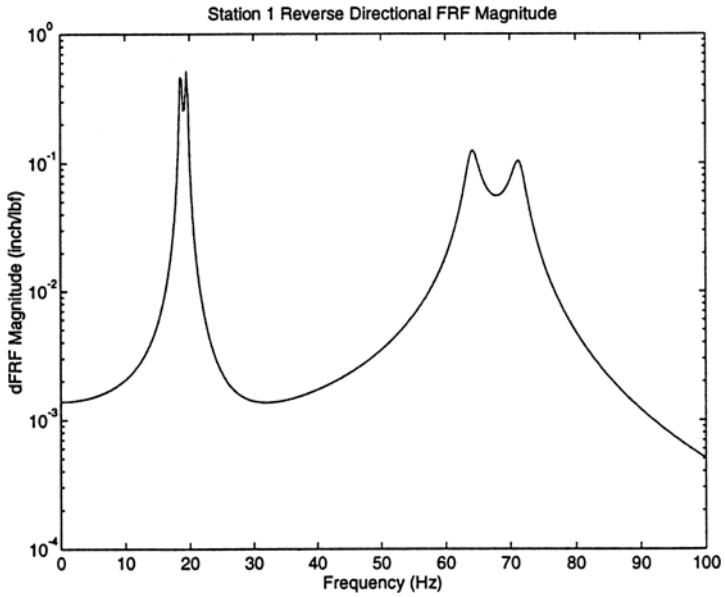

Figure 4.8: Magnitude of Reverse dFRFs of Anisotropic Rigid Rotor at Station 1

from limited frequency resolution in the calculation). The fact that magnitudes of the

forward normal and reverse dFRFs are equal at the bounce mode frequencies indicates that the mode is such that the rotor moves along a line (see Figure 4.3) as expected from Equation (4.21) with $|P_f| = |\overline{P_b}|$ and from the real form of the governing equations.

4.8 Results / Conclusions

It was shown in this chapter that planar excitation, as well as planar motion, can be represented as the sum of counter-rotating vectors using a complex variable representation. Directional frequency response functions (dFRFs) which implicitly include directionality were defined to relate these components.

The method of formulating the natural mode as the sum of forward rotating and backward rotating sub-modes is proposed. A definition to classify forward and backward natural modes was proposed in conjunction with this definition of the sub-modes. It was shown that the dFRFs for general rotors may be obtained by modal superposition of these modes in a manner consistent with conventional modal analysis of non-rotating systems. Because these dFRFs contain the directional response characteristics, they are very useful in practical applications such as modal identification and diagnostics.

With the natural mode defined here, dynamic analysis of rotating systems can be conducted in essentially the same way as in modal analysis of non-rotating systems. In fact, it is realized that vibration of the non-rotating system can be treated as a special case of the rotating system.

CHAPER 5: EXPERIMENTAL MODAL ANALYSIS AND THEORETICAL VALIDATION

5.1 Chapter Abstract

Impact testing is shown to be a practical method of verifying the speed-dependent dynamic characteristics of a rotating system, and it could also be applied to assess changes in a rotating machine's condition without interfering with scheduled operation. A pendulum-mounted multi-axis force sensor is used as an impact device to enable measurement of the tangential force component induced by friction. Complex modal analysis is applied to clearly distinguish forward and backward modes and separate them in the frequency domain. The fact that mixed whirl of a rigid rotor on anisotropic supports can be excited by rotating mass imbalance is demonstrated. Analytical developments are verified with experimental data obtained from a simply supported rigid rotor test rig with significant gyroscopic effects.

5.2 Introduction

This chapter establishes the fact that impact testing of a rotating shaft using a multi-axis force sensor is a reasonable approach to acquiring data for the application of complex modal analysis. To accomplish this, an overview of complex modal analysis is first presented.

Other researchers have presented work on modal analysis of spinning rotors. Nordmann[1] was among the first to look at modal analysis of non-self-adjoint rotating systems. Muszynska[3] reported perturbation devices capable of independent forward and backward excitation. Rogers and Ewins[19] pointed out some of the practical issues associated with testing spinning rotors and conducted testing with a dynamic exciter

attached to the shaft through a stinger riding on the fixed race of a bearing. Blough, et. al.,[20-22] have done extensive work on signal processing related to rotating systems and have impacted the shaft through a low-friction stationary flap.

Lee, et. al., [8-16] have developed complex modal analysis theory and testing. They have demonstrated the method primarily on magnetically levitated rotors. The stator of a magnetic bearing provides a convenient noncontact excitation source which is necessarily well-controlled. Ehrich[2] has discussed the representation of general elliptical motion by rotating complex vectors. Bently, et. al., [4-7] have applied these concepts to monitoring response components in machinery diagnostics.

This chapter explains an interpretation of complex modal analysis which is based upon representing excitations and responses as the sum of rotating components. Initial experimental verification of the approach is included. Chapter 3 introduced the concept for free vibration and a detailed development of the method for forced vibration was provided in Chapter 4.

5.3 Conceptual Overview of Complex Modal Analysis

A brief overview of complex modal analysis is made as necessary. For further details on complex modal analysis of rotors, see the bibliography. The geometry of a simple rotor is shown in Figure 5.1:

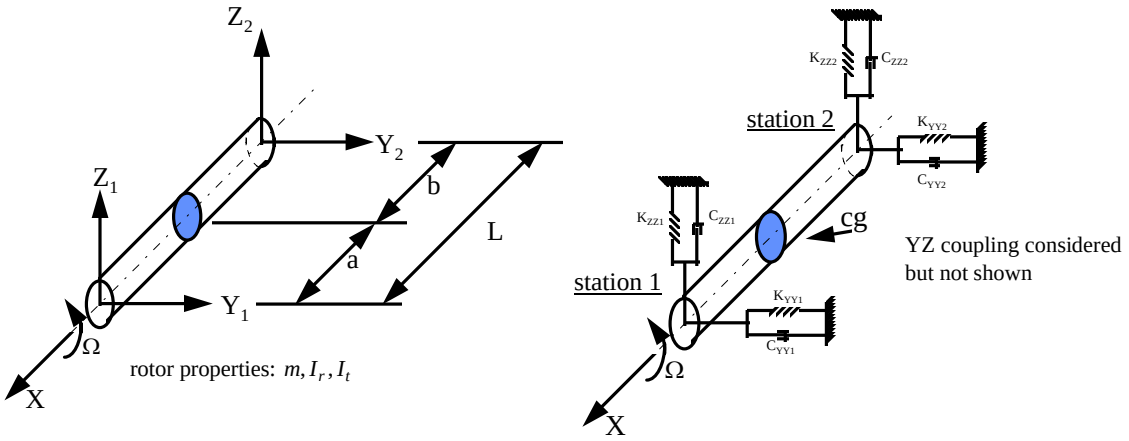

Figure 5.1: Rigid Rotor Geometry, Supports and Coordinate System

The relationship between the planar excitations and responses of a rotor as described by real variables in the frequency domain is:

$$\begin{Bmatrix} Y(\omega) \\ Z(\omega) \end{Bmatrix} = \begin{bmatrix} H_{YY}(\omega) & H_{YZ}(\omega) \\ H_{ZY}(\omega) & H_{ZZ}(\omega) \end{bmatrix} \begin{Bmatrix} F_Y(\omega) \\ F_Z(\omega) \end{Bmatrix} \tag{5.1}$$

Unlike non-rotating structures, $H_{ZY}(\omega) \neq H_{YZ}(\omega)$ due to the unique dynamics of rotating machines.

In complex modal analysis response and excitation are described by complex variables *p(t)* and *g(t)*, respectively, where:

$$\begin{aligned} p(t) &= y(t) + jz(t) \\ g(t) &= f_Y(t) + jf_Z(t) \end{aligned} \tag{5.2}$$

The single complex variables *p(t)* and *g(t)* represent two-dimensional displacement and force vectors which are in motion.

Using the complex Fourier series representations of real signals in Equation (5.2) and grouping $e^{+j\omega_k t}$ and $e^{-j\omega_k t}$ terms as illustrated in Figure 5.2, it is realized that two vectors (in fact, any vectors) in planar motion can be considered to be composed of forward rotating and backward rotating components.

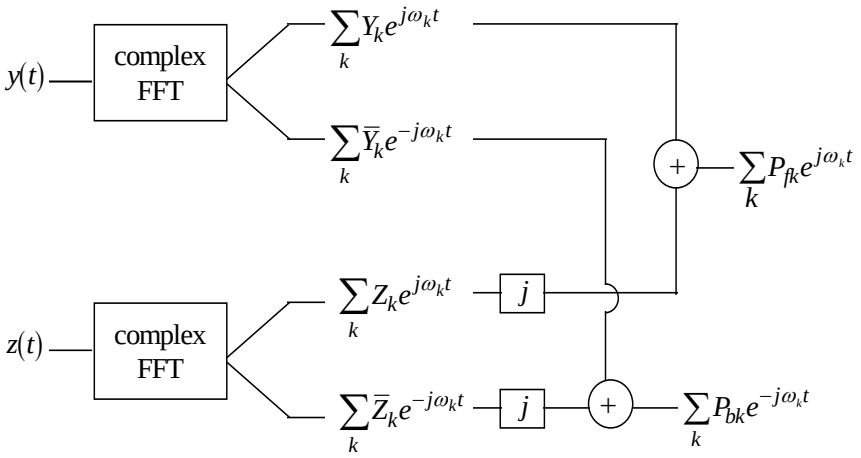

Figure 5.2: Decomposition of Response Into Rotating Components

The same decomposition applies to the excitation *g(t)*. Now one can relate the forward and backward rotating components of the displacement (response) and the force (excitation) at each frequency. The continuous description of this relationship is:

$$\begin{Bmatrix} P_f(\omega) \\ \overline{P}_b(\omega) \end{Bmatrix} = \begin{bmatrix} H_{gp}(\omega) & H_{\hat{g}p}(\omega) \\ H_{g\hat{p}}(\omega) & H_{\hat{g}\hat{p}}(\omega) \end{bmatrix} \begin{Bmatrix} G_f(\omega) \\ \overline{G}_b(\omega) \end{Bmatrix} \tag{5.3}$$

Elements of this frequency response matrix are referred to as "directional frequency response functions" (dFRFs) because they implicitly include directionality. Partitions H_{gp} and $H_{\hat{g}\hat{p}}$ relate excitations and responses of the same direction and are called "normal dFRFs"; the partitions $H_{\hat{g}p}$ and $H_{g\hat{p}}$ relate excitations and responses in opposite directions and are called "reverse" dFRFs. Figure 5.3 illustrates this concept in the frequency domain:

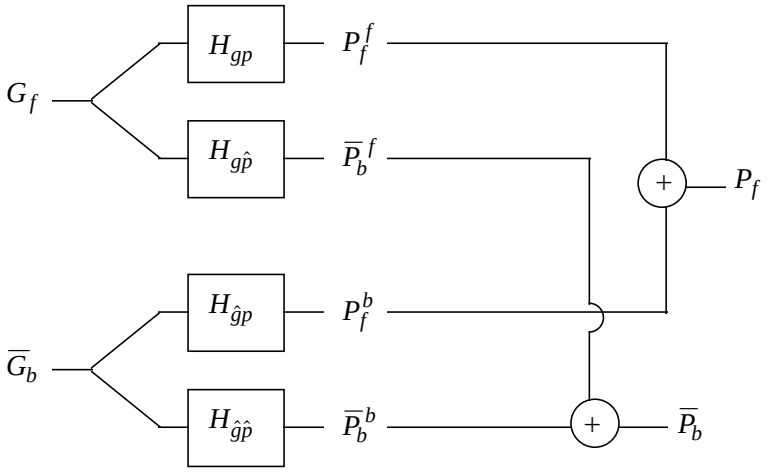

Figure 5.3: Frequency Domain Illustration of dFRF Matrix

Lee[8-16] has pioneered the development of complex modal analysis. Here, a physically-based derivation of the approach was used in which the dFRFs are viewed not to relate the complex signals *p(t)* and *g(t)* but their rotating components which are derived from real measurable signals.

5.4 Complex Analysis of Rigid Rotor

For illustration, complex modal analysis is applied to the simply supported rigid rotor (the model and equations can be found in Appendix A). The frequency response relation from the real description becomes:

$$\begin{Bmatrix} Y_1(\omega) \\ Y_2(\omega) \\ Z_1(\omega) \\ Z_2(\omega) \end{Bmatrix} = \begin{bmatrix} H_{Y1Y1}(\omega) & H_{Y1Y2}(\omega) & H_{Y1Z1}(\omega) & H_{Y1Z2}(\omega) \\ H_{Y2Y1}(\omega) & H_{Y2Y2}(\omega) & H_{Y2Z1}(\omega) & H_{Y2Z2}(\omega) \\ H_{Z1Y1}(\omega) & H_{Z1Y2}(\omega) & H_{Z1Z1}(\omega) & H_{Z1Z2}(\omega) \\ H_{Z2Y1}(\omega) & H_{Z2Y2}(\omega) & H_{Z2Z1}(\omega) & H_{Z2Z2}(\omega) \end{bmatrix} \begin{Bmatrix} F_{Y1}(\omega) \\ F_{Y2}(\omega) \\ F_{Z1}(\omega) \\ F_{Z2}(\omega) \end{Bmatrix} \tag{5.4}$$

First consider an isotropic rotor system. The rotor considered is steel with a bearing span of 203 mm, shaft diameter of 10 mm, and support parameters

of $K_{ZZi} = K_{YYi} = 7\,^{N}/_{mm}$ and $C_{ZZi} = C_{YYi} = 4.4e-4\,^{N\cdot sec}/_{mm}; i = 1,2$ A disk of 25.4 mm axial length, 76.2 mm diameter, and 0.8 kilograms is located at midspan. At 500 rpm, the driving point *Y*-direction dynamic compliance FRF at station 1(H_{Y1Y1}) of this isotropic rotor is shown in Figure 5.4:

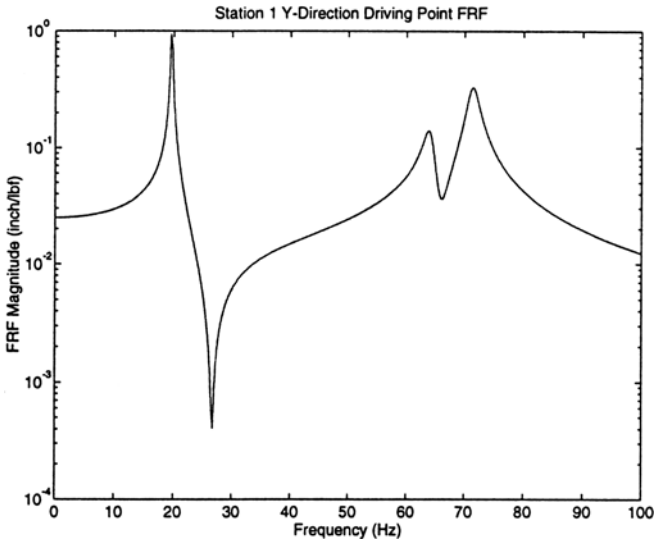

Figure 5.4: Magnitude of Y-direction Driving Point FRF at Station 1 (H_{Y1Y1})

The peak near 20 Hz is due to the bounce mode; the peaks near 65 Hz are due to forward and backward pitch modes which are separated at speed by gyroscopic effects.

The complex dFRF matrix (dFRM) for this model is:

$$\begin{Bmatrix} P_{f1}(\omega) \\ P_{f2}(\omega) \\ \overline{P}_{b1}(\omega) \\ \overline{P}_{b2}(\omega) \end{Bmatrix} = \begin{bmatrix} H_{g1p1}(\omega) & H_{g2p1}(\omega) & H_{\hat{g}1p1}(\omega) & H_{\hat{g}2p1}(\omega) \\ H_{g1p2}(\omega) & H_{g2p2}(\omega) & H_{\hat{g}1p2}(\omega) & H_{\hat{g}2p2}(\omega) \\ H_{g1\hat{p}1}(\omega) & H_{g2\hat{p}1}(\omega) & H_{\hat{g}1\hat{p}1}(\omega) & H_{\hat{g}2\hat{p}1}(\omega) \\ H_{g1\hat{p}2}(\omega) & H_{g2\hat{p}2}(\omega) & H_{\hat{g}1\hat{p}2}(\omega) & H_{\hat{g}2\hat{p}2}(\omega) \end{bmatrix} \begin{Bmatrix} G_{f1}(\omega) \\ G_{f2}(\omega) \\ \overline{G}_{b1}(\omega) \\ \overline{G}_{b2}(\omega) \end{Bmatrix} \tag{5.5}$$

Normal dFRFs H_{g1p1} (forward) and $H_{\hat{g}1\hat{p}1}$ (backward) at station 1 are shown in Figure 5.5:

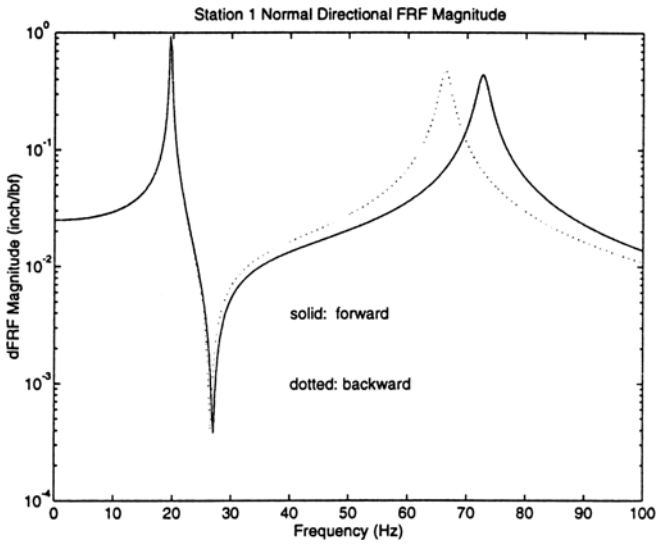

Figure 5.5: Magnitude of Normal dFRFs of Isotropic Rotor at Station 1

Since the rotor is isotropic the reverse dFRFs are zero ($H_{\hat{g}ipj} = H_{gi\hat{p}j} \equiv 0; i, j = 1,2$), therefore they are not shown. For a rigorous discussion of shaft anisotropy see reference [8].

The forward pitch mode, which is elevated in frequency by gyroscopic stiffening, appears only in H_{g1p1}; the backward pitch mode does not contribute to this dFRF. Similarly, the backward pitch mode, the frequency of which is decreased by the gyroscopic effect, appears in $H_{\hat{g}1\hat{p}1}$; the forward pitch mode does not contribute to this dFRF. Forward and backward bounce modes exist at the same frequency near 20 Hz and contribute to their respective dFRFs.

Now assume that the support system becomes anisotropic: $K_{ZZi} = 0.9K_{YYi} = 6.3\,{}^{\mathrm{N}}\!/_{mm}$; $i = 1,2$. Because of the system anisotropy, now reverse dFRFs in Equation (5.3) become nonzero. Figure 5.6 shows the normal dFRFs and Figure 5.7 shows the reverse dFRFs (reverse dFRFs have same magnitude but opposite phase; phase

plots have been omitted since the important concepts are sufficiently illustrated with magnitude plots) at station 1.

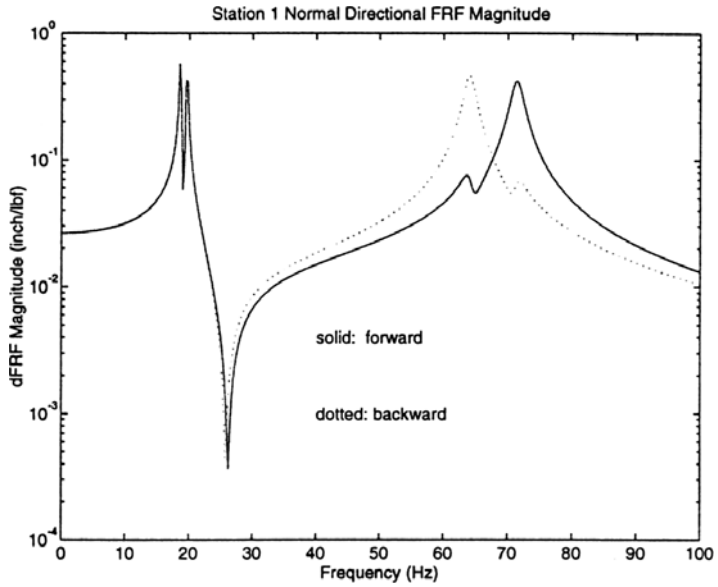

Figure 5.6: Magnitude of Normal dFRFs of Anisotropic Rotor at Station 1

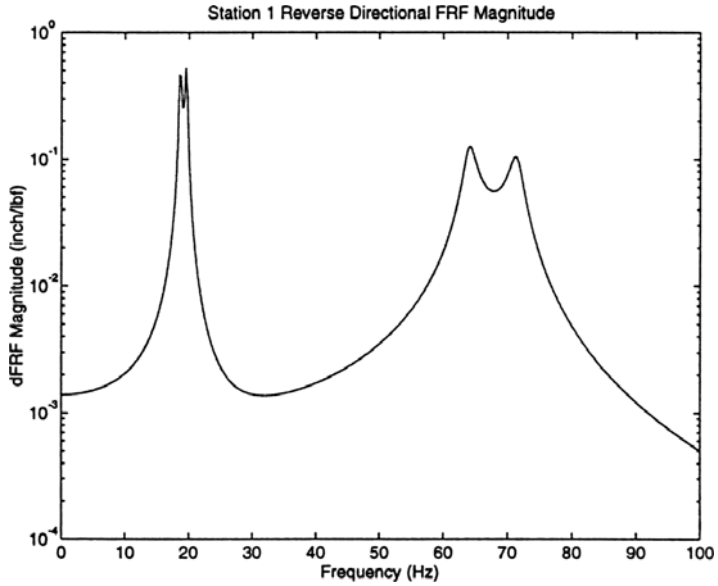

Figure 5.7: Magnitude of Reverse dFRFs of Anisotropic Rotor at Station 1

Now consider the case when the rotor is excited synchronously by a concentrated mass imbalance at station 1. Then, $G_{f2} = \overline{G}_{b1} = \overline{G}_{b2} \equiv 0$, and response is described by the first column of the dFRM. The ratio of forward to backward response at station 1 is

defined by the ratio of H_{g1p1} to $H_{g1\hat{p}1}$; the ratio of forward to backward response at station 2 is defined by the ratio of H_{g1p2} to $H_{g1\hat{p}2}$. If the magnitude of this ratio for a particular station is >1, the whirl orbit is an ellipse rotating forward; if the value is 1 the orbit is a line, and if the value is <1 the orbit is an ellipse rotating backward. Figure 5.8 shows the value of these ratios for the synchronous response, where the dFRM has been recalculated at each shaft speed:

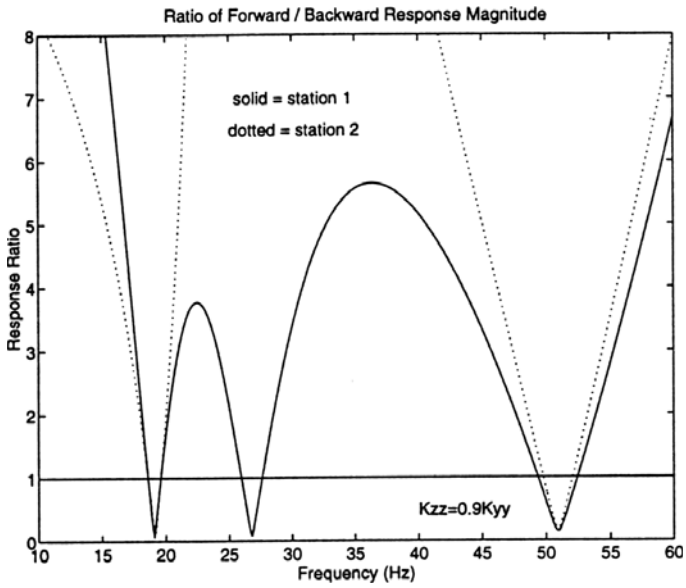

Figure 5.8: Station Response Ratio Magnitude (Anisotropic Rotor)

In two frequency ranges near 50 Hz (3000 rpm), the rotor's whirl response is mixed with station 1 undergoing backward whirl and station 2 undergoing forward whirl. These frequency ranges increase with the level of stiffness anisotropy.

5.5 dFRF Estimation By Impact Testing

Consider a single station rotor for simplicity. Impacting the spinning rotor results in a tangential excitation component as well as the normal component. If both components of the impact force are measured, these forces can be transformed into

forward and backward components in the frequency domain according to the procedure illustrated in Figure 5.2. For the calculation, the tangential forces are projected to the center of the rotor so that the effect of the torsional moment is ignored. At each frequency, the forward displacement due to the input force becomes:

$$\begin{bmatrix} G_f & \overline{G}_b \end{bmatrix}_i \begin{Bmatrix} H_{gp} \\ H_{\hat{g}p} \end{Bmatrix} = \begin{bmatrix} P_f \end{bmatrix}_i ; i = 1,2,3,\ldots, N_{avg} \tag{5.6}$$

where N_{avg} is the number of measurements, which should be equal to or larger than the number of the frequency response functions to be determined. In the case of the single station rotor, it has to be at least 2. In practice, the equation may be over-determined by using more measurement sets than the minimum necessary to improve the accuracy of the test as follows:

$$\begin{bmatrix} \begin{bmatrix} G_f & \overline{G}_b \end{bmatrix}_1 \\ \vdots \\ \begin{bmatrix} G_f & \overline{G}_b \end{bmatrix}_{N_{avg}} \end{bmatrix}_{N_{avg}x2} \begin{Bmatrix} H_{gp} \\ H_{\hat{g}p} \end{Bmatrix}_{2x1} = \begin{Bmatrix} \begin{bmatrix} P_f \end{bmatrix}_1 \\ \vdots \\ \begin{bmatrix} P_f \end{bmatrix}_{N_{avg}} \end{Bmatrix}_{N_{avg}x1} \tag{5.7}$$

Or,

$$[G]_{N_{avg}x2} \begin{Bmatrix} H_{gp} \\ H_{\hat{g}p} \end{Bmatrix}_{2x1} = \begin{Bmatrix} P_f \end{Bmatrix}_{N_{avg}x1} \tag{5.8}$$

Estimates of dFRFs are obtained in a least squares sense using the pseudoinverse of [G]:

$$\begin{Bmatrix} H_{gp} \\ H_{\hat{g}p} \end{Bmatrix}_{2x1} \cong [G]^{+}_{2xN_{avg}} \begin{Bmatrix} P_f \end{Bmatrix}_{N_{avg}x1} \tag{5.9}$$

In order for the pseudoinverse to be numerically well-conditioned, at least as many independent measurements as frequency response functions to be determined must be used. This translates to a requirement that each impact orientation must be unique.

The dFRFs in the second row of Equation (5.3) are estimated similarly using the measured backward response components:

$$\begin{Bmatrix} H_{g\hat{p}} \\ H_{\hat{g}\hat{p}} \end{Bmatrix}_{2x1} \cong [G]^{+}_{2xN_{avg}} \left\{ \overline{P}_b \right\}_{N_{avg}x1} \tag{5.10}$$

Special Case: Excitation by Frictionless Impact

This case is represented by excitation made with a noncontact method or when the tangential component is negligible. Referring back to Equation (5.3), the response of the single station rotor is given by:

$$\begin{Bmatrix} P_f \\ \overline{P}_b \end{Bmatrix} = \begin{bmatrix} H_{gp} & H_{\hat{g}p} \\ H_{g\hat{p}} & H_{\hat{g}\hat{p}} \end{bmatrix} \begin{Bmatrix} G_f \\ \overline{G}_b \end{Bmatrix} \tag{5.11}$$

Two successive impact tests are conducted with the impact in different orientations, once in *Y* and then once in *Z* in this example.

Test *I*: (*Y* direction impact) $f_y(t) \neq 0, f_z(t) = 0$

so that: $$G_f(\omega_k) = F_y(\omega_k), \overline{G}_b(\omega_k) = F_y(\omega_k) \tag{5.12}$$

Data from Test *I* satisfy the first row of Equation (5.11):

$$\left[P_f\right]_I = H_{gp}\left[G_f\right]_I + H_{\hat{g}p}\left[\overline{G}_b\right]_I = \left(H_{gp} + H_{\hat{g}p}\right)\left[F_y\right]_I \tag{5.13}$$

Test *II*: (*Z* direction impact) $f_y(t) = 0, f_z(t) \neq 0$

so that: $$G_f(\omega_k) = jF_z(\omega_k), \overline{G}_b(\omega_k) = -jF_z(\omega_k) \tag{5.14}$$

Data from Test *II* also satisfy the first row of Equation (5.11):

$$\left[P_f\right]_{II} = H_{gp}\left[G_f\right]_{II} + H_{\hat{g}p}\left[\overline{G}_b\right]_{II} = \left(H_{gp} - H_{\hat{g}p}\right)j\left[F_z\right]_{II} \tag{5.15}$$

Data from these two successive tests is used to estimate the dFRFs. Adding Equations (5.13) and (5.15), after division by the appropriate force coefficient, leads to:

$$\frac{(5.13)}{[F_y]_I} + \frac{(5.15)}{j[F_z]_{II}} = 2H_{gp} \tag{5.16}$$

or:
$$2H_{gp} = \frac{[P_f]_I}{[F_y]_I} + \frac{[P_f]_{II}}{j[F_z]_{II}} \tag{5.17}$$

Subtracting Equations (5.13) and (5.15), after division by the appropriate force coefficient, leads to:

$$\frac{(5.13)}{[F_y]_I} - \frac{(5.15)}{j[F_z]_{II}} = 2H_{\hat{g}p} \tag{5.18}$$

or:
$$2H_{\hat{g}p} = \frac{[P_f]_I}{[F_y]_I} - \frac{[P_f]_{II}}{j[F_z]_{II}} \tag{5.19}$$

A similar process results in the backward normal and reverse dFRFs in the second row of Equation (5.11). Averaging of the estimates from these tests may be done if multiple measurements are made in each direction. A least square procedure may also be applied if testing is conducted in more than two directions. From Equation (5.19), it is obvious that the reverse dFRFs will become zero if the system is isotropic.

5.6 Experimental Verification

A simple experimental verification example was conducted to establish the validity of the previous development. The test article was the isotropic rotor modeled above and described in Appendix A. It was supported by rolling element bearings which were suspended from a rigid frame by springs in the *Y* and *Z* coordinate directions. It was driven by a variable speed DC motor through a flexible coupling. Responses were measured with a standard orthogonal pair of eddy-current probes as used in industrial machinery monitoring applications. A triaxial force sensor was fitted with an impact cap

to become a triaxial impact hammer; two of the available three channels were used to record the normal and tangential components of excitation. Controlling the direction of shaft impacts is key to acquiring useable data; a simple pendulum was used to do this with improved repeatability. Impacts were performed in each of two directions (i.e., the *Y* and *Z* coordinates) and in order to improve estimation accuracy five measurements were made in each direction.

Figures 5.9 through 5.12 present the magnitude of the linear spectra recorded for a typical measurement made with a *Y*-direction impact while the rotor was spinning from *Y* toward *Z* at 500 rpm (8.33 Hz). Figure 5.9 shows the linear spectra of the recorded excitations in the *Y* and *Z* directions.

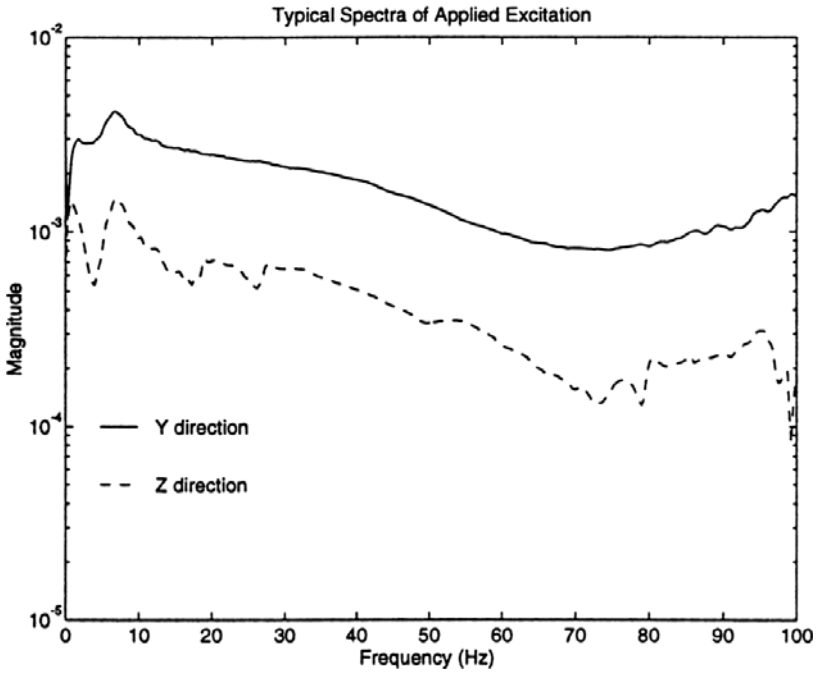

Figure 5.9: Magnitude of Linear Spectra of Excitation Measured at Station 1

In this case, the force in the *Y* direction is the "normal" component of the impact and the force in the *Z* direction is the "tangential" component. As expected, the magnitude of the

tangential component is less than that of the normal component with the scale factor being roughly the value of the coefficient of friction.

Figure 5.10 shows the forward and backward spectral components of the excitation as calculated from the concept illustrated in Figure 5.2. Under ideal conditions the impact force would be measured as one with a certain fixed line of action, resulting in forward and backward components of the same magnitude.

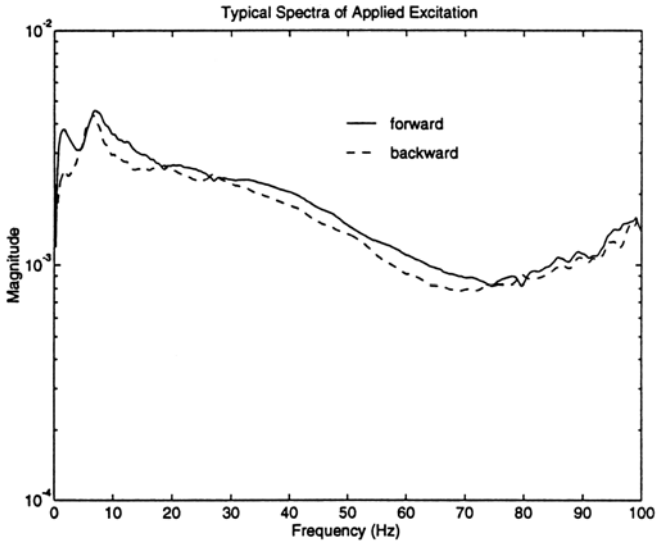

Figure 5.10: Magnitude of Directional Linear Spectra of Excitation at Station 1

Figure 5.11 shows the linear spectra of the recorded responses in the *Y* and *Z* directions as measured by the proximity probes. The peaks at 8.33 Hz are due to the synchronous imbalance response; no effort was made to filter the input signals.

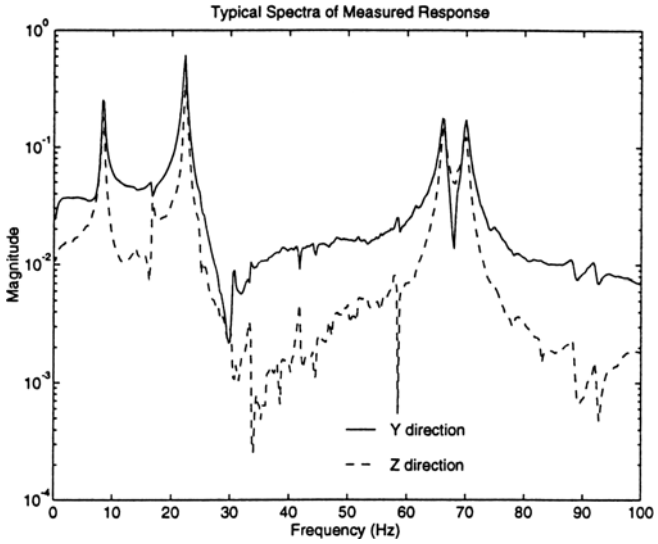

Figure 5.11: Magnitude of Linear Spectra of Response Measured at Station 1

Figure 5.12 shows the forward and backward spectral components of the response. The backward response is noticeably cleaner than the forward response. This is explained by the fact that the rotor rig was very nearly isotropic: from concepts developed in Chapter 4, the isotropic rotor will have no backward response due to forward excitations

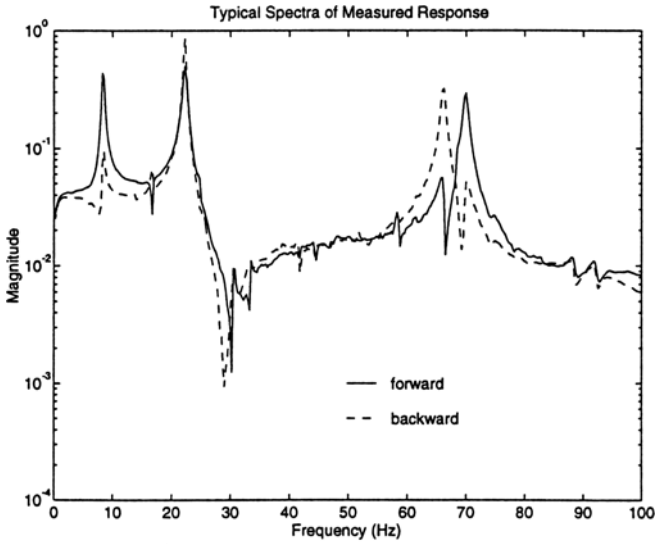

Figure 5.12: Magnitude of Directional Linear Spectra of Response at Station 1

(e.g., mass imbalance and harmonics due to ball bearings, etc.). Thus, all system noise due to rotor spin is in the forward direction and should appear only on forward response measurements as demonstrated in the figure.

Based upon the results of all ten measurements, Figure 5.13 shows the estimated normal dFRFs at station 1 which were calculated with the pseudoinverse approach described above. They correspond to the analytical dFRFs previously shown in Figure 5.5:

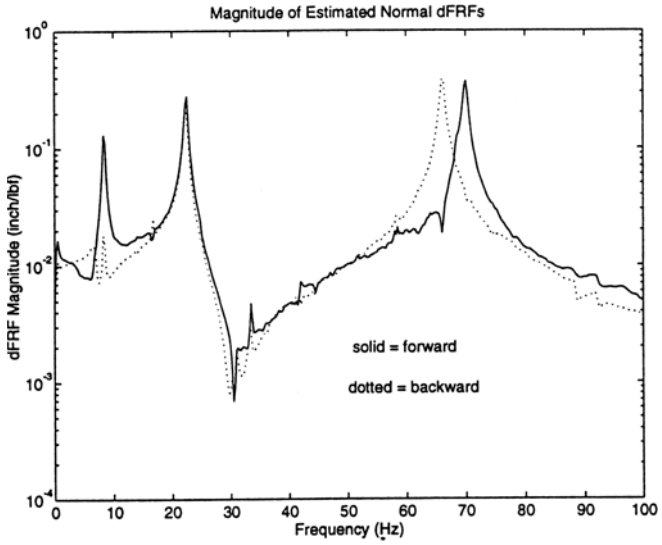

Figure 5.13: Magnitude of Estimated Normal dFRFs at Station 1

Several comments are in order relating to these measurements. Since no attempt was made to filter out the mass imbalance response which was not considered in the analytical model that led to Figure 5.5, a small peak appears in the forward normal dFRF and a much smaller peak in the reverse normal dFRF at the synchronous frequency (8.33 Hz) and at harmonics. Comparing Figures 5.5 and 5.13, it was shown that very good qualitative agreement is achieved.

5.7 **Results / Conclusions**

The dFRF as used in complex modal analysis in relation to signals measured in conventional modal testing was explained. Impact testing of spinning rotors with a multi-axis force sensor appears to have promise as a method to acquire data for complex modal analysis which does not require the well-controlled, noncontact excitation found in magnetically suspended systems.

Issues associated with modal analysis of rotating systems are divided into two classes:

- those associated with the approach to complex modal analysis presented in this work
- generic difficulties associated with impact modal testing of rotor systems: how to generate excitation, proper signal processing and test methods, filtering of imbalance response, effects of shaft runout, hydrodynamic bearing nonlinearities, etc.

The main intent of this chapter was to explain the laws of complex modal analysis and show its practical implementation in the context of impact testing. Difficulties which exist in real modal analysis will have parallel difficulties in complex modal analysis, and these were not the objective of this work.

Complex dFRFs of anisotropic systems were explained based upon the understanding of the complex natural mode given in Chapter 3. Also, a modal expansion theorem analogous to classical modal analysis was presented in Chapter 4.

CHAPTER 6: SUMMARY AND RECOMMENDED EXTENSIONS

6.1 Summary and Conclusions

The fundamental work presented herein provides a unique way to look at rotor dynamics problems. The approach offers significant benefits in understanding the dynamic behavior of rotor systems as compared to conventional analysis using real variables. Simple models were used in order to present the concepts clearly; the method is readily extended to more complicated geometries with a simple matrix transformation. Actually, analysis of higher order sets of equations, such as those formulated with finite elements, more clearly demonstrates the power of the method but at the expense of basic understanding. In keeping with the fundamental nature, a simple experimental rotor rig and testing approach was used to conceptually verify the method.

Basic theory for free vibration analysis of general anisotropic rotor systems by the complex description has been presented. Interpretation of the complex representation of planar motion, formulation of the equation of motion, solution of the free vibration equation, natural frequencies and complex natural modes were explained in a logical progression. Most importantly, it was proposed that complex natural modes should be expressed using two sub-components: a forward rotating component and a backward rotating component. It was shown that assuming such a form is the only way to satisfy the general complex free vibration equation. The resulting complex mode description carries not only frequency and amplitude information but also directivity.

One benefit of the concept of complex modes is clear definition of forward and backward modes enabled by the physical interpretation of the homogeneous solution, the

complex modal vector and natural frequency. Using an anisotropic rotor system model it was shown that the forward (backward) mode can be defined as that mode whose forward (backward) sub-mode is stronger than its backward (forward) sub-mode. It was shown that physically, the forward (backward) mode represents an elliptic whirl motion rotating forward (backward).

It was shown that general plane excitations can also be represented as the sum of counter-rotating vectors using complex variables. Directional frequency response functions (dFRFs) were defined to relate the independent rotating components of excitation and response. It was shown that dFRFs for general rotors may be obtained by modal superposition in a manner consistent with conventional modal analysis of non-rotating systems; in fact, vibration of the non-rotating system can be considered a special case of the rotating system. Because dFRFs contain directional response characteristics they are very useful in practical applications such as modal identification and machinery diagnostics of rotating equipment.

Tracing the rotating components of dFRFs back to the real signals measured in conventional modal testing was explained. A simple but effective method of experimental identification for complex modes of rotors was explained, again by considering the physical meanings of directional modes and excitations. Ideally a non-contact force would be preferred for excitation because it does not introduce an unwanted circumferential input in the identification method. However, impact testing of spinning rotors using a multi-axis force sensor was shown to be a useful method for acquiring data for complex modal analysis which does not require the well-controlled, noncontact

excitation found in magnetically suspended laboratory systems. It can be directly applied to rotors currently operating in the field.

Issues associated with experimental modal analysis of rotating systems may be divided into two classes: those associated with the approach to complex modal analysis presented in this work and those generic difficulties associated with impact testing of rotor systems. The main objective in this work was to develop and explain complex modal analysis and show its practical implementation in the context of impact testing. Difficulties which exist in real modal analysis, for example the repeated roots issue, will have parallel difficulties in complex modal analysis, and these were not the focus.

It is believed that the definition of complex modes and the complex formulation method proposed in this work enable all existing techniques and procedures in classical modal analysis theory to be utilized for rotor analysis. For example, experimental analysis for mode identification and forced vibration analysis by the modal superposition theory can be implemented in the complex description for general rotor systems exactly the same way as has been done in the real analysis of non-rotating structures.

This work was based upon and motivated by the complex modal analysis theory that has been pioneered by Lee and his collaborators and cited extensively herein. However, it offers a significant advancement to this theory and a comparison between the two should be presented. First, Lee's dFRF matrix was derived by transforming the frequency response matrix relating real system responses and excitations; it was not derived from physical relationship between complex excitation and response. It appears that he interprets this matrix as relating the complex excitation and its conjugate to the complex response and its conjugate. An implication is that any nonzero excitation also

has a nonzero conjugate so that the system must be considered to have two inputs. The approach presented herein, developed from fundamental input / output relationships, relates components of complex excitation and response. This is significant for several reasons, one of which is that rotating mass imbalance and other excitations which are multiples of the synchronous speed are a single input. That is, the most common forms of excitation are purely in the forward direction; they have no backward components. Also of fundamental significance is that this work offers the definition of the complex natural mode for anisotropic rotor systems, which is the foundation of the general modal superposition theory and the major contribution of this work.

6.2 Recommendations for Future Work

This work has laid a foundation for basic understanding of complex modal analysis, its application, and its benefits. Necessary future efforts to continue the development have also been identified. They are:

- Extension of the theory to the analysis of asymmetric rotors (i.e., those which are not axisymmetric). This problem is typically formulated in a rotating (rotor-fixed) coordinate system to avoid periodic terms in the system matrices and is of interest in the detection of cracked shafts and the analysis of certain high speed electrical machinery such as compulsators and some switched reluctance motor designs.
- Application of the theory to real rotor systems for analysis, particularly on-line monitoring and control problems. Two items are mentioned in particular. First, clear understanding of distinctions between forward and backward modes as well as the physical understanding gained through the approach may lead to tailoring of active magnetic bearings to independently consider these modes and the control laws which

control their stability characteristics. Second is the observation that for the typical isotropic or weakly anisotropic system, mass imbalance excitation and its harmonics generate only forward responses. An impact or controlled excitation which occurs along a fixed line of action contains broadband forward and backward components of equal magnitude. The measured response of the rotor to such a perturbation will contain forward responses due to the ambient forward rotating excitations as well as the perturbation response; the backward response will be due to the perturbation response only so that it would theoretically be free of noise due to rotation. For monitoring changes in machinery over time, such as bearing journal wear, cracked shafts, etc., measured backward dFRFs may be much more useful. Monitoring the operating response over time to see that no significant backward components exist would indicate whether or not the system remains isotropic. This is conceptually simple, but the application would need to be practically investigated.

- Extension of the work to include more realistic bearing models, such as hydraulic bearings, bearings riding on squeeze film dampers and actively controlled magnetic bearings. Since the method builds from the transformation from the real formulation (i.e. system responses, excitations, and mass/stiffness/damping properties expressed in a Cartesian coordinate system), this generalization would deal more with how to treat the variation of support properties with rotor speed and other variables which may be addressed well with lambda matrix theory[8,17]. Active magnetic bearings offer the ability to directly specify the eight coefficients for each bearing, at least over certain frequency ranges, so that they offer an excellent tool to study rotor dynamics. However, the control law is more likely such that the performance is not well

represented by these coefficients and improved methods are needed to mate the frequency-dependent nature of their performance with the speed-dependent nature of the rotor itself.

- Refining experimental and on-line monitoring techniques, both in hardware and software and algorithims related to signal processing. In particular, active magnetic bearings offer much promise for on-line monitoring applications due to their ability to serve as a controlled non-contact excitation mechanism and their innate need for proximity sensors. In regards to impact testing, calibration of the triaxial impact hammer used in this work was not exhaustive. It is felt that further experimental development of this apparatus is justified by the quality and usefulness of the initial measurements made here.
- Application of the complex analysis approach to continuous systems, particularly applying forward and backward descriptions to the rotating shell vibration problem. A potential application of this theoretical development is the study of turbine blades in aircraft engines which are prone to catastrophic failure due to high cycle fatigue induced by high frequency vibration.

BIBLIOGRAPHY:

[1] Nordmann, R., "**Dynamics of Rotors: Stability and System Identification**", Edited by O. Mahrenholtz, Springer-Verlag, 1984, Chapter Title: "Modal Analysis in Rotor Dynamics", Nordmann, R.

[2] Ehrich, Fredric F.; "**Handbook of Rotordynamics**", McGraw-Hill, 1992, Chapter authors: Nelson, Harold D. and Crandall, Stephen H.

[3] Muszynska, A.; *Modal Testing of Rotor/Bearing Systems*, The International Journal of Analytical and Experimental Modal Analysis, 1986, pp 15-34

[4] Muszynska, A.; *Forward and Backward Precession of a Vertical Anisotropically Supported Rotor*; Journal of Sound and Vibration, Vol. 192(1), 1996

[5] Muszynska, Agnes; Hatch, Charles T.; and Bently, Donald E.; *Dynamics of Anisotropically Supported Rotors*, International Journal of Rotating Machinery, Vol. 3(2), 1993

[6] Franklin, Wesley; Goldman, Paul; Bently, Donald E.; and Muszynska, Agnes; *Early Cracked Shaft Detection in Pumps Using Rotor Lateral Vibration Analysis*, 1997 ASME Fluids Engineering Division Summer Meeting (available through Bently Nevada)

[7] Laws, Bill; "*Toolbox Tips: When you use spectrum, don't use it halfway*", Orbit Magazine, a Bently Nevada publication, June 1998

[8] Lee, Chong-won; "**Vibration Analysis of Rotors**", Kluwer Academic Publishers, 1993

[9] Lee, Chong-Won and Joh, Young-Don; *Theory of Excitation Methods and Estimation of Frequency Response Functions in Complex Modal Testing of Rotating Machinery*; Mechanical Systems and Signal Processing, Vol. 7(1), 1993

[10] Lee, Chong-Won, Ha, Young-Ho, Joh, Chee-Young, Kim, Cheol-Soon; *In-Situ Identification of Active Magnetic Bearing System Using Directional Frequency Response Functions*, Transactions of the ASME, Journal of Dynamic Systems, Measurement, and Control, Vol. 118, September 1996

[11] Lee, Chong-Won; *Rotor Dynamics and Control in Complex Modal Space*, Keynote Speech of 1st International Conference on Motion and Vibration Control, 1992

[12] Lee, C. -W., and Kim, Jong-Sun; *Modal Testing and Suboptimal Vibration Control of Flexible Rotor Bearing System by Using a Magnetic Bearing*, Transactions of the ASME, Journal of Dynamic Systems, Measurement, and Control, Vol. 114, June 1992

[13] Joh, Chee-Young and Lee, Chong-Won; *Use of dFRFs for Diagnosis of Asymmetric/Anisotropic Properties in Rotor-Bearing System*, Transactions of the ASME, Journal of Vibration and Acoustics, Vol. 118 Jan 1996

[14] Lee, Chong-Won; *A Complex Modal Testing Theory For Rotating Machinery*, Mechanical Systems and Signal Processing, 1991, Vol. 5(2), pages 119-137

[15] Lee, Chong-won, and Joh, Chee-Young; *Development of the Use of Directional Frequency Response Functions for the Diagnosis of Anisotropy and Asymmetry in Rotating Machinery: Theory*, Mechanical Systems and Signal Processing, 1994, Vol. 8(6)

[16] Joh, Y.-D., and Lee, C.-W.; *Excitation Methods and Modal Parameter Identification in Complex Modal Testing of Rotating Machinery*, Modal Analysis: the International Journal of Analytical and Experimental Modal Analysis, vol. 8(3), July 1993

[17] Lancaster, P.; "**Lambda Matrices and Vibrating Systems**"; Pergamon Press, 1966

[18] Jreyzubger-Janik, T., and Irretier, H.; *On Modal Testing of Flexible Rotors for Unbalance Identification*, Proceedings of 17th International Modal Analysis Conference, 1998

[19] Rogers, P. J., and Ewins, D. J.; *Modal Testing of an Operating Rotor System Using a Structural Dynamics Approach*, Proceedings of the 7th International Modal Analysis Conference, 1989

[20] Blough, J., Landgraf, M., Brown, D., and Vold, H.; *Signal Processing Procedures for Trouble Shooting Rotating Equipment*, Proceedings of International Seminar of Modal Analysis 19 - Tools for Noise and vibration Analysis, Volume II, pp 621-632, 1994

[21] Blough, J. R., and Brown, D. L.; *Machine Balancing Using the Inverse Frequency Response Function Method*, Proceedings of 16th International Modal Analysis Conference, 1997

[22] Blough, Jason R., and DeClerck, James P.; *Application and Development of Some Signal Processing Procedures to Estimate Frequency Response Functions of a System During Operation*, Proceedings of the 15th International Modal Analysis Conference, 1996

[23] Childs, Dara; "**Turbomachinery Rotordynamics: Phenomena, Modeling, and Analysis"**; John Wiley & Sons, 1993

[24] Vance, John M.; "**Rotordynamics of Turbomachinery**"; John Wiley & Sons, Inc, 1988

[25] Dimentberg, F. M.; "**Flexural Vibrations of Rotating Shafts**", Butterworths, 1959 (English translation, 1961)

Other Related References:

Kessler, C.; Kim,J.; *Complex Modal Analysis and Interpretation for Rotating Machinery*, Proceedings of the 16th International Modal Analysis Conference, 1998, pp 782-787

Kessler, C.; Kim,J.; *Complex Modal Analysis and Modal Superposition for Rotating Machinery*, Proceedings of the 17th International Modal Analysis Conference, 1999

Kessler, C.; Kim,J.; *Application of Triaxial Force Sensor to Impact Testing of Spinning Rotor Systems*, Proceedings of the 17th International Modal Analysis Conference, 1999

Genta, G.; *Whirling of Unsymmetrical Rotors: A Finite Element Approach Based on Complex Co-ordinates*, Journal of Sound and Vibration, vol. 124(1), 1988

von Karman Institute for Fluid Dynamics, "**Vibration and Rotor Dynamics, Lecture Series 1992-06**", 1992

Gunter, Edgar J., "**Dynamic Stability of Rotor-Bearing Systems**", 1966

Rao, C., Bhat, R. B., and Xistris, G. D.;*Experimental Verification of Simultaneous Forward and Backward Whirling at Different Points of a Jeffcott Rotor Supported on Identical Journal Bearings*, Journal of Sound and Vibration, 1996, Vol. 198(3), Letters to the Editor

Okada, Y., Nagai, B., Shimane, T.; *Cross-Feedback Stabilization of the Digitally Controlled Magnetic Bearing*, Transactions of the ASME, Journal of Vibration and Acoustics, Vol. 114, January,1992

Jei, Y.-G, and Lee, C.-W.; *Modal Characteristics of Asymmetrical Rotor-Bearing Systems*, Journal of Sound and Vibration, 1993, Vol. 162(2)

Shafai, B., Beale, S., LaRocca, P., and Cusson, E.; *Magnetic Bearing Control Systems and Adaptive Forced Balancing*, IEEE Control Systems, April 1994

Alford, J. S.; *Protecting Turbomachinery from Self-Excited Rotor Whirl*, Journal of Engineering for Power, October 1965

Ehrich, F; *Observations of Subcritical Superharmonic and Chaotic Response in Rotordynamics*, Journal of Vibration and Acoustics, Vol. 114, January 1992

Goodwin, M. J.; *Experimental Techniques for Bearing Impedance Measurement*, Journal of Engineering for Industry, Vol. 113, August 1991

Hawkins, Larry A. and Imlach, Joseph; *Eigenvalue Analysis Techniques for Magnetic Bearing Supported Rotating Machinery*, SAE 931387

Mosher, P. A., Scharrer, J. K., and Greenhill, L. M.; *Development of a High Speed Pump Impeller Test Apparatus*, AIAA 95-2406

Keogh, P. S., Burows, C. R., Berry, T.; *On-Line Controller Implementation for Attenuation of Synchronous and Transient Rotor Vibration*, Journal of Dynamic Systems, Measurement, and Control, June 1996, Vol. 118

Wang, W. and Kirkhope, J.; *New Eigensolutions and Modal Analysis for Gyroscopic/Rotor Systems, Part 1: Undamped Analysis*, Journal of Sound and Vibration, 1994, Vol. 175(2)

Hong, S. -W., and Lee, C. -W.; *Frequency and Time Domain Analysis of Linear Systems with Frequency Dependent Parameters*, Journal of Sound and Vibration, 1988, Vol. 127(2)

Youcef-Toumi, K., and Reddy, S.; *Dynamic Analysis and Control of High Speed and High Precision Active Magnetic Bearings*, Journal of Dynamic Systems, Measurement, and Control, Vol. 114, December 1992

Petala, G., and Boros, K. T.; *Magnetic Bearing Control of Flexible Shaft Vibrations Based on Multi-access Velocity-Displacement Feedback*, Transactions of the ASME, January 1995

MBC 500 Magnetic Bearing Experiments, University of California, Santa Barbara, http:\\www-ccec.ece.ucsb.edu\magbearing

Jensen, Raymond, and Muszynska, Agnes; *Use of Forward Response Data for the Balancing of Anisotropic Rotors*, BRDRC (Bently Rotor Dynamic Research Company) Report 5/1997

Rajalingham, C., Ganesan, N., and Prabhu, B. S.; *Conditions for Backward Whirling Motion of a Flexible Rotor Supported on Hydrodynamic Journal Bearings*, Journal of Sound and Vibration 1986 Vol. 111(1)

NOTE: **book titles in bold**, *paper titles in italics*, journal titles in standard font

APPENDIX A: RIGID ROTOR MODEL DEVELOPMENT

A.1 Development of General Rigid Rotor Equations

This section summarizes development of the rigid rotor governing equations. The rigid rotor assumption is valid for a rotor on soft supports operating at speeds well below those corresponding to the natural frequency of its first bending mode. This model is typically used as the plant for at least the initial design of magnetic bearings. This particular development follows from application of Newton's law and is inertially decoupled using the dynamic relationships resulting from the angular momentum equations. Rotational speed dependent coupling exists in the damping matrix between the Y and Z coordinates due to the gyroscopic effect. Speed-independent planar coupling also exists in the stiffness and damping matrices.

The geometry considered is shown in Figure A.1, where the rotor can be considerably more complex in appearance provided the conditions mentioned above are met. If it behaves as a rigid body, it is characterized by the location of the center of gravity as defined by *a* and *b* as well as inertial properties listed in the figure where I_r is the moment of inertia about the spin axis and I_t is the moment of inertia about a transverse axis through the center of gravity. Cartesian coordinate systems 1 and 2 translate with the rotor but do not rotate.

The following results from application of Newton's law in the X, Y, and Z coordinate directions through the center of gravity of the rigid rotor as shown in Figure A.1:

$$m\ddot{x}_c = F_{X1} + F_{X2} + F_{Xc} \tag{A.1}$$

$$m\ddot{y}_c = F_{Y1} + F_{Y2} + F_{Yc} \tag{A.2}$$

$$m\ddot{z}_c = F_{Z1} + F_{Z2} + F_{Zc} \tag{A.3}$$

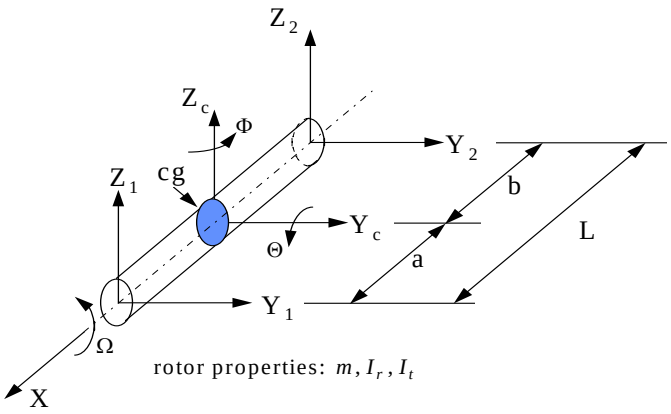

Figure A.1: Rigid Rotor Geometry and Coordinate Systems

The following equations governing the rotation of the rotor about its center of gravity result from considering the angular momentum of the spinning shaft and applying small angle approximations:

$$\frac{d}{dt}\left(L_Y\right) = \frac{d}{dt}\left(I_t\dot{\Theta} + I_r\Omega\Phi\right) = M_Y \tag{A.4}$$

which leads to:

$$I_t\ddot{\Theta} + I_r\Omega\dot{\Phi} = -aF_{Z1} + bF_{Z2} \tag{A.5}$$

Also,

$$\frac{d}{dt}\left(L_Z\right) = \frac{d}{dt}\left(I_t\dot{\Phi} - I_r\Omega\Theta\right) = M_Z \tag{A.6}$$

which leads to:

$$I_t\ddot{\Phi} - I_r\Omega\dot{\Theta} = aF_{Y1} - bF_{Y2} \tag{A.7}$$

The following geometric relations can be applied for the rigid rotor:

$$\begin{aligned} y_1 &= y_c + a\Phi \\ y_2 &= y_c - b\Phi \\ z_1 &= z_c - a\Theta \\ z_2 &= z_c + b\Theta \end{aligned} \quad \text{or,} \quad \begin{aligned} y_c &= y_1 - a\Phi \\ y_c &= y_2 + b\Phi \\ z_c &= z_1 + a\Theta \\ z_c &= z_2 - b\Theta \end{aligned} \tag{A.8}$$

The rotation angles which represent the rigid body rotation about the Y_c and Z_c axes are given by:

$$\Theta = \frac{z_2 - z_1}{L} \qquad \text{and} \qquad \Phi = \frac{y_1 - y_2}{L} \tag{A.9}$$

Substituting relations for displacement of the center of gravity, y_c, into the equations of motion:

$$m\left(\ddot{y}_1 - a\ddot{\Phi}\right) = F_{Y1} + F_{Y2} + F_{Yc} \tag{A.10}$$

or,

$$\ddot{y}_1 = \frac{1}{m}F_{Y1} + \frac{1}{m}F_{Y2} + \frac{1}{m}F_{Yc} + a\ddot{\Phi} \tag{A.11}$$

With the dynamic relationship from Equation (A.7), this becomes:

$$\ddot{y}_1 = \frac{1}{m}\left(F_{Y1} + F_{Y2} + F_{Yc}\right) + \frac{a}{I_t}\left(aF_{Y1} - bF_{Y2} + I_r\Omega\dot{\Theta}\right) \tag{A.12}$$

Now applying the rigid body geometric relationship from Equation (A.9) for the rotation angle Θ results in:

$$\ddot{y}_1 = \frac{1}{m}\left(1 + \frac{ma^2}{I_t}\right)F_{Y1} + \frac{1}{m}\left(1 - \frac{mab}{I_t}\right)F_{Y2} + \frac{1}{m}F_{Yc} + \frac{a\Omega I_r}{LI_t}\dot{z}_2 - \frac{a\Omega I_r}{LI_t}\dot{z}_1 \tag{A.13}$$

A similar process results in the remaining equations of motion for the rigid rotor:

$$\ddot{y}_2 = \frac{1}{m}\left(1 - \frac{mab}{I_t}\right)F_{Y1} + \frac{1}{m}\left(1 + \frac{mb^2}{I_t}\right)F_{Y2} + \frac{1}{m}F_{Yc} - \frac{b\Omega I_r}{LI_t}\dot{z}_2 + \frac{b\Omega I_r}{LI_t}\dot{z}_1 \tag{A.14}$$

$$\ddot{z}_1 = \frac{1}{m}\left(1 + \frac{ma^2}{I_t}\right)F_{Z1} + \frac{1}{m}\left(1 - \frac{mab}{I_t}\right)F_{Z2} + \frac{1}{m}F_{Zc} + \frac{a\Omega I_r}{LI_t}\dot{y}_1 - \frac{a\Omega I_r}{LI_t}\dot{y}_2 \tag{A.15}$$

$$\ddot{z}_2 = \frac{1}{m}\left(1 - \frac{mab}{I_t}\right)F_{Z1} + \frac{1}{m}\left(1 + \frac{mb^2}{I_t}\right)F_{Z2} + \frac{1}{m}F_{Zc} - \frac{b\Omega I_r}{LI_t}\dot{y}_1 + \frac{b\Omega I_r}{LI_t}\dot{y}_2 \tag{A.16}$$

Now define the following dimensionless geometric parameters:

$$\alpha = 1 + \frac{ma^2}{I_t} \qquad \beta = 1 + \frac{mb^2}{I_t} \qquad \gamma = 1 - \frac{mab}{I_t} \tag{A.17}$$

The rigid rotor equations, with no consideration of the form of the support system parameters, can then be expressed as:

$$\begin{Bmatrix} \ddot{y}_1 \\ \ddot{y}_2 \\ \ddot{z}_1 \\ \ddot{z}_2 \end{Bmatrix} + \frac{\Omega I_r}{L I_t} \begin{bmatrix} 0 & 0 & a & -a \\ 0 & 0 & -b & b \\ -a & a & 0 & 0 \\ b & -b & 0 & 0 \end{bmatrix} \begin{Bmatrix} \dot{y}_1 \\ \dot{y}_2 \\ \dot{z}_1 \\ \dot{z}_2 \end{Bmatrix} = \frac{1}{m} \begin{bmatrix} \alpha & \gamma & 0 & 0 \\ \gamma & \beta & 0 & 0 \\ 0 & 0 & \alpha & \gamma \\ 0 & 0 & \gamma & \beta \end{bmatrix} \begin{Bmatrix} F_{Y1} \\ F_{Y2} \\ F_{Z1} \\ F_{Z2} \end{Bmatrix} \tag{A.18}$$

or,

$$\left\{\ddot{Y}\right\} + [G]\left\{\dot{Y}\right\} = [P]\{F\} \tag{A.19}$$

where

$$\{Y\} = \begin{Bmatrix} y_1 \\ y_2 \\ z_1 \\ z_2 \end{Bmatrix} \qquad \text{and} \qquad \{F\} = \begin{Bmatrix} F_{Y1} \\ F_{Y2} \\ F_{Z1} \\ F_{Z2} \end{Bmatrix} \tag{A.20}$$

and matrices *G* and *P* are defined to represent the gyroscopic effect and the mass-normalized planar coupling, respectively. The vector *F* is comprised of all forces acting at stations 1 and 2.

At this point, forces applied to the rotor at stations 1 and 2 are completely arbitrary. If it is assumed that there is no interaction between the supports at stations 1 and 2 and that the performance of the support system is adequately represented by the combination of a spring and damper element, the equations representing the support system are:

$$\begin{Bmatrix} F_{Y1} \\ F_{Y2} \\ F_{Z1} \\ F_{Z2} \end{Bmatrix}_{\text{bearing}} = -\begin{bmatrix} K_{YY1} & 0 & K_{YZ1} & 0 \\ 0 & K_{YY2} & 0 & K_{YZ2} \\ K_{ZY1} & 0 & K_{ZZ1} & 0 \\ 0 & K_{ZY2} & 0 & K_{ZZ2} \end{bmatrix} \begin{Bmatrix} y_1 \\ y_2 \\ z_1 \\ z_2 \end{Bmatrix} - \begin{bmatrix} C_{YY1} & 0 & C_{YZ1} & 0 \\ 0 & C_{YY2} & 0 & C_{YZ2} \\ C_{ZY1} & 0 & C_{ZZ1} & 0 \\ 0 & C_{ZY2} & 0 & C_{ZZ2} \end{bmatrix} \begin{Bmatrix} \dot{y}_1 \\ \dot{y}_2 \\ \dot{z}_1 \\ \dot{z}_2 \end{Bmatrix} \tag{A.21}$$

or,

$$\{F\}_{\text{bearing}} = -[K]\{Y\} - [C]\left\{\dot{Y}\right\} \tag{A.22}$$

Governing equations for the rigid rotor mounted on spring-damper supports then become:

$$\left\{\ddot{Y}\right\} + [G + PC]\left\{\dot{Y}\right\} + [PK]\{Y\} = \{F\}_{\text{external}} \tag{A.23}$$

where the external force vector represents external forces acting at stations 1 and 2.

In full form, the equations of motion become:

$$\begin{Bmatrix} \ddot{y}_1 \\ \ddot{y}_2 \\ \ddot{z}_1 \\ \ddot{z}_2 \end{Bmatrix} + \left[\frac{\Omega I_r}{L I_t} \begin{bmatrix} 0 & 0 & a & -a \\ 0 & 0 & -b & b \\ -a & a & 0 & 0 \\ b & -b & 0 & 0 \end{bmatrix} + \frac{1}{m} \begin{bmatrix} \alpha C_{YY1} & \gamma C_{YY2} & \alpha C_{YZ1} & \gamma C_{YZ2} \\ \gamma C_{YY1} & \beta C_{YY2} & \gamma C_{YZ1} & \beta C_{YZ2} \\ \alpha C_{ZY1} & \gamma C_{ZY2} & \alpha C_{ZZ1} & \gamma C_{ZZ2} \\ \gamma C_{ZY1} & \beta C_{ZY2} & \gamma C_{ZZ1} & \beta C_{ZZ2} \end{bmatrix} \right] \begin{Bmatrix} \dot{y}_1 \\ \dot{y}_2 \\ \dot{z}_1 \\ \dot{z}_2 \end{Bmatrix} +$$
$$\frac{1}{m} \begin{bmatrix} \alpha K_{YY1} & \gamma K_{YY2} & \alpha K_{YZ1} & \gamma K_{YZ2} \\ \gamma K_{YY1} & \beta K_{YY2} & \gamma K_{YZ1} & \beta K_{YZ2} \\ \alpha K_{ZY1} & \gamma K_{ZY2} & \alpha K_{ZZ1} & \gamma K_{ZZ2} \\ \gamma K_{ZY1} & \beta K_{ZY2} & \gamma K_{ZZ1} & \beta K_{ZZ2} \end{bmatrix} \begin{Bmatrix} y_1 \\ y_2 \\ z_1 \\ z_2 \end{Bmatrix} = \frac{1}{m} \begin{bmatrix} \alpha & \gamma & 0 & 0 \\ \gamma & \beta & 0 & 0 \\ 0 & 0 & \alpha & \gamma \\ 0 & 0 & \gamma & \beta \end{bmatrix} \begin{Bmatrix} F_{Y1} \\ F_{Y2} \\ F_{Z1} \\ F_{Z2} \end{Bmatrix} \tag{A.24}$$

And the physical rotor model is as shown in Figure A.2 on the following page:

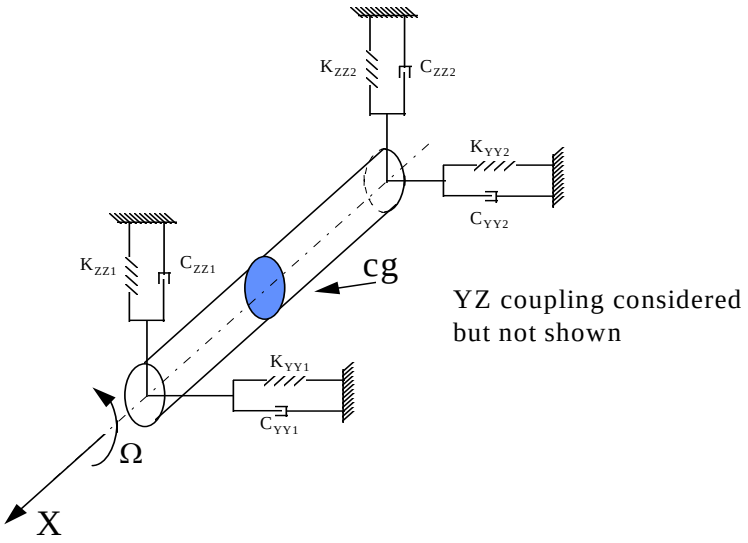

Figure A.2: Rigid Rotor Geometry and Supports

Equations A.24 are appropriate for a rigid rotor of any geometry on spring-damper supports. The coordinate systems translate with their respective stations but do not rotate.

A.2 Simplification of Rigid Rotor Equations to 2 DOF Gyroscopic Motion Equation

The motion considered above is simplified in this section to the pitch motion shown in Figure A.3. Motion is circular at each end with a typical side view as shown in the top of the figure. If the rotor behaves as a rigid body, it is characterized by the inertial properties listed in the figure, where I_r is the moment of inertia about the spin axis, I_t is the moment of inertia about a transverse axis through the center of gravity, L is the bearing span, and m is the rotor mass.

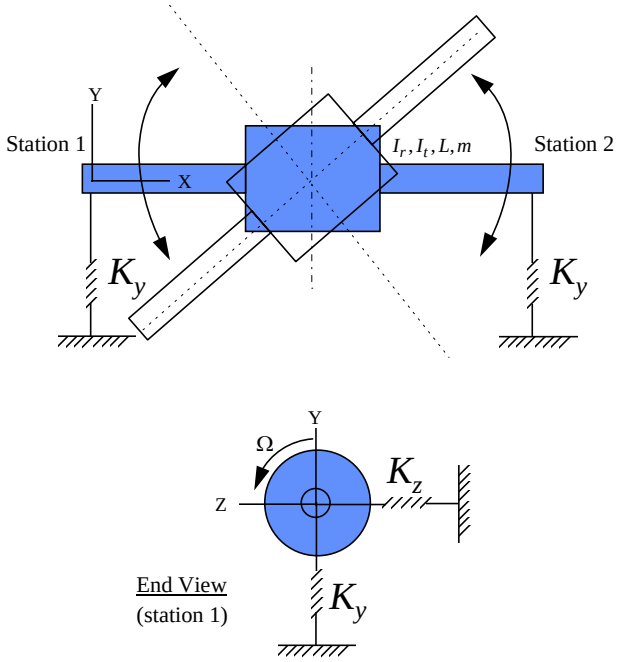

Figure A.3: Rigid Rotor Geometry and Pitch Motion

The simplified coordinate system is defined in Figure A.4:

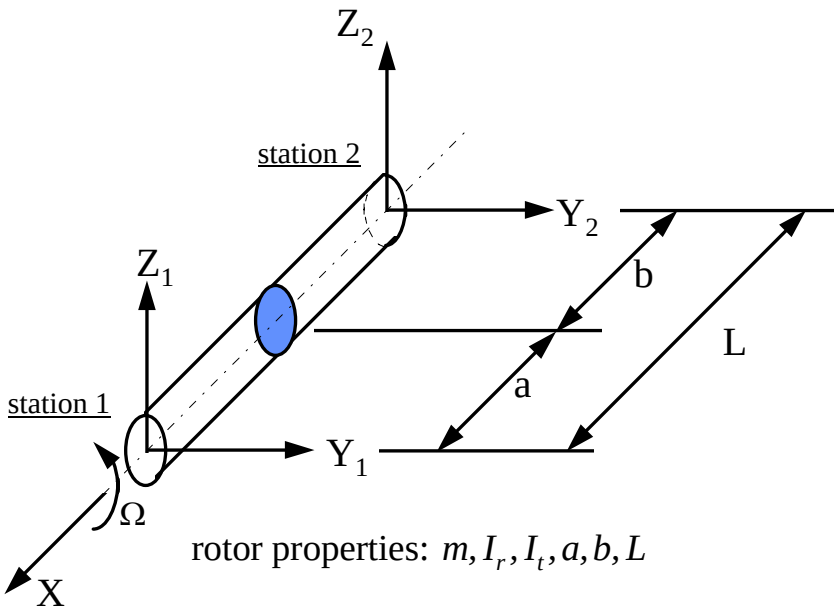

Figure A.4: Simplified Rigid Rotor Coordinate System

Support conditions are assumed to be represented by a spring and damper at each rotor station. With these assumptions the governing equations for the rigid rotor can be expressed as Equations A.24. A modification of the homogeneous rigid rotor equations is of interest which is derived by examining conditions corresponding to the antisymmetric ("pitch") modes of the symmetric rigid rotor:

$$y_1 = -y_2 \qquad \text{and} \qquad z_1 = -z_2 \tag{A.25}$$

Symmetry requirements which are imposed on the support system are such that the bearings at either end of the shaft behave identically and the symmetry requirement on the shaft is that the center of mass be at midspan ($a = b = L/2$) which leads to:

$$\alpha = \beta \tag{A.26}$$

For the pitch modes the undamped homogeneous equations of motion reduce to:

$$\begin{Bmatrix} \ddot{y}_1 \\ \ddot{z}_1 \end{Bmatrix} + \frac{\Omega I_r}{I_t} \begin{bmatrix} 0 & 1 \\ -1 & 0 \end{bmatrix} \begin{Bmatrix} \dot{y}_1 \\ \dot{z}_1 \end{Bmatrix} + \frac{\alpha - \gamma}{m} \begin{bmatrix} K_{YY} & 0 \\ 0 & K_{ZZ} \end{bmatrix} \begin{Bmatrix} y_1 \\ z_1 \end{Bmatrix} = \begin{Bmatrix} 0 \\ 0 \end{Bmatrix} \tag{A.27}$$

The following parameters are defined:

$$\bar{k} = \left(\frac{\alpha - \gamma}{m}\right)\frac{K_{YY} + K_{ZZ}}{2}\,;\, \lambda^2 = \frac{\bar{k}}{m}\,;\; \Delta = \frac{K_{YY} - K_{ZZ}}{K_{YY} + K_{ZZ}}\,;\, \Omega_p = \frac{\Omega I_r}{I_t} \qquad \text{(A.28)}$$

The parameter Δ defines the level of support anisotropy and Ω_p defines the level of the gyroscopic effect. The nondimensional equations for pitch motion then become:

$$\begin{Bmatrix} \ddot{y}_1 \\ \ddot{z}_1 \end{Bmatrix} + \begin{bmatrix} 0 & \Omega_p \\ -\Omega_p & 0 \end{bmatrix}\begin{Bmatrix} \dot{y}_1 \\ \dot{z}_1 \end{Bmatrix} + \begin{bmatrix} 1+\Delta & 0 \\ 0 & 1-\Delta \end{bmatrix}\begin{Bmatrix} y_1 \\ z_1 \end{Bmatrix} = \begin{Bmatrix} 0 \\ 0 \end{Bmatrix} \qquad \text{(A.29)}$$

where the dimensionless time parameter $\tau = \lambda t$ is used and the dot notation[1] now denotes differentiation with respect to the parameter τ.

The particular parameters of the rigid rotor used in this work are:

$a = 4$ inch (101.6 mm)
$b = 4$ inch (101.6 mm)
$L = 8$ inch (203.2 mm)
$m = 5.270e-3$ $\text{lbf}\cdot\text{sec}^2/\text{inch}$ (0.924 Kg)
$I_r = 5.1e-3$ $\text{lbf}\cdot\text{sec}^2\cdot\text{inch}$ ($5.77e2$ $\text{Kg}\cdot\text{mm}^2$)
$I_t = 6.7e-3$ $\text{lbf}\cdot\text{sec}^2\cdot\text{inch}$ ($7.58e2$ $\text{Kg}\cdot\text{mm}^2$)
$\Omega = 500$ rpm (52.36 rad/sec)

The support system damping parameters are:

$$\begin{aligned} C_{YYi} = C_{ZZi} &= 2.5e-3 \ \text{lbf}\cdot\text{sec}/\text{in}\ (4.4e-4\ \text{N}\cdot\text{sec}/\text{mm}) \\ C_{YZi} = C_{ZYi} &= 0 \ \text{lbf}\cdot\text{sec}/\text{in}\ (0\ \text{N}\cdot\text{sec}/\text{mm}) \end{aligned} \quad ; i = 1,2$$

The isotropic rotor support system stiffness parameters are:

$$\begin{aligned} K_{YYi} = K_{ZZi} &= 40.0 \ \text{lbf}/\text{in}\ (7.00\ \text{N}/\text{mm}) \\ K_{YZi} = K_{ZYi} &= 0 \ \text{lbf}/\text{in}\ (0\ \text{N}/\text{mm}) \end{aligned} \quad ; i = 1,2$$

The anisotropic rotor support system stiffness parameters are:

$$\begin{aligned} K_{YYi} &= 40.0 \ \text{lbf}/\text{in}\ (7.00\ \text{N}/\text{mm}) \\ K_{ZZi} &= 36.0 \ \text{lbf}/\text{in}\ (6.30\ \text{N}/\text{mm}) \quad ; i = 1,2 \\ K_{YZi} = K_{ZYi} &= 0 \ \text{lbf}/\text{in}\ (0\ \text{N}/\text{mm}) \end{aligned}$$

Further analytical developments based upon the rigid rotor model are available[2,3].

Appendix A References:

[1] Childs, Dara; ”**Turbomachinery Rotordynamics; Phenomena, Modeling, and Analysis**”, John Wiley & Sons, 1993

[2] Lee, Chong-won; “**Vibration Analysis of Rotors**”, Kluwer Academic Publishers, 1993

[3] Ehrich, Fredric F.; “**Handbook of Rotordynamics**”, McGraw-Hill, 1992